

**A SENSITIVE AND SELECTIVE RATIO-METRIC
NEAR IR FLUORESCENT PROBES FOR ZINC AND MERCURY IONS
BASED ON THE DISTYRYL-BODIPY
FLUOROPHORE**

**A THESIS SUBMITTED TO
THE GRADUATE SCHOOL OF NATURAL AND APPLIED SCIENCES
OF
MIDDLE EAST TECHNICAL UNIVERSITY**

**BY
SERDAR ATILGAN**

**IN PARTIAL FULFILLMENT OF THE REQUIREMENTS
FOR
THE DEGREE OF DOCTOR OF PHILOSOPHY
IN
CHEMISTRY**

JUNE 2009

Approval of the thesis:

**A SENSITIVE AND SELECTIVE RATIOMETRIC NEAR-IR
FLUORESCENT PROBES FOR ZINC AND MERCURY IONS BASED ON
THE DI-STYRYL-BODIPY FLUOROPHORE**

submitted by **SERDAR ATILGAN** in partial fulfillment of the requirements for the degree of **Doctor of Philosophy in Chemistry Department, Middle East Technical University** by,

Prof. Dr. Canan Özgen
Dean, Graduate School of **Natural and Applied Sciences**

Prof. Dr. Ahmet M. Önal
Head of Department, **Chemistry**

Prof. Dr. Mahinur Akkaya
Supervisor, **Chemistry Department, METU**

Examining Committee Members

Prof. Dr. Metin Balcı
Chemistry Dept., METU

Prof. Dr. Mahinur Akkaya
Chemistry Dept., METU

Prof. Dr. Mevlüt Ertan
Pharmacy Dept., Hacettepe University

Prof. Dr. Ahmet M. Önal
Chemistry Dept., METU

Prof. Dr. Metin Zora
Chemistry Dept., METU

Date: June 3, 2009

I hereby declare that all information in this document has been obtained and presented in accordance with academic rules and ethical conduct. I also declare that, as required by these rules and conduct, I have fully cited and referenced all material and results that are not original to this work

Name, Last name : SERDAR ATILGAN

Signature :

ABSTRACT

A SENSITIVE AND SELECTIVE RATIOMETRIC NEAR IR FLUORESCENT PROBES FOR ZINC AND MERCURY IONS BASED ON THE DISTYRYL-BODIPY FLUOROPHORE

ATILGAN, SERDAR

Doctor of Philosophy, Department of Chemistry

Supervisor: Prof.Dr. Mahinur Akkaya

June 2009, 170 pages

Near-IR dyes that absorb and emit in the red visible or near-IR region have attracted great interest in the fields of medicinal chemistry and biochemistry for the last few decades. This interest is due to the multiple notes of metal ions in biological and environmental processes. Therefore the development of cation selective and sensitive sensors have been a hot subject for many researchers. Consequently, fluorescence based sensors are the most efficient and favorable ones among its counterparts in the field of sensor research.

In this study, we have targeted to synthesize BODIPY based near-IR dyes as a selective fluorophore for Zn (II) and Hg (II) cations. We have also demonstrated that the versatile BODIPY fluorophore can be functionalized for long wavelength emission on the 3 and 5 position of the BODIPY core with multiple and distinct functional groups in a stepwise manner. Thus we are able to link two BODIPY cores with a different absorption wavelengths to each other first time with click chemistry strategy to generate a chemosensor for Hg (II) cation.

Keywords: Near-IR dyes, boradiazaindacene dyes, chemosensor

ÖZ

ÇİNKO VE CİVA İYONLARI İÇİN Dİ-STİRİL BODIPY FLOROFORUNA DAYALI HASSAS VE SEÇİCİ ORANSAL YAKIN KIZIL ÖTESİ FLORESANS PROBLARI

ATILGAN, SERDAR

Doktora, Kimya Bölümü

Tez Yöneticisi: Prof. Dr. Mahinur Akkaya

Haziran 2009, 170 sayfa

Son yıllarda, kırmızı görünür ya da yakın-IR bölgede yayan ve absorbe eden yakın-IR boyalar, tıbbi kimya ve biyokimya alanlarında büyük ilgi çekmiştir. Bu ilgi, biyolojik ve çevresel süreçlerindeki metal iyonlarının çeşitli notlarından kaynaklanmaktadır. Bundan dolayı katyon oluşumunda seçici ve duyarlı sensörler her zaman birçok araştırmacı için ilgi çekici bir konu olmuştur. Sonuç olarak, algılayıcı alanındaki araştırmalar arasında, floresan tabanlı algılayıcılar benzerlerine kıyasla en verimli ve en uygun olanlarıdır.

Bu çalışmamızda Zn (II) ve Hg (II) katyonları için seçici bir florofor olan BODIPY tabanlı yakın-IR boyaların sentezlenmesini hedefledik. Ayrıca çok yönlü BODIPY floroforu 3 ve 5 pozisyonlarından uzun dalga boyu emisyon için basamak basamak birden çok ve farklı fonksiyonel gruplar ile fonksiyonlabileceğini gösterdik. Bu çalışmada ayrıca farklı soğurma dalga boyuna sahip iki BODIPY çekirdeği Hg (II) katyonuna uygun bir moleküler algılayıcı oluşturmak için birbirlerine ilk kez Click kimyası stratejisi ile bağlanmıştır.

Anahtar Kelimeler: Yakın-IR boyalar, boradiazaindacene boyalar, moleküler algılayıcılar

***Dedicated to my wife, Neslihan,
for her continuous support and encouragement
and also to our son***

ACKNOWLEDGEMENTS

I would like to express my sincere thanks to my supervisor Prof. Dr. Engin U. Akkaya from Bilkent University for his guidance, support, endless imagination, stimulating suggestions, patience, and writing of this thesis. I will never forget his support throughout my life.

I would like to express my gratitude to Prof. Dr. Mahinur Akkaya

I was extraordinarily fortunate in having such a wonderful mother, father and sister.

I was very lucky to work with Tugba Özdemir and also have such a sister. I could never have succeeded without her support. The preparation of this thesis would not been possible without her. Additional thanks to İlker Kütük for his help during the laboratory studies and also for his brotherhood.

My especial thanks are due to Bora Bilgiç and Tamer Tezel for their help, support and friendships

I wish to express my sincere appreciation to Dr. Ö. Altan Bozdemir. Thank you very much.

I am obliged to each and every member of Supramolecular Chemistry Laboratory, Yusuf, Ruslan, Onur, Safacan, Sündüz, Sencer, Bilal for the great atmosphere in the laboratory. They are very precious for me.

And to my lovely wife. Her patience, help and being my wife always gave me extra power to overcome the problems.

Finally, I want to thank the Chemistry department of the Middle East Technical University for giving me permission to collect necessary data and to do the necessary working for preparation of my doctoral thesis.

TABLE OF CONTENTS

ABSTRACT.....	iv
ÖZ.....	v
ACKNOWLEDGEMENTS.....	vii
TABLE OF CONTENTS.....	viii
LIST OF FIGURES.....	xiii
LIST OF ABBREVIATIONS.....	xxvi
CHAPTERS	
1. INTRODUCTION.....	1
1.1. Fluorescent Molecular Sensors	1
1.1.1 Fundamental aspects.....	1
1.1.2 Photoinduced Electron Transfer (PET).....	5
1.1.3 Internal Charge transfer systems (ICT).....	7
1.1.4 Fluorescence Resonance Energy Transfer (FRET).....	10
1.1.5 Near-IR Dyes.....	12
1.2 Designing a Zinc selective chemosensor.....	13
1.2.1 Zinc in biological systems.....	13
1.2.2 Molecular sensor design for Zn (II).....	15
1.3 Hg(II) selective Chemosensors and Importance of mercury Selection.....	25

1.3.1	Hg(II) in Nature and Human Life.....	25
1.3.2	Employing Chromophores For Mercury Detection.....	27
1.3.3	Designed fluorophore with Fluorescence turn-off mechanism for Hg(II) detection.....	29
1.3.4	Turn-On strategy for Hg(II) detection	31
1.3.5	Ratiometric Fluorescence Sensors For Hg ²⁺	34
1.4	BODIPY.....	39
1.4.1	The nomenclature of BODIPY.....	39
1.4.2	The fundamental properties of BODIPY.....	40
1.4.3	Synthesis of BODIPY.....	43
1.4.4	The chemistry of BODIPY.....	44
1.4.4.1	Electrophilic Substitution.....	44
1.4.4.2	Active Methyl Groups (condensation reaction).....	45
1.4.5	Optical Properties.....	46
1.4.5.1	Photoinduced electron transfer on BODIPY core...	46
1.4.5.2	ICT on BODIPY core.....	51
1.4.5.3	Both ICT and PET mechanism on the same BODIPY core.....	51
1.4.5.4	FRET (Fluorescence resonance energy transfer) on BODIPY core	53
1.4.5.5	Near-IR BODIPY Dyes.....	55

2. EXPERIMENTAL.....	58
2.1 Synthesis of Zn (II) selective Chemosensor.....	59
2.1.1 Synthesis of ethyl 3, 4, 5-trihydroxybenzoate (43).....	59
2.1.2 Synthesis of triethylene glycol methyl ether tosylate.....	60
2.1.3 Synthesis of the compound 46.....	61
2.1.4 Synthesis of the compound 47.....	62
2.1.5 Synthesis of the compound 48.....	63
2.1.6 4,4-difluoro-8-[3,4,5-tris(2-(2-(2methoxyethoxy) ethoxy) ethoxy)] benzaldehyde-2,6-diethyl-1,3,5tetramethyl -4-bora-3a,4a -diza-s-indacene (50).....	64
2.1.7 N,N-Bis(pyridine-2-ylmethyl) aniline (53).....	65
2.1.8 4- (bis(pyridin-2-ylmethyl)amino)benzaldehyde 54.....	66
2.1.9 Monostyryl functionalization of the BODIPY dye 55....	67
2.1.10 Synthesis of the target distyryl-BODIPY.....	68
2.2 Synthesis of Hg ²⁺ selective double-chealated chemosensor...	70
2.2.1 Synthesis of N,N-bis(bromoethyl)aniline, 58.....	70
2.2.2 Synthesis of 10-phenyl-1,4-dioxa-7,13-dithia-10-azacyclopentadecane.....	71
2.2.3 Synthesis of 4-(1,4-dioxa-7,13-dithia-10-azacyclopentadecan-10-yl) benzaldehyde, 61.....	72
2.2.4 Synthesis of 2,6-diethyl-4,4-difluoro-1,3,5,7-tetramethyl-8-(4-terti-arybutylphenyl)-4-bora-3a,4a-diaza-s-indacene.....	73

2.2.5	Synthesis of distyryl BODIPY, 64.....	74
2.3	Synthesis of ratiometric FRET based fluorescent chemosensor for Hg ²⁺	76
2.3.1	Synthesis of 4-(prop-2-ynyloxy)benzaldehyde	76
2.3.2	Synthesis of 4,4-difluoro-8-(4-(prop-2-ynyloxy)phenyl)- 1,3,5,7-tetramethyl-4-bora-3a,4a-diaza-s-indacene.....	77
2.3.3	Synthesis of 4-(6-bromohexyloxy)benzaldehyde, 71.....	78
2.3.4	Synthesis of 4-(6-azidohexyloxy)benzaldehyde, 72.....	79
2.3.5	Synthesis of Mono-styryl BODIPY (Blue-BODIPY), 73...	80
2.3.6	Synthesis of the di-styryl BODIPY, 74.....	81
2.3.7	Synthesis of the targeted Di-styryl BODIPY, 75.....	83
3.	RESULTS AND DISCUSSION.....	85
3.1	A Sensitive and Selective Ratiometric Near IR Fluorescent Probe for Zinc Ions Based on the Distyryl-Bodipy Fluorophore, 56.....	85
3.2	Double chealated near-IR di-styryl BODIPY based ratiometric fluorescent chemosensor for Hg ²⁺ , 64.....	97
3.3	Ratiometric analysis of Hg ²⁺ with near-IR fluorescent chemosensor via energy- transfer system, 75.....	109
4.	CONCLUSION.....	124

REFERENCES.....	126
APPENDICES	
A. AUXILLIARY.....	142
B. ¹ H, ¹³ C NMR and MALDI-ToF Mass Spectrum	144
VITA.....	168

LIST OF FIGURES

Figure 1	Main classes of fluorescent molecular sensors ions or molecules.....	4
Figure 2	Molecular orbital diagrams for oxidative and reductive PET.....	6
Figure 3	Schematic diagram for spectral displacement of a fluorophore following a cation binds.....	9
Figure 4	Spectral representations for Acceptor absorption and Donor emission overlapping.....	10
Figure 5	Molecular orbital schematic for resonance energy transfer.....	11
Figure 6	Structure of N,N,N,N-tetrakis (2- pyridylmethyl) ethylenediamine, 1.....	16
Figure 7	A schematic representation for PET process.....	17
Figure 8	Structure of DPA-based anthracene dye, 2	18
Figure 9	Structure of the fluorescein based chemosensors, 3, 4	19

Figure 10 a) Structure of complexation of Zn ²⁺ to coumarin-based chromophore. b) Uv-vis spectral titration and fluorescence response of compound 5, with Zn ²⁺	20
Figure 11 Structure of Zn ²⁺ selective Squaraine dye, 6	21
Figure 12 Changes in the emission spectrum of squaraine derivative 6 with increasing amounts of Zn ²⁺ . a) [Zn ²⁺]=0; b) [Zn ²⁺]=1.0 μM, c[Zn ²⁺]=0.025 M.....	21
Figure 13 a)Fluorescence ratiometric images (340 nm/380 nm) of zinc in macrophages (RAW 264.7) labeled with ZnAF-R2 EE in PBS buffer, pH 7.4 a) Bright –field transmission image. b) Ratiometric image of a. c) Pyrithione (zinc ionophore; 15 μM) and ZnSO ₄ (150 μM) were added to b. d) TPEN (400 μM) was added 15 min after the addition of pyrithione.....	23
Figure 14 a) Structural representation of Zn ²⁺ complexation with dye, 9 . b) Absorption, excitation spectra of compound 9 (1 μM) at various Zn ²⁺ concentrations (in 100 mm HEPES buffer, pH 7.4).....	24
Figure 15 Organic soluble turn-off fluorescent chemosensors for Hg ²⁺ cation.....	30
Figure 16 Structure of Hg ²⁺ selective dye designed with a turn-off strategy, 13	31
Figure 17 Structure of compounds 14 , 15 , 16	33

Figure 18 Structure of the compounds based on Ratiometric fluorescence sensing for Hg ²⁺ , 17 , 18	36
Figure 19 Ratiometric fluorescence response of 2 μM 18 to 0-40 μM Hg(II) in 30:70 THF/H ₂ O (20 μM HEPES, Ph 7.2). Excitation was provided at 540 nm.....	36
Figure 20 a) Structure of the compound 19 . b)The emission response of the dye 19 in THF (1.0 μM) to an increasing concentration (0-25 μM) of Hg(II) ions. A small decrease in the intensity at 540 nm is indicative of larger EET.....	38
Figure 21 Structural representation of numbering of BODIPY core....	40
Figure 22 BODIPY cores.....	42
Figure 23 Synthetic pathway for BODIPY.....	43
Figure 24 General procedure for electrophilic substitution reaction on BODIPY core.....	44
Figure 25 Modification of BODIPY core on 3, 5 positions.....	45
Figure 26 Formation of reductive PET with oxidation of diamine to triazole on BODIPY core.....	47
Figure 27 Coordination of Zn ²⁺ to ionophore core causes oxidative PET.....	48

Figure 28 Molecular orbital representation of a-PET and d-PET on BODIPY core.....	49
Figure 29 BODIPY based fluorophore designed with the advantages of the strategy of ICT process for cation analysis.....	51
Figure 30 Representation of ICT and PET on BODIPY core.....	52
Figure 31 BODIPY, as a cation sensor, with two coordination site with strategies ICT and PET.....	53
Figure 32 Structure of cassette where an FRET is observed from BODIPYs to PDI core.....	55
Figure 33 BODIPY based Near-IR dyes.....	57
Figure 34 The synthesis of ethyl 3,4,5-trihydroxybenzoate.....	59
Figure 35 The synthesis of compound 45	60
Figure 36 Synthesis of the compound 46	61
Figure 37 Synthesis of the compound 47	62
Figure 38 Synthesis of the compound 48	63
Figure 39 Synthesis of the BODIPY, 50	65
Figure 40 Synthesis of the compound, 53	66
Figure 41 The Synthesis of the compound, 54	67

Figure 42	Synthesis of mono-styryl-BODIPY, 55	68
Figure 43	Synthesis of di-styryl-BODIPY, 56	69
Figure 44	Synthesis of the compound 58	70
Figure 45	The synthesis of crownether moiety, 60	71
Figure 46	Vilsmeier reaction of the compound 61	72
Figure 47	Synthesis of BODIPY, 63	74
Figure 48	Synthesis of double armed Hg(II) selective chemosensor, 64	75
Figure 49	Synthesis of 4-(prop-2-ynyloxy)benzaldehyde, 67	76
Figure 50	Synthesis of BODIPY dye, 69	77
Figure 51	Structural representation of the production of compound 71	78
Figure 52	Synthesis of 4-(6-azidohexyloxy)benzaldehyde, 72	79
Figure 53	Synthesis of mono-styryl BODIPY, 73	81
Figure 54	Structural representation of the synthesis of the compound, 74	82
Figure 55	Synthesis of the targeted di-styryl BODIPY, 75	84

Figure 56 Representation of the modulation of BODIPY unit as a Zn ²⁺ selective chemosensor.....	85
Figure 57 Absorbance change of the dye 56 (2.5 μM) in response to different metal ions(5.0 μM) in aqueous solutions. The solutions are buffered with 0.1 M HEPES pH 7.2. 5% EtOH was added as cosolvent.....	88
Figure 58 The change in absorption spectrum of the dye (2.5 μM) as a function of increasing Zn(II) concentration. Concentration of Zn(II) is varied between 0 to 100 μM.....	88
Figure 59 Change in the emission spectrum of the Dye (2.5 μM) in response to increasing concentrations of Zn(II) in ethanol-water mixture (%5 in ethanol). Zinc concentrations were varied in the following order: 0, 0.25, 0.5, 1, 2, 5, 10, 20, 50, 100 μM. Excitation was at 630 nm, with slit widths of 5 nm.....	90
Figure 60 Fluorescence intensity ratio (F_{675}/F_{730}) of 1 versus increasing concentration of log [Zn ²⁺]. The concentration of 56 was 2.5 μM. Hill plot analysis yielded to 1:1 stoichiometry with a slope 0.97.....	91
Figure 61 Normalized emission intensities at 680 nm (the emission intensity of the free dye= 1) of the chemosensor (1.2 μM) in the presence of selected metal ions (1.0 mM). Excitation was done at 630 nm with 5 nm slit widths. Solvent: ethanol-aqueous buffer mixture (5% in ethanol, HEPES 0.1 M, pH= 7.2).....	92

Figure 62 Results of the competition experiments between Zn(II) and selected metal ions. The free dye 56 (chemosensor) concentrations was set at 2.5 μM . Excitation was at 630 nm; emission intensity values at 680 nm were collected; and all metal ions were added at 200 μM concentration. Solvent: ethanol-aqueous buffer mixture (5% in ethanol, HEPES 0.1 M, pH = 7.2)	93
Figure 63 Digital photographs of the chemosensor solutions (5.0 μM) in the presence of different metal ions at 100 μM concentration. The upper plate is taken under ambient light, and the bottom one under UV illumination at 360 nm. Solvent: ethanol-aqueous buffer mixture (5% in ethanol, HEPES 0.1 M, pH= 7.2).....	93
Figure 64 Curve of fluorescence intensity at 675 nm of the dye versus increasing concentration of Zn^{2+} . The concentration of the dye was 5.0 μM . Dissociation constant was calculated as 2.0×10^{-5} M.....	94
Figure 65 Curve of fluorescence ratio of the dye at 675 nm and 730 nm (5.0 μM) versus increasing concentration of Zn^{2+}	95
Figure 66 Logarithmic value for the fluorescence intensity of dye at 675 nm versus $\log[\text{Zn}^{2+}]$. Hill coefficients (2.1038) fits with 1:1 coordination of dye- Zn^{2+}	96
Figure 67 Structural representation of chemosensor 64 as a mercury selective fluorophore.....	97

Figure 68 Normalized absorption spectra of di-styryl BODIPY (1.5 μ M) in the presence of different cations (10.0 μ M) in THF.....	99
Figure 69 Change in the emission spectrum of di-styryl BODIPY (1.5 μ M) in response to the different cation with a cation concentration 10.0 μ M in THF. Excitation wavelength was 640 nm with a slit width 2.5 nm.....	100
Figure 70 Fluorescence response of di-styryl BODIPY (1.5 μ M) to various cations (10.0 μ M) in THF. Excitation was done at 640 nm with a slit width 2.5 nm.....	101
Figure 71 The fluorescence intensity response of di-styryl BODIPY (1.5 μ M) with 20 μ M metal followed by 10 μ M Hg ⁺² in THF. Excitation wavelength was 640 nm with a slit width 2.5 nm.....	101
Figure 72 Absorption spectra of di-styryl BODIPY (1.5 μ M) in the presence of increasing concentration of Hg ⁺² (cation concentrations; 0, 0.5, 0.75, 1.0,1.5, 2.0, 2.5, 4.0, 5.0, 7.5, 10 μ M) in THF solution.....	103
Figure 73 Emission spectrum of the chemosensor, di-styryl BODIPY (1.5 μ M), at Increasing concentration of the Hg ⁺² (cation concentrations; 0, 0.5, 0.75,1.0, 1.5, 2.0, 2.5, 4.0, 5.0, 7.5, 10 μ M). Excitation wavelength was 630 nm with a slit width 2.5 nm.....	104

Figure 74 Curve of fluorescence intensity at 655 nm of the dye versus increasing concentration of Hg ²⁺ . The concentration of the dye was 1.5 μM. dissociation constant was calculated as 1.8x10 ⁻⁶	105
Figure 75 Curve of fluorescence ratio of the dye (1.5 μM) versus increasing concentration of Hg ²⁺ .The dissociation constant was calculated as 2.4x10 ⁻⁶ M.....	106
Figure 76 Logarithmic value for the fluorescence intensity of dye at 655 nm versus log[Hg ²⁺]. Hill coefficients (2.1038) fits with 1:2 coordination of dye-Hg ²⁺	107
Figure 77 Logarithmic value for the fluorescence intensity ratio of dye at 655 and 720 nm versus log[Hg ²⁺]. Hill coefficients (2.3598) fits with 1:2 coordination of dye-Hg ²⁺	108
Figure 78 Structural representation of working scheme for Hg ²⁺ selective FRET based near-IR BODIPY dye, 75 . Green color declare the process where no interaction is exist between dye and metal cation. Yellow color represents the process where an interaction is provided between dye and metal.....	109
Figure 79 Absorption spectra of the dye 75 (1,5 μM) in the presence of some selected metal cations (20 μM) in THF.....	112
Figure 80 Fluorescence spectrum of the dye (1.5 μM) with various cation (10.0 μM). Excitation was done at 500 nm with a slit width 5.0 nm.....	113

Figure 81	Fuorescence intensity ratio at 670 nm and 510 nm of the dye with responds to metal interaction in THF solution.....	114
Figure 82	Fluorescence ratio of the dye at 670 nm and 723 nm corresponds to metal cation interactions.....	115
Figure 83	Results of the competition experiments between Hg(II) and selected ions. The free dye 75 (chemosensor) concentrations was set at 1.5 μ M, where the concentration of the competing cation 100 mM and concentration of Hg ²⁺ was 10 Mm. Excitation was at 500 nm with a slit width 5.0 nm.....	116
Figure 84	Absorption spectrum of the dye 75 (1.5 μ M) with increasing concentration of Hg ²⁺ in THF. Hg ²⁺ concentration is varied from 0 to 15 μ M.....	117
Figure 85	Change in the emission spectrum of the dye in responds to the increasing concentration of Hg ²⁺ in THF. Cation concentration is varied from 0 to 15 μ M. Excitation was done at 500 nm with a slit width 5.0 nm.....	118
Figure 86	Demonstration of energy transfer with fluorescense intensity of BODIPY, dye 75 and dye+Hg ²⁺	119
Figure 87	Logarithmic value for the fluorescence intensity ratio of dye 75 at 670 and 725 nm versus log[Hg ²⁺]. A Hill coefficient (1.13) fits with 1:1 coordination of dye-Hg ²⁺	120

Figure 88	Logarithmic value for the fluorescence intensity of dye 75 at 670 nm versus $\log[\text{Hg}^{2+}]$	121
Figure 89	Curve of fluorescence ratio of the dye (1.5 μM) versus increasing concentration of Hg^{2+} . The dissociation constant was calculated as $3.1 \times 10^{-6} \text{M}$	122
Figure 90	Curve of fluorescence intensity ratio at 670 nm and 725 nm of the dye versus increasing concentration of Hg^{2+} . The concentration of the dye was 1.5 μM . Dissociation constant was calculated as 3.2×10^{-6}	123
Figure 91	^1H NMR spectra of the compound 43	144
Figure 92	^1H NMR spectra of the compound 45	145
Figure 93	^1H NMR spectra of the compound 46	146
Figure 94	^1H NMR spectra of the compound 47	146
Figure 95	^1H NMR spectra of the compound 48	147
Figure 96	^{13}C NMR spectra of the compound 48	147
Figure 97	^1H NMR spectra of the compound 50	148
Figure 98	^{13}C NMR spectra of the compound 50	148
Figure 99	^1H NMR spectra of the compound 53	149

Figure 100	^1H NMR spectra of the compound 54	149
Figure 101	^1H NMR spectra of the compound 56	150
Figure 102	^{13}C NMR spectra of the compound 56	150
Figure 103	^1H NMR spectra of the compound 58	151
Figure 104	^1H NMR spectra of the compound 60	151
Figure 105	^1H NMR spectra of the compound 61	152
Figure 106	^{13}C NMR spectra of the compound 61	152
Figure 107	^1H NMR spectra of the compound 63	153
Figure 108	^{13}C NMR spectra of the compound 63	153
Figure 109	^1H NMR spectra of the compound 64	154
Figure 110	^{13}C NMR spectra of the compound 64	154
Figure 111	^1H NMR spectra of the compound 67	155
Figure 112	^1H NMR spectra of the compound 69	155
Figure 113	^{13}C NMR spectra of the compound 69	156
Figure 114	^1H NMR spectra of the compound 71	156
Figure 115	^{13}C NMR spectra of the compound 71	157

Figure 116	¹ H NMR spectra of the compound 72	157
Figure 117	¹³ C NMR spectra of the compound 72	158
Figure 118	¹ H NMR spectra of the compound 73	158
Figure 119	¹³ C NMR spectra of the compound 73	159
Figure 120	¹ H NMR spectra of the compound 74	159
Figure 121	¹³ C NMR spectra of the compound 74	160
Figure 122	¹ H NMR spectra of the compound 75	161
Figure 123	¹³ C NMR spectra of the compound 75	162
Figure 124	MALDI-TOF Mass spectra of the compound 50	163
Figure 125	MALDI-TOF Mass spectra of the compound 55	164
Figure 126	MALDI-TOF Mass spectra of the compound 56	165
Figure 127	MALDI-TOF Mass spectra of the compound 64	166
Figure 128	MALDI-TOF Mass spectra of the compound 75	167

LIST OF ABBREVIATIONS

CEQ	Cheation enhancement of quenching
CEF	Chelation enhancement of fluorescence
PET	Photoinduced energy transfer
RET	Resonance energy transfer
ICT	Internal charge transfer
NIR	Near infrared
AAS	Atomic Absorption Spectroscopy
ICP-MS	Inductively-coupled Plasma
BODIPY	Boradiazaindacene Dye
FRET	Fluorescence Resonance Energy Transfer

CHAPTER 1

INTRODUCTION

1.1 Fluorescent Molecular Sensors

1.1.1 Fundamental aspects

In the past 20 years, there has been a dramatic growth in the use of fluorescence in analytical chemistry, clinical biochemistry, medicine and in the environment. Fluorescence is now a dominant methodology used extensively in biotechnology ^[1], flow cytometry ^[2], medical diagnostics ^[1], DNA sequencing ^[1], forensics ^[2], and genetic analysis ^[3]. Concurrently with fluorescence methods numerous chemical and biochemical analytes can be detected; cations, anions, neutral molecules and gases. Fluorescence detection is highly sensitive, and also there is one more point that no longer the need for the expense and difficulties of handling radioactive tracers for most biochemical measurements. Nowadays, fluorescent cellular and molecular imaging are also observed together with the enhancement of fluorescence imaging for chemical application.

The first known fluorophore, quinine^[4], was responsible for stimulating the development of the first spectrofluorometers that appeared in the 1950s. During World War II in Europe, the Department of War was interested in monitoring antimalaria drugs, including quinine. This early drug assay resulted in a subsequent program at the National Institutes of Health to develop the first practical spectrofluorometer.^[5]

A fluorescence emission spectrum is a plot of the fluorescence intensity versus wavelength (nanometers) or wavenumber (cm^{-1}). Emission spectra vary widely and are dependent upon the chemical structure of the fluorophore and the solvent in which it is dissolved. The spectra of some compounds, such as perylene^[6], show significant structure due to the individual vibrational energy levels of the ground and excited states. Other compounds, such as quinine^[7], show spectra devoid of vibrational structure.

An important feature of fluorescence is its detection with high sensitivity. In 1877, the sensitivity of fluorescence was used to demonstrate that the rivers Danube and Rhine were connected by underground streams.^[8] This connection was demonstrated by placing fluorescein (highly fluorescent dye) into the Danube. Sixty hours later, its characteristic green fluorescence appeared in a small river.

In fluorescent molecular sensors, the fluorophore is the signaling species, it means that it acts as a signal transducer that converts the information into an optical signal due to the analyte.

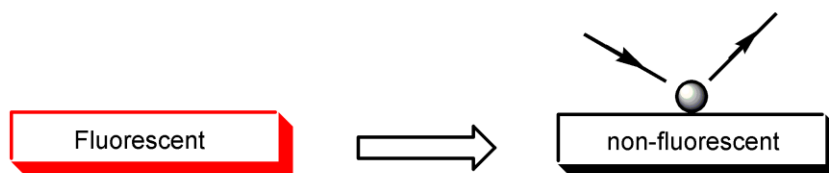
Three type of strategies can be distinguished to illustrate a fluorescent molecular sensor.

1. Any collision of an analyte cause a fluorescence quenching such as gas particles collision.
2. An analyte can reversibly bind to fluorophore. In this situation there are two possibility; fluorescence can be quenched upon binding of analyte

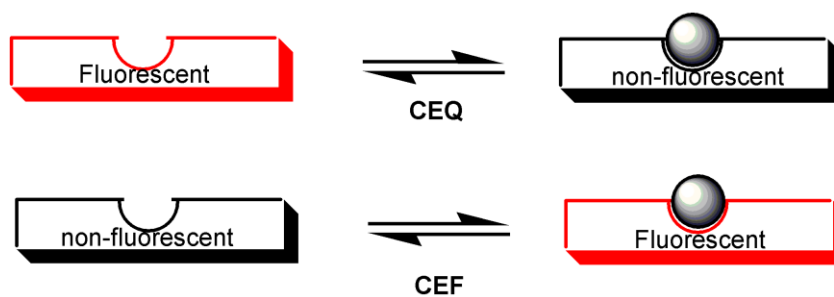
known as chelation enhancement of quenching (CEQ) and fluorescence can be enhanced upon binding of analyte, that is known as chelation enhancement of fluorescence (CEF).

3. Fluorophores can be linked to the receptor with a spacer or not. The changes in photophysical properties of the fluorophore upon interaction with analyte is resulted to the some optical processes such as electron transfer, charge transfer, energy transfer, excimer or exciplex formation or disappearance. Again fluorescence can be quenched (CEQ) or enhanced (CEF) following with analyte coordination.

1.type no association quenching by collision with analyte



2.type complexing fluorophores



3. Fluorophores linked to a receptor

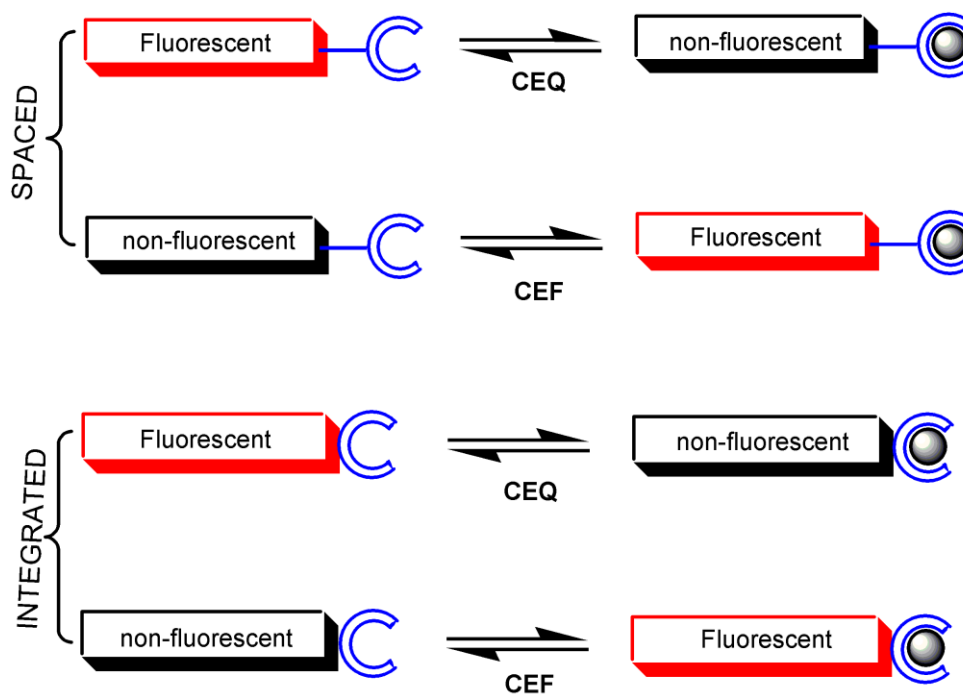


Figure 1 Main classes of fluorescent molecular sensors, ions or molecules

1.1.2 Photoinduced Electron Transfer (PET)

Photoinduced electron transfer (PET) ^[9] is often responsible for fluorescence quenching. In many organic photochemical reactions this process is enclosed. It is exhibited in many natural event and take a major role, such as photosynthesis and in artificial systems for the conversion of solar energy based on photoinduced charge separation.

The terminology for PET can be confusing because the excited fluorophore can be either the electron donor or acceptor. ^[10] The direction of electron transfer in the excited state is determined by the oxidation and reduction potential of the ground and excited states. When discussing PET the term donor refers to the species that donates an electron to an acceptor. In PET the terms donor and acceptor do not identify which species is initially in the excited state. It is different from the resonance energy transfer (RET), in this phenomena the fluorophore is always donors. ^[10]

The nature of PET quenching is illustrated with many examples. The more common situation is when the excited state of a fluorophore acts as an electron acceptor (Figure 2). ^[11] One typical example is an electron-rich species such as dimethylaniline (DMA), which can donate electrons to a wide range of polynuclear aromatic hydrocarbons, which act as electron acceptors. ^[11]

PET quenching can also occur by electron transfer from the excited fluorophore to the quencher as illustrated in Figure 2. Examples include electron transfer from excited indoles to electron-deficient imidazolium or acrylamide quenchers ^[12] (Table 1.1). Quenching by halocarbons can also occur by electron transfer from the fluorophore to the electronegative halocarbon. Electron-rich dimethoxynaphthalene can donate electrons to pyridinium. ^[13]

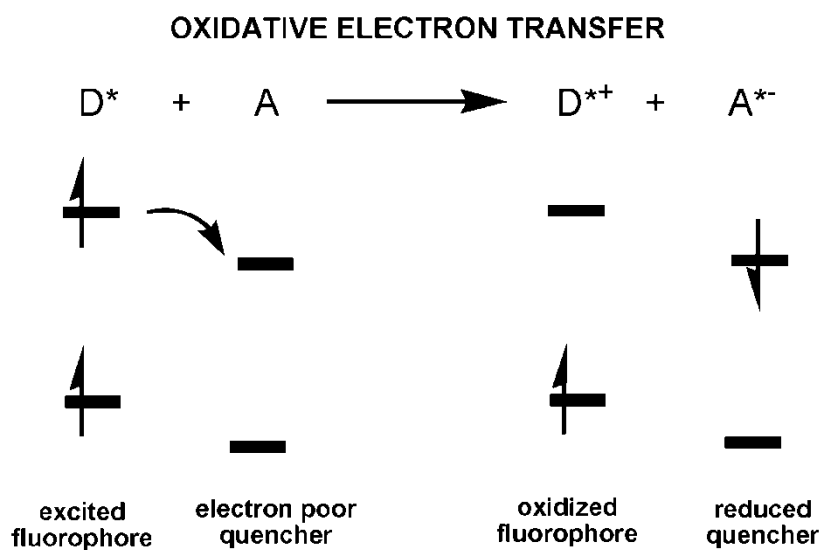
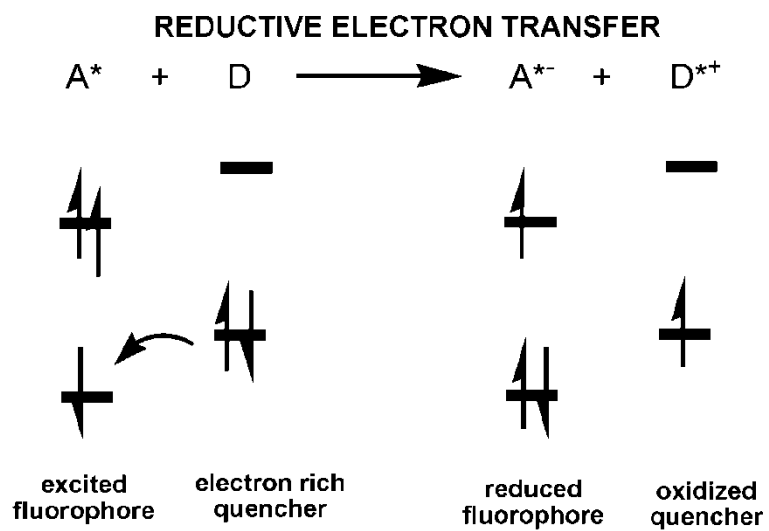


Figure 2 Molecular orbital diagrams for oxidative and reductive PET

1.1.3 Internal Charge transfer systems (ICT)

When a fluorophore contains an electron-donating group (often an amino group) conjugated to an electron with-drawing group, it undergoes intramolecular charge transfer from the donor to the acceptor upon excitation by light. The consequent change in dipole moment results in a Stokes' shift that mainly depends on the microenvironment of the fluorophore. Coordination of the metal to the electron donating group will change the photophysical property of the fluorophore because the complexed cation change the efficiency of the intramolecular charge transfer. ^[19]

When an electron donating group such as amino group interact with the cation, the latter reduces the electron donating character of this group, this is because of reduction in conjugation, following a blue shift absorption is result on the photophysical environment of the fluorophore (Figure 3). On the other hand, a cation may interact with the acceptor group enhances the electron withdrawing character of this group which results in red shift of the absorption spectrum of the fluorophore (Figure 3). All these photophysical effects obviously dependent on the charge and the size of the cation and so selectivity of these effects expected. ^[19]

The photophysical changes upon cation binding can also be described in terms of charge-dipole interaction. In the situation where the dipole moment in the excited state is larger than that in the ground state, the cation interact with the donor group, the excited state is more strongly destabilized by the cation than the ground state, a blue shift absorption and emission is result. Conversely when the cation interact with an acceptor group the excited state is more stabilized by the cation than the ground state and this leads to a red shift in the absorption and emission spectra on the ionophores.

In ICT sensors, the changes in fluorescence quantum yield with cation binding with respect to fluorophore free are not very large compared to these observed in PET. However, cation binding can be monitored as a shift in both absorption and emission wavelength maxima so that an appropriate choice of the excitation and observation wavelengths are often allows to observe quite larger changes in fluorescence intensity. Additionally ratiometric measurements are possible: the ratio of the fluorescence intensities at two appropriate emission or absorption wavelengths provide a notice about the concentration of the analyte, which is independent from the concentration of the fluorophore and is insensitive to the intensity of the incident light.

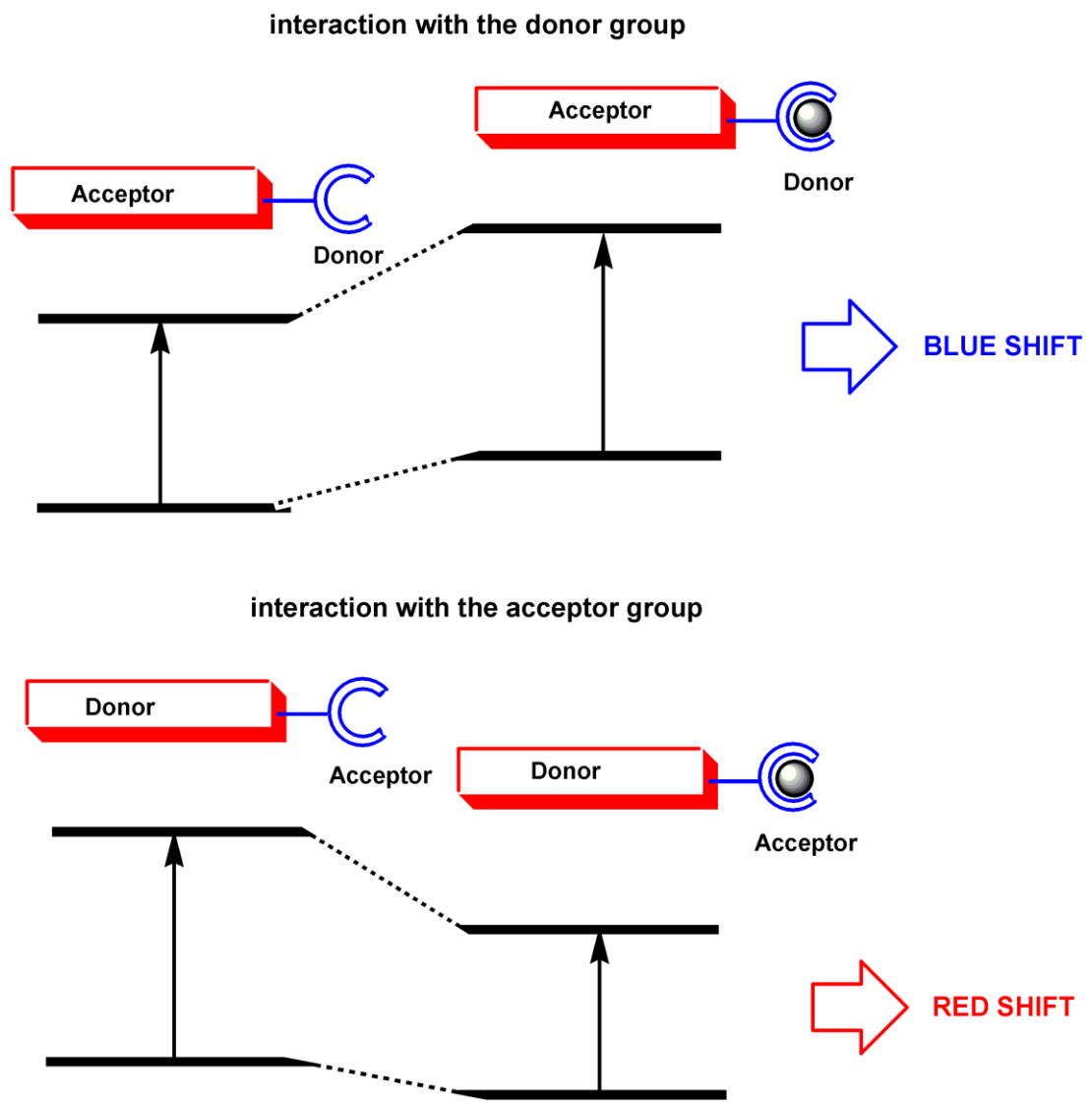


Figure 3 Schematic diagram for spectral displacement of an fluorophore following a cation binds

1.1.4 Fluorescence Resonance Energy Transfer (FRET)

Fluorescence resonance energy transfer (FRET) has become widely used in all applications of fluorescence, including medical diagnostics, DNA analysis, and optical imaging. FRET is widely used to measure the size of the protein or the thickness of the membrane in biological application with its energy transfer distance.^[20-21]

FRET is an electrodynamic phenomenon that classical physics is explaining it in theoretically. FRET occurs between a donor (D) molecule in the excited state and an acceptor (A) molecule in the ground state. The donor molecules typically emit at shorter wavelengths that overlap with the absorption spectrum of the acceptor^[22]. Such an overlap is illustrated in figure 4.

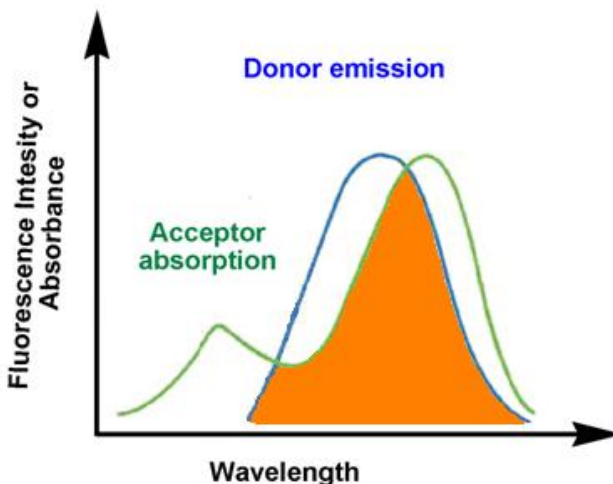


Figure 4 Spectral representations for Acceptor absorption and Donor emission overlapping

Energy transfer occurs without the appearance of a photon and is the result of long range dipole–dipole interactions between the donor and acceptor.^[23] Figure 5 shows a molecular orbital diagram for FRET. The fluorophore initially has two electrons in the highest-occupied molecular orbital (HOMO). Absorption of light results in elevation of one electron to the lowest-unoccupied orbital (LUMO). When RET occurs the electron in the excited donor (D_R^*) returns to the ground state. Simultaneously an electron in the acceptor (A_R) goes into a higher excited-state orbital. If the acceptor is fluorescent it may then emit. If the acceptor is nonfluorescent the energy is dissipated as heat. FRET decreases the intensity of the donor and transfers the energy to an acceptor. The acceptor can be fluorescent or nonfluorescent, but in both cases the fluorescence intensity of the initially excited molecule is decreases

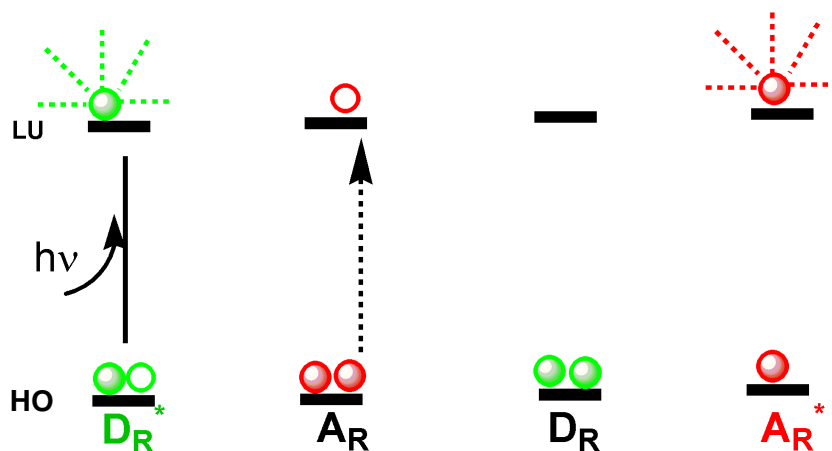


Figure 5 Molecular orbital schematic for resonance energy transfer.

The rate of energy transfer depends upon the extent of spectral overlap of the emission spectrum of the donor with the absorption spectrum of the acceptor, the quantum yield of the donor, the relative orientation of the donor and acceptor transition dipoles, and the distance between the donor and

acceptor molecules. The distance at which RET is 50% efficient is called the Förster distance ^[22] which is typically in the range of 20 to 60 Å. The molecules has a Förster distance between 20-90 Å are convenient for studies of biological macromolecules. These distances are comparable to the size of biomolecules and/or the distance between sites on multi-subunit proteins. Any condition that affects the D–A distance will affect the transfer rate, allowing the change in distance to be quantified. In this type of application, one uses the extent of energy transfer between a fixed donor and acceptor to calculate the D–A distance, and thus obtain structural information about the macromolecules. ^[23] Intramolecular distances determined by energy transfer: dependence on orientational freedom of donor and acceptor. ^[24]

1.1.5 NEAR-IR Dyes

In the last decades, the study of organic compounds mainly focused on the chromophores in which the π -electron system is excited by absorbed light in the ultraviolet and visible regions of the electromagnetic spectrum. Various new applications, such as the use of conjugated organic compounds as dye lasers or as materials for storing information with the help of diode lasers, led to the synthesis of new compounds which absorb light in the near infrared (NIR). ^[25] The advantages of imaging in the NIR region (700–1100 nm) are numerous and have been extensively discussed. ^[26-30]

Prominent among these advantages is the absence or significant reduction of background absorption, fluorescence, and light scattering ^[31-32] along with the availability of low-cost sources of irradiation. Compounds which absorb light strongly in the near IR (NIR) region of the spectrum have numerous

potential applications, including (i) optical data storage devices, in which reading and writing is performed by diode lasers; (ii) Q-switching of lasers, whereby continuous low-energy output in the NIR region is converted to very short, intense bursts; and (iii) photodynamic therapy, which takes advantage of the relative transparency of living tissue to NIR radiation.^[33-35]

There has been recent intense interest in the preparation and study of near-infrared (NIR)-absorbing dyes as well as their applications as safe, noninvasive imaging/contrasting probes. Thus, nowadays NIR dyes play a prominent role in many fields of medicinal chemistry and biotechnology, ranging from tomography^[36] through endoscopic imaging^[37] and tumor diagnostics^[38] to drug discovery^[39] and nucleic acid detection.^[40]

1.2 Designing a Zinc selective chemosensor

1.2.1 Zinc in biological systems

Zinc is only moderately abundant in nature ranking 23rd of the elements in periodic table. In the body it is observed that zinc is the second most abundant transition metal following iron. An adult human body almost contains 2-3 g of zinc.^[41-42]

In the body almost thousands of proteins contain zinc.^[43] The structure of approximately 200 enzymes containing zinc have been characterized up to now. Zinc proteins can be divided into several groups according to the role played by zinc within the proteins.^[44] In the catalytic group zinc is a direct

participant in the catalytic function of the enzyme. Enzymes in which zinc serves as a co-catalytic function, one or several zinc ions may be used for catalytic, regulatory, and structural functions. In addition there are a large number of transcription factors that utilize zinc, the so-called zinc fingers.^[45]

Considering the wide variety of metabolic functions requiring zinc, it is not surprising that any zinc deficiency or imbalanced zinc distribution within the body, organ, or cell, leads to a broad range of diseases. Some reported diseases about the neurological disorders of the zinc in brain are Alzheimer's disease^[46-48], amyotrophic lateral sclerosis (ALS)^[49], Parkinson's disease^[50], and epilepsy.^[51-52] Furthermore, zinc plays a crucial role in insulin secretion and apoptosis^[53].

Besides growth, numerous body functions are affected by zinc ions, including the immune, endocrine, and gastroenterological systems. The huge scope for the exploration of the diverse physiological roles of biological zinc demands sensitive and noninvasive techniques for real-time detection and imaging. The relative concentration of free Zn^{2+} within biological cells varies from 1 nM in the cytoplasm of many cells to 1 mM in the vesicles of presynaptic neurons in the human brain. Although the total concentration of zinc in a cell is relatively high, the concentration of free zinc, which is not strongly bound to proteins, is extremely low. Total cellular zinc can be relatively determined by standard analytical techniques such as AAS or ICP-MS however the estimation of free zinc has proved to be difficult with such kind of methods. This has led to emergence of the new type of molecular recognition these are the molecular sensors which can make the zinc cation visible even if it is trace amount.

1.2.2. Molecular sensor design for Zn (II)

There are many criteria for a fluorescent Zn(II) sensor that operates in biological samples. In biological systems zinc ion found in d^{10} electronic configuration, abbreviated as Zn^{2+} . The lack of d-d transition makes Zn^{2+} ion as a colorless cation. The Zn^{2+} ion is very stable and undergoes redox reactions only under extreme conditions excluding the occurrence of ligand-to-metal charge-transfer bands in its complexes. These effects render UV-Visible spectroscopy unsuitable for the detection of free or complexed Zn^{2+} . These concerns make it a top priority of chemists to develop selective and efficient probes or so-called chemosensors for zinc ions. There are some criteria for the selection of the chemosensor such as; It must be selective for Zn^{2+} over all other constituents in the biological media, including millimolar concentrations of Na^+ , K^+ , Ca^{2+} , and Mg^{2+} , and provide Zn^{2+} detection with spatial and temporal resolution. The probe affinity, measured by its dissociation constant (K_d), should approach the median concentration of Zn^{2+} in the sample for monitoring its flux. Other desirable characteristics include rapid and reversible Zn^{2+} coordination, excitation and emission wavelengths in the visible/near-IR/IR regions for single photon excitation, a bright ($\Phi \times \epsilon$) signal, water-solubility, nontoxicity, and photostability.

Many fluorescent sensor molecules that can selectively detect Zn^{2+} have been reported in the past three years. A fluorescent sensor molecule typically consists of a fluorophore and an appropriate switch, which can induce characteristic fluorescence changes by Zn^{2+} binding, either in fluorescence intensity, in the excitation or emission wavelength, or both.

The first reported selective fluorescent sensor molecule for Zn^{2+} was p-toluenesulfonamide quinoline (TSQ) ^[54]. Several TSQ derivatives were

synthesized to increase the water solubility. Among these derivatives, Zinquin can be used to monitor Zn^{2+} concentrations in living cells. Zinquin forms a 1:2 complex by Zn^{2+} addition. ^[55] It was evident earlier, however, that the Zn^{2+} -zinquin stability constants is apparently not large enough to permit interaction of Zinquin with extremely tightly bound ($K_d \ll 1$ nm) Zn^{2+} in metalloenzymes or zinc finger proteins.

So new strategies for the ionophore is of great current interest and a typical intracellular Zn^{2+} chelator *N,N,N,N*-tetrakis(2-pyridylmethyl)ethylenediamine (TPEN) ^[56], **1**, was reported as a novel chelator for Zinc ion in vivo and vitro studies, which apparently has a much higher affinity for Zn^{2+} , masked the Zn^{2+} -dependent fluorescence of Zinquin in lymphocyte cells. ^[53] Thus, it was quantitatively confirmed that TPEN with much higher affinities is a well-suited chelating unit for Zn^{2+} cation and moreover it is confirmed that Zinquins do not mobilize tightly bound Zn^{2+} from enzymes such as carbonic anhydrase.

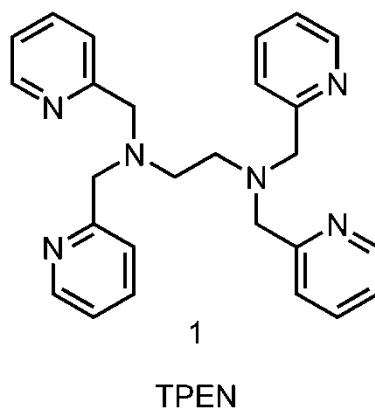


Figure 6 Structure of *N,N,N,N*-tetrakis(2-pyridylmethyl)ethylenediamine, **1**

With TPEN application as a chelator for zinc ion, ionophores which are specific to Zn^{2+} are limited to certain groups such as quinolines, bis(2-pyridylmethyl)amine (or di-2-picoylamine, DPA), linear and cyclic polyamines, and some bio-ligands such as zinc-finger domains. Among these ionophores, DPA^[57-58] is the most widely used ligand for Zn^{2+} binding.

There are many examples for Zn^{2+} sensors with different optical strategy. A fluorescent molecular probe may consist of a fluorophore attached to a chelating agent or an ionophore with or without a spacer group. Analyte binding to the ionophore will cause a change in absorption and emission spectra of the fluorophore, which leads to signal output (Figure 7). The mechanism of signal transduction through change in fluorescence occurs by a process such as charge transfer,^[59-60] electron transfer,^[61] energy transfer,^[62] excimer formation,^[63] or conformational change.^[64] Among these mechanisms, photoinduced electron transfer (PET) is widely used in chemosensor design as it significantly influences the fluorescence emission.

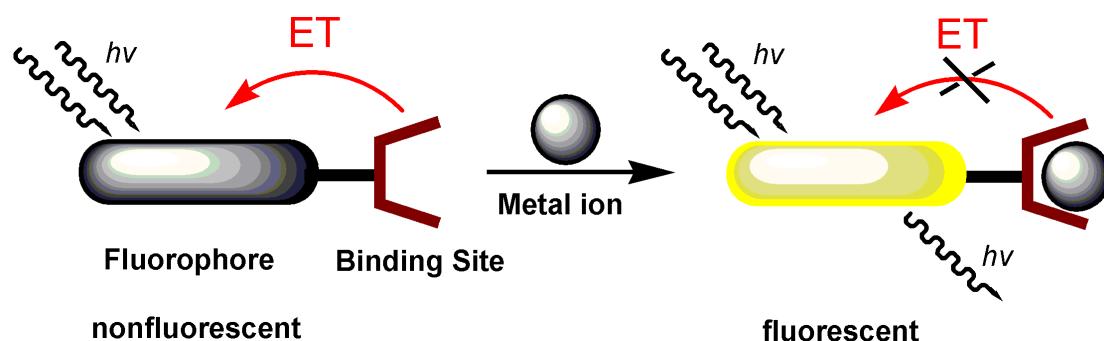


Figure 7 A schematic representation for PET process

The amine nitrogen atom of DPA is a good electron donor in the PET process. DPA-based sensor, **2**, is a typical PET sensor for protons and Zn^{2+} .^[65]

Upon binding of the metal ion, the electron-transfer process of the probe is interrupted, and the fluorescence quantum yield is increased.

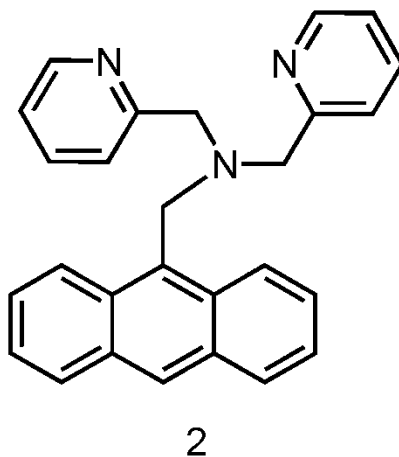


Figure 8 Structure of DPA-based anthracene dye, **2**

Fluorescent sensor molecules that are excited by visible light are advantageous over sensors with shorter wavelength excitation, because excitation at ultraviolet wavelengths can cause cell damage, and cellular autofluorescence can interfere with the measurement. Fluorescein is one of the most widely used fluorophores in biological experiments and is advantageous in that it has a high quantum yield of fluorescence in aqueous solution, and its excitation wavelength is in the visible range. Thus, fluorescein can be a favorable fluorophore for Zn^{2+} fluorescent sensor molecules and several such sensors have been reported in the past couple of years that can be used in biological applications.

Fluorescein derivatives **3** and **4** have the advantage of absorption in the visible region, which facilitates excitation at those frequencies. ^[66] Only the anionic form of fluorescein emits strongly, which means that the pK_a values are an important factor for the pH-dependent performance. Attachment of electron-

withdrawing groups renders better performance over a much-broader pH range. Newport Green DCF (**3**) and Newport Green DPX (**4**) are DPA-based sensors that show fluorescence enhancement upon binding to zinc.^[66]

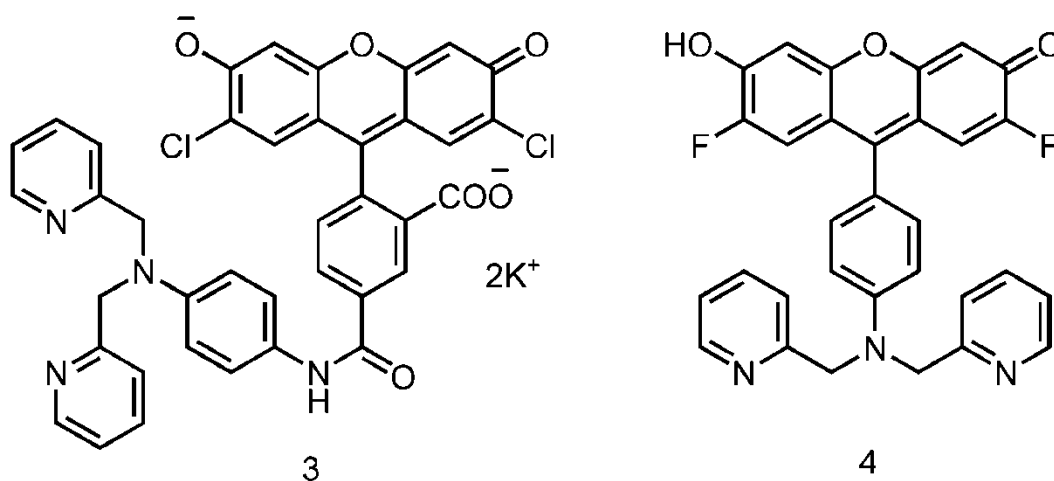


Figure 9 Structure of the fluorescein based chemosensors, **3**, **4**

Recently, other types of fluorescent probes have also been reported. One particularly interesting type is probes that enable ratiometric imaging. This is a technique that involves observing the changes in the ratio of fluorescence intensities at two wavelengths. Thus, a fluorescent ratiometric sensor responds to an analyte by a shift in its emission maximum, which may or may not be concomitant with the variation in intensity. This shift in the emission wavelength should be enough to distinguish the emission maximum of the coexisting free and bound Zn^{2+} species, thus allowing the determination of the ratio of emission maxima of two species. Together with the known binding constant of the sensor, the unknown zinc concentration can be determined.^[67]

Lim, Brückner, and co-workers reported the coumarin-derived ratiometric sensor for Zn^{2+} .^[68] The lactone oxygen atom of the coumarin moiety is a potential donor atom

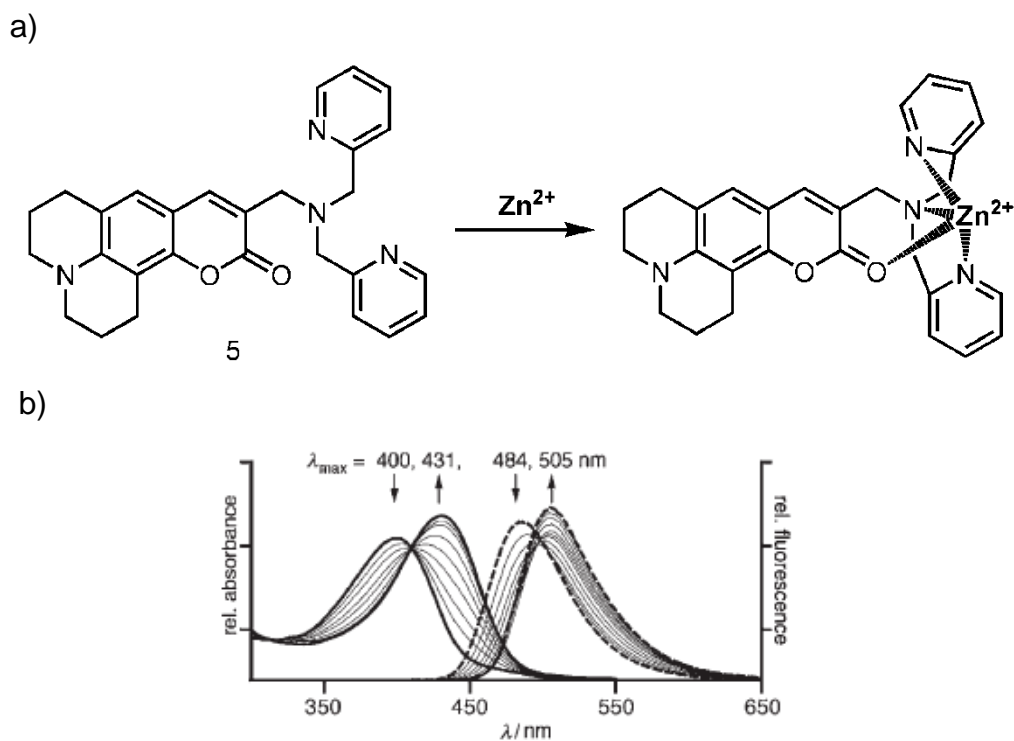


Figure 10 a) Structure of complexation of Zn^{2+} to coumarin-based chromophore. b) Uv-vis spectral titration (—) and fluorescence response (----) of compound 5, with Zn^{2+} .^[68]

and, hence, participates in chelation with Zn^{2+} , resulting in a change in the electronic properties of the chromophore. Although a range of metal ions can bind to the sensor, most lose out when in competition with Zn^{2+} , thus making a suitable probe for biological systems.

In another study, squaraine based dyes are represented as zinc cation sensitive fluorophore published by Akkaya and co-workers.^[69] Squaraine dyes are excellent chromophores for the design of molecular probes for biologically relevant cations and binds to Zn^{2+} to result in a three-state fluorescence response to a single input.

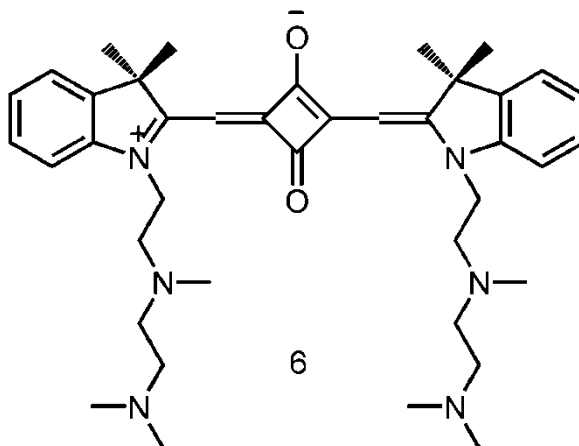


Figure 11 Structure of Zn^{2+} selective Squaraine dye, **6**.

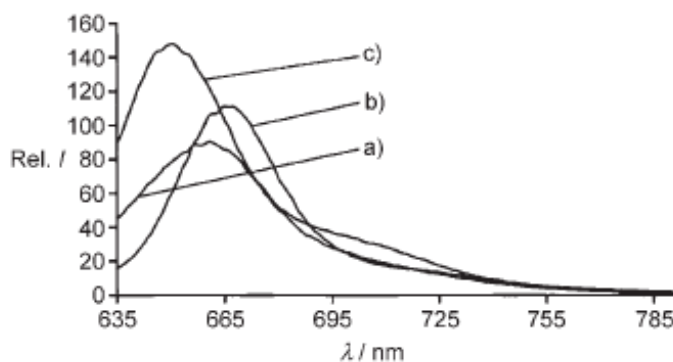
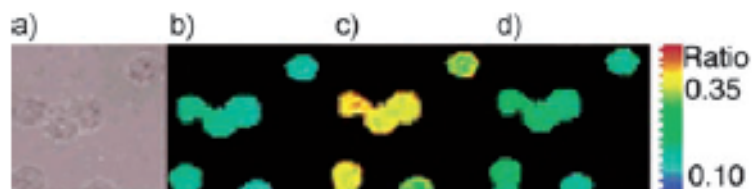


Figure 12 Changes in the emission spectrum of squaraine derivative **6** with increasing amounts of Zn^{2+} . a) $[Zn^{2+}]=0$; b) $[Zn^{2+}]=1.0 \mu M$, c) $[Zn^{2+}]=0.025 M$.^[69]

Maruyama et al. made use of the internal charge transfer (ICT) mechanism in electron-donating DPA conjugated to an electron-withdrawing benzofuran derivative in the design of ratiometric Zn²⁺ probes.^[70] The probes **7** (ZnAF-R1) and **8** (ZnAF-R2), Figure **13**, upon complexation with Zn²⁺, exhibited a blue shift in the excitation maxima, whereas the emission maxima remained unchanged. Sensor **8** is more soluble and has a better fluorescence quantum yield than **7** in water, thus making it useful for biological applications as illustrated by the fluorescence ratiometric imaging of Zn²⁺.

As mentioned before, NIR fluorescent probes have the advantages in vivo imaging, low absorptivity and following with the alive and undamaged cells is the one well-known property of these kind of dyes in biological application. In literature there are several NIR fluorescent probes reported and applied to biological studies. However, zinc sensitive NIR dyes are rare. One of the most used and well-known fluorescent NIR probe is cyanine dyes. Recently, Nagano and co-workers synthesized a series of carbocyanine dyes **9**, which are useful as ratiometric NIR probes for Zn²⁺.^[71] The dipicolylethylenediamine attached to the chromophore acts as the metal-ion chelator.

a)



b)

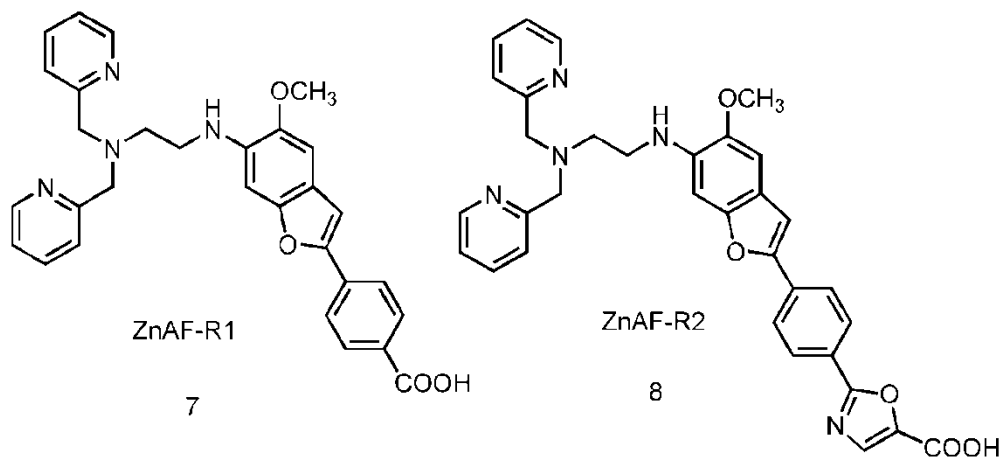


Figure 13 a) Fluorescence ratiometric images (340 nm/380 nm) of zinc in macrophages (RAW 264.7) labeled with ZnAF-R2 EE in PBS buffer, pH 7.4 a) Bright -field transmission image. b) Ratiometric image of a). c) Pyrithione (zincionophore; 15 μ M) and ZnSO₄ (150 μ M) were added to b). d) TPEN (400 μ M) was added 15 min after the addition of pyrithione. **b)** Structure of dyes **7**, **8**.^[70]

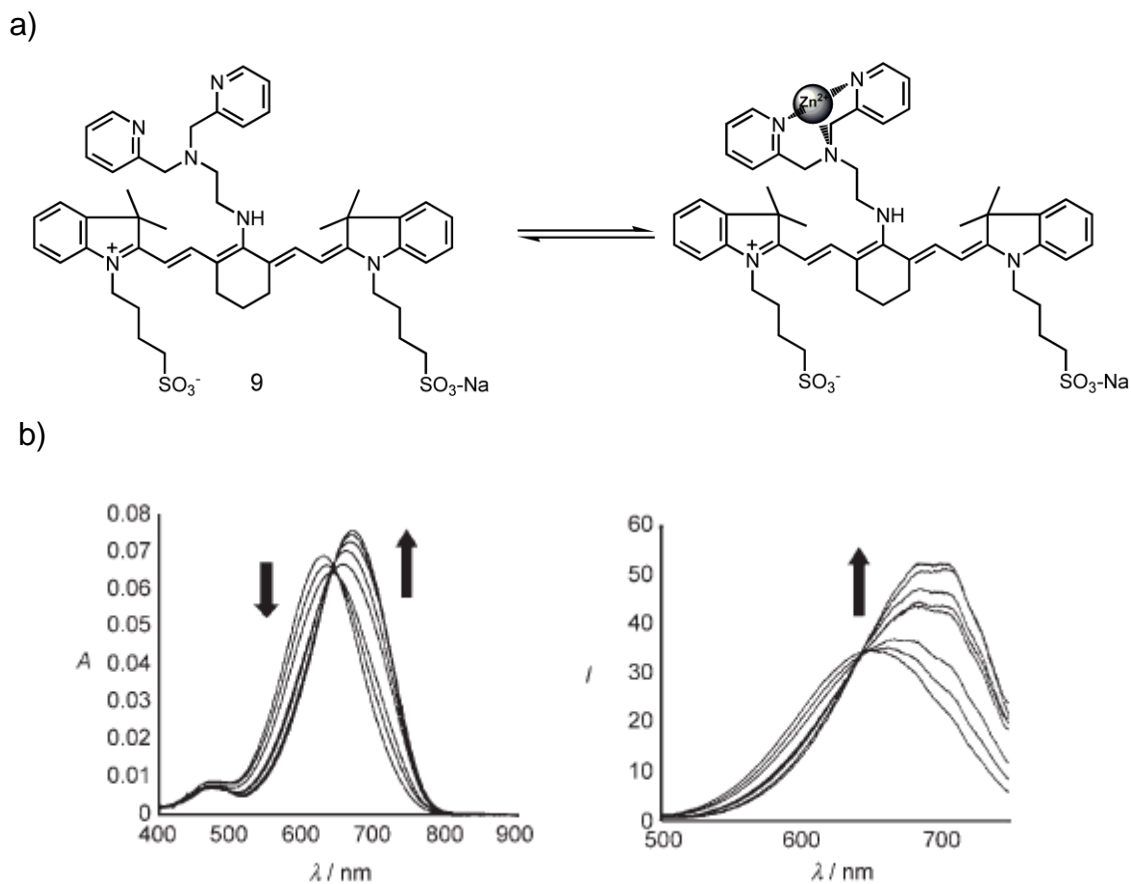


Figure 14 a) Structural representation of Zn^{2+} complexation with dye, **9**. b) Absorption, excitation spectra of compound **9** ($1 \mu\text{M}$) at various Zn^{2+} concentrations (in 100 mM HEPES buffer, pH 7.4).^[72]

The molecule has a high extinction coefficient ($7.0 \times 10^4 \text{ m}^{-1} \text{ cm}^{-1}$) and a large Stokes' shift.^[71] Upon binding to Zn^{2+} , the electron-donating ability of the amine to the chromophore decreases, and the color of the solution changes from blue to teal (dark greenish-blue) owing due to 1:1 complexation (Figure 14b).

1.3 Hg(II) selective Chemosensors and Importance of mercury selection

1.3.1 Hg(II) in Nature and Human Life

Mercury pollution is a global problem and a major source of human exposure stems from contaminated natural waters.^[72-74] Inorganic mercury, Hg(0) and Hg(II), is released into the environment through a variety of anthropogenic and natural sources. Industrial sources of mercury include coal and gold mining, solid waste incineration, wood pulping, fossil fuel combustion, and chemical manufacturing.^[75-78]

Emitted elementary mercury vapors are easily transported in the atmosphere, often across continents and oceans, and are eventually oxidized to Hg(II). Atmospheric deposition of Hg(II) results in its accumulation on plants, in topsoil, and in waters. Irrespective of the source and initial site of deposition, Hg(II) ultimately enters freshwater and marine ecosystems. A fraction of this Hg(II) is reduced to Hg(0) by microorganisms, including algae and cyanobacteria, and is subsequently released back to the atmosphere.^[79] Another portion of the Hg(II) accumulates in underwater sediments. Some prokaryotes that live in these sediments convert this inorganic mercury to methylmercury, which we define as any CH₃HgX species, as do bacteria that reside in fish gills and gut. In addition to this acknowledged source, some ecological studies point to the occurrence of abiotic mercury methylation under certain environmental conditions, but more work is needed to evaluate this hypothesis.^[80] Because methylmercury is lipophilic, readily absorbed, and

poorly excreted, it enters the food chain and biomagnifies in higher organisms, especially in the muscles of large predatory fish, including tuna, swordfish, and whales, and is subsequently ingested by humans.^[81.85]

Although often overlooked, at least in the chemical literature, mercury bioaccumulation also occurs in plants, which provides additional routes of entry into the food web.^[86] Mosses take up Hg(II) from atmospheric deposition and tree leaves are another Hg(II) repository. Mercury reduces photosynthesis and transpiration in plants, the former of which may impact the global carbon cycle. The bioaccumulated mercury reenters soils and natural water following plant decay or is consumed by birds and mammals, and thereby further enters the food chain. Additional sources of human exposure to mercury include the household^[87] and workplace,^[88] religious practices,^[89-90] dental amalgams,^[91-93] and vaccines.^[94-95]

The biological targets and toxicity profile of mercury depend on its chemical composition.^[96-97] Methylmercurials, the species of greatest concern, are readily absorbed by the human GI (gastrointestinal tract), cross the blood-brain barrier, and target the central nervous system. In the absence of accidental poisoning, the only known source of human exposure to methylmercury is through seafood consumption. Many acute poisonings occurred in Minamata, Japan (1950–1960s) following the release of mercury into the Agano River; the subsequent case studies provided a significant portion of our knowledge about methylmercury intoxication.^[98-101] Another noteworthy epidemic occurred in Iraq after methylmercury tainted seed grain was used for bread.^[102-103] Neurological problems associated with methylmercury intoxication are manifold and include prenatal brain damage, cognitive and motion disorders, vision and hearing loss, and death. The ramifications of long-term and low-level exposure to methylmercury are less clear and warrant thorough toxicological investigations. This mode of exposure is currently of particular

concern for human embryos, the developing fetus, and children.^[104-107] At the molecular and cellular levels, methylmercury causes oxidative stress and lipid peroxidation,^[108] and it inhibits the division and migration of neurons. It accumulates in astrocytes, preventing glutamate uptake, and thereby causes excitotoxic injury to neurons.^[109] Inorganic mercury targets the renal epithelial cells of the kidney, causing tubular necrosis and proteinuria.^[110-111] It is also a neurotoxin and causes immune system dysfunction. The global cycling of mercury and consequential human health risks present the scientific community with some important tasks, which include the development of safer manufacturing practices, performance of more detailed toxicological studies, and implementation of environmental remediation. Efforts directed toward the design and implementation of new mercury detection tools will ultimately aid these endeavors.

1.3.2 Employing Chromophores for Mercury Detection

Commercial quantitative mercury detection is done with many analytical techniques that includes atomic absorption spectroscopy, cold vapor atomic fluorescence spectrometry, and gas chromatography. Most of these methods are very complicated and time consuming analysis for mercury. Moreover, in many of these techniques multistep sample preparation is needed. Recent years, to avoid these kind of problems to detect mercury, liquid chromatography capillary electrophoresis is introduced as an alternative technique for monitoring both inorganic mercury and organomercurials.

The instrumental techniques discussed above often give a knowledge about Hg concentration in mercury containing material. However they are not

useful for quick detection in vivo studies of biological analysis. Mercury responsive ligands with some ionophores are developed as an alternative analytical techniques. The use of mercury-responsive small-molecule ligands that provide immediate optical feedback can overcome such limitations because their use does not require sophisticated instrumentation or sample preparation.

Mercury(II) ion has closed d^{10} configuration so it has no optical spectroscopic signature which limits the methods for its detection. Optical methods, such as changes in fluorescence in solution shifting in absorption wavelength, are indisputable well-suited way for mercury detection in either biological or environmental studies.

There are a few considerations that could influence the design of the mercury detection ligands. The well-known criteria for any of the metal are selectivity. Thus, the probe firstly designed as for only mercury selective over all other components in environmental and biological sample, including thiols, organic acids, alkali and alkaline earth metal ions, and various transition metal ions. For fluorescence detection of Hg(II), enhancement (“turn-on”) is preferable to fluorescence quenching (“turn-off”) because it lessens the chance of false positives and is more amenable to multiplexing, the simultaneous use of several detectors that uniquely respond to different analytes. Because Hg(II) is a heavy metal ion that can quench fluorescence by several mechanisms, ^[112-117] achieving turn-on detection can be a significant challenge. Ratiometric sensing offers several additional advantages. ^[118] In this approach, a change in absorption or emission with analyte binding is monitored at two wavelengths. Ratiometric sensing is less prone to artifacts and is superior for studies of inhomogeneous samples. It can also facilitate analyte quantification.

The affinity and selectivity can both be tuned through modifications of the Hg(II) binding unit. In this regard, principles of Hg(II) coordination chemistry should be considered in selecting a Hg(II) responsive moiety for incorporation

into the probe. Because of its $5d^{10}6s^2$ electronic configuration and lack of ligand field stabilization energy, Hg(II) can accommodate a range of coordination numbers and geometries. Two-coordinate linear and four coordinate tetrahedral species are common. Hg(II) is a soft acid and the use of soft donor atoms, including thiols and thioethers, in a chelating unit will generally increase its affinity and selectivity for Hg(II). Mechanisms commonly invoked to explain the response of optical sensors to Hg(II) are electron transfer (ET) and charge transfer (CT). These general categories include photoinduced electron transfer (PET) and internal charge transfer (ICT). Fluorescence quenching by Hg(II) is often attributed to electron transfer and, more generally, the heavy atom effect.

1.3.3 Designed fluorophore with Fluorescence turn-off mechanism for Hg(II) detection

In literature there are rare fluorescence quenching chemosensors and these compounds are classified as depending on their solubilities in appropriate solvents, soluble in organic or in aqueous media. Several azacrown ethers linked to 4,4'-bis(dimethylamino) biphenyl receptors was reported, **10–12**, provide fluorescence turn-off for the optical detection of mercury ion in MeCN ($\lambda_{\text{ex}}=270$ nm; $\lambda_{\text{em}}= 370$ nm).^[119] These ionophores have low selectivity for Hg(II) because other divalent metal ions, including Ni(II), Zn(II) and Cd(II), also cause fluorescence turn-off. Furthermore, fluorescence enhancement is observed for **10** in the presence of Pb(II) ($\lambda_{\text{em}} \sim 420$ nm) and **12** provides turn-on Cu(II) detection in MeCN ($\lambda_{\text{em}} = 525$ nm). As a result, these macrocycles are not well-suited for Hg(II) detection in any complicated mixture.

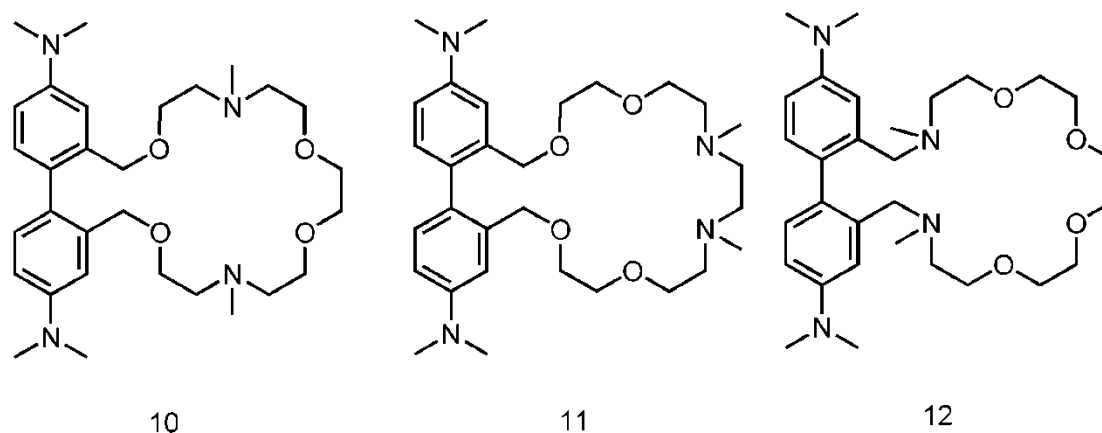


Figure 15 Organic soluble turn-off fluorescent chemosensors for Hg^{2+} cation

In another study, turn-off strategy for Hg(II) detection in visible region was recognized with a novel binding site which is dithia-dioxa-monoaza crown binding unit was linked to a phenoxazinone scaffold. ^[119] Compound **13** has a quantum yield of 0.08, which decreases to 0.04 following addition of Hg(II) . A shifting occurs from 634 to 615 nm also which is the evidence of the blue-shift in wavelength with Hg(II) coordination. Solution studies indicate 1:1 coordination, a dissociation constant for Hg(II) of $0.83 \mu\text{M}$, reversibility, and a lower detection limit of 100 nM. relative to most other binding unit considered thus far for Hg(II) detection sensitivity is greater for this chelating group. In conclusion the fluorescence response of this sensor is exclusively Hg(II) -specific.

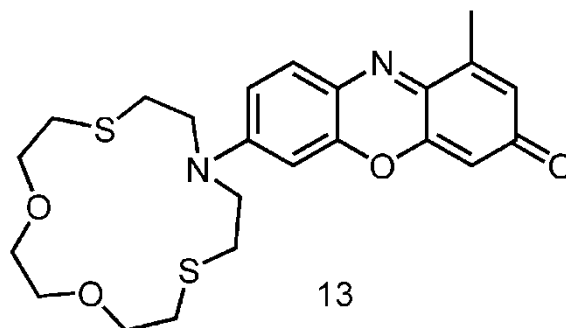


Figure 16 Structure of Hg^{2+} selective dye designed with a turn-off strategy, **13**

1.3.4 Turn-On strategy for $\text{Hg}(\text{II})$ detection

The design of sensors that give fluorescent enhancement (FE) upon $\text{Hg}(\text{II})$ binding is a particular challenge because, like many other heavy metals, $\text{Hg}(\text{II})$ often causes fluorescent quenching via enhanced spin-orbit coupling associated with the heavy atom effect, which will facilitate the intersystem crossing process.^[120-124]

Thus, design and development of new strategies for mercury selective fluorescent chemosensor is considered by the scientists. As a result of this topic, a novel optical study is conceived for mercury detection, turn-on strategy, it is flourish and current focus in last decades.

Nitrobenzoxadiazolyl (NBO), naphthalimide, boron dipyrromethene (BODIPY), and anthraquinone based chromophores with macrocyclic chelates have been used for turn-on $\text{Hg}(\text{II})$ detection in the appropriate solvent (Figure 17).^[125-129]

Compound **14** ($\Phi_{\text{free}} = 0.034$, $\lambda_{\text{ex}} = 476$ nm, $\lambda_{\text{em}} = 539$ nm) exhibits fluorescence enhancement following Hg(II) addition in MeOH, but few other details regarding its photophysical properties and Hg(II) selectivity are documented.^[125] The macrocyclic chelates in **15-16** contain multiple thioether components, which help to provide selectivity and high affinity for soft metal ions such as Hg(II). Both sensors **15** and **16** are example for fluorescence turn-on strategies following Hg(II) coordination in MeCN.^[130-131]

Sensor **15** contains a naphthalimide acceptor linked to the 3-position of a 1,3,5-trisubstituted Δ^2 -pyrazoline ring with an anilino NS₄ crown donor in the 5-position (Figure 17).^[127] It exhibits a low fluorescence in the absence of Hg(II) ($\Phi = 0.007$) and has a emission wavelength in the NIR region ($\lambda_{\text{em}} = 680$ nm). Electron transfer of the fluorophore is blocked with the coordination of Hg(II) to macrocycle binding unit. A 13-nm blue-shift in the wavelength of maximum emission and a 20-fold enhancement in quantum yield following Hg(II) addition occur. Sensor **15** also responds to Ag(I) with a 15-fold enhancement in quantum efficiency.

In another study, BODIPY fluorophore was investigated as a fluorescent sensor in which anilino thiaazacrown donor chelate is receptor.^[128] The BODIPY chromophore, as illustrated in the foregoing chapter, has high extinction coefficient and large quantum yield resulting in bright emission, relative to most other chromophores considered thus far. In the absence of metal ion, BODIPY fluorophore **16** shows a very low quantum yield of 1×10^{-4} in MeCN ($\lambda_{\text{em}} = 509$ nm). Addition of Hg(II) cause a two-nm red-shift in the wavelength of maximum emission and a dramatic 5900-fold enhancement in quantum yield. Titration studies indicate 1:1 stoichiometry for Hg(II) complexation. Detection of Hg(II) in ppb level is possible with this highly bright fluorophore. Fluorescence

enhancement also observed following addition of Cu(II) (2500-fold) and Ag(I) (2200-fold) to **16** in MeCN and these metal ions can also be detected at ppb levels.

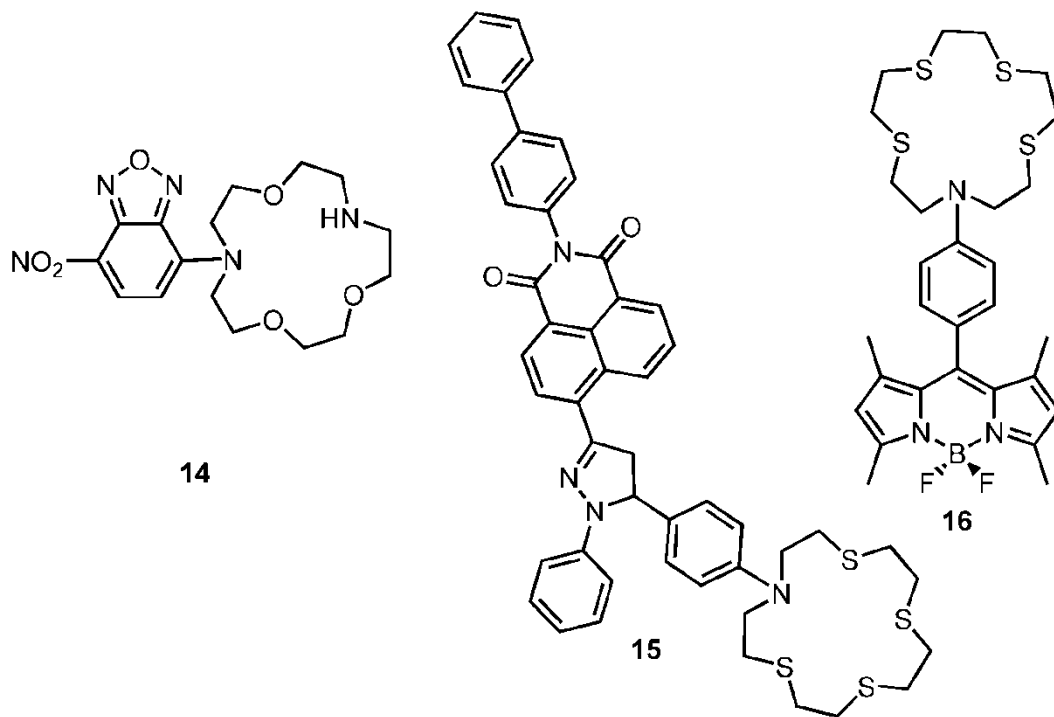


Figure 17 Structure of compounds **14**, **15**, **16**.

1.3.5 Ratiometric Fluorescence Sensors For Hg (II)

Up to now, intensity based Hg(II) probes relying on fluorescence turn-off or turn-on following Hg(II) recognition were desired. Ratiometric fluorescence monitoring is an alternative approach and also considerable challenge for Hg(II) sensing. As mentioned before, this optical approach involves a comparison of fluorescence intensities at two different wavelengths before and after analyte recognition. Although only a few examples of ratiometric Hg(II) detectors have been documented,^[132–140] this technique is gaining attention in the mercury sensing community and provides an opportunity for further studies.

In a recently reported study, anthracene, **17**, is linked with two dithiocarbamate ligands and a ratiometric monitoring study was provided with this desired fluorophore following Hg(II) recognition in 1:1 MeCN/H₂O and 1:1 EtOH/H₂O.^[141] A characteristic anthracene emission spectrum is exhibited, two sharp maxima at ~390 and ~410 nm and a broad emission band centered at 525 nm attributed to charge transfer between the dithiocarbamate and anthracene moieties. A decrease in emission intensity is observed with addition of Hg(II) to **17** which illustrates the ceasing of charge transfer. Incidentally some fluorescence enhancement at ~390 and ~410 nm also occurs. This probe also replies to some fluorescence change following addition of Zn(II) and Cd(II). Substitution of the triethylamine moieties with morpholine cuts the ratiometric response because only quenching of the charge transfer band is observed upon Hg(II) addition.

In another research, a BODIPY chromophore in which chelating substituent is dithiadioxaza macrocycles, **18**, was illustrated for the ratiometric detection of Hg(II) by both fluorescence and color changes.^[142] Emission intensity of compound BODIPY is weak ($\Phi_{\text{free}} = 0.04$, $\lambda_{\text{em}} = 668$ nm) in 30:70

THF/H₂O (20 mM HEPES, pH 7.2) because macrocyclic nitrogen atom is quenching the BODIPY excited state which results in PET process.^[142] A slight decrease in the emission at 668 nm and a remarkable increase at 578 nm is observed with coordination of Hg(II) to dithiadioxaza functionalized binding site ($\Phi_{\text{Hg}} = 0.33$) (Figure 19). The I_{578}/I_{668} ratio increases ~30-fold with addition of 20 equiv of Hg(II).^[142] Addition of Mg(II), Fe(III), Co(II), Ni(II), Cu(II), Zn(II), Cd(II), Pb(II), Ag(I), or Al(III) to BODIPY 95 results in negligible fluorescence change. Job plots indicate formation of a 1:2 **18**:Hg(II) complex, where one Hg(II) binds to each macrocycle, with K_d values of 23 and 34 μM . Both PET and ICT were invoked to rationalize the fluorescence response of **18** to Hg(II). Donor nitrogen atom of the macrocycle causes an ICT to the BODIPY chromophore and thus red-shifted emission of **18** relative to unfunctionalized BODIPY occurs. Introduction of Hg(II) to the macrocyclic nitrogen atom decreases its electron-donating ability and frustrate ICT, which results in a hypsochromic shift of the emission band.^[142] In addition, Hg(II) complexation to **18** decreases PET quenching of the BODIPY excited-state by the nitrogen lone pair electrons, which causes the fluorescence enhancement (Figure 19). Meanwhile fluorophore **18** also provides colorimetric ratiometric Hg(II) detection.

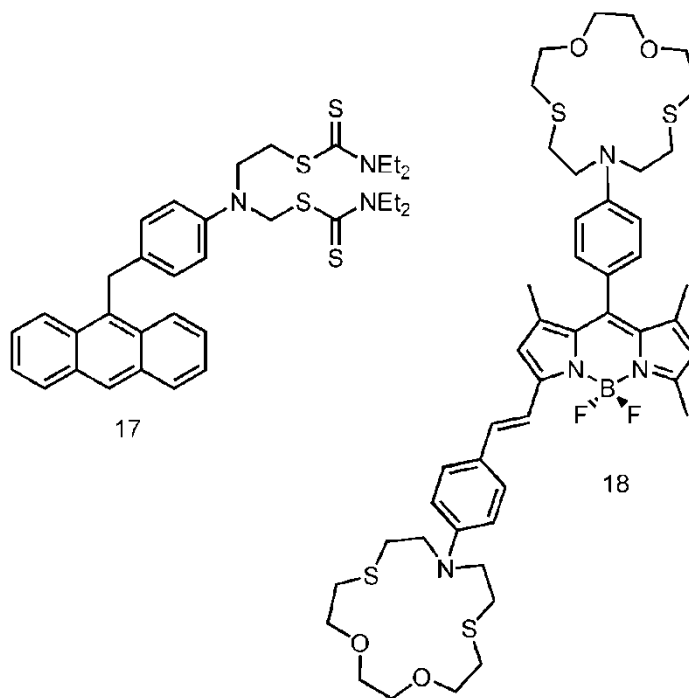


Figure 18 Structure of the compounds based on Ratiometric fluorescence sensing for Hg^{2+} , **17**, **18**.

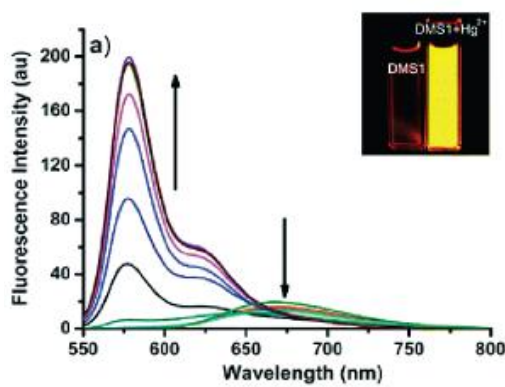
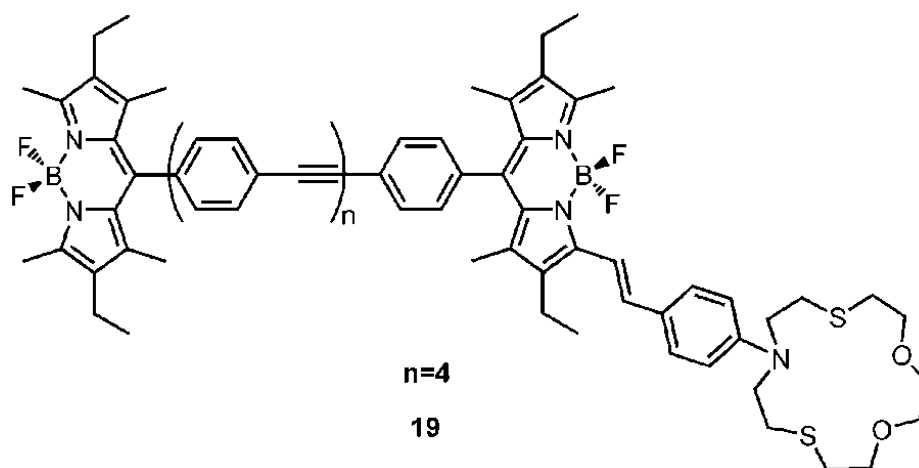


Figure 19 Ratiometric fluorescence response of 2 μM **18** to 0-40 μM $\text{Hg}(\text{II})$ in 30:70 THF/ H_2O (20 μM HEPES, Ph 7.2). Excitation was provided at 540 nm. ^[142]

There are some requirements to design a ratiometric chemosensor, one of the most important criteria is, to catch a relation between the magnitude of the range of signal ratios of emission intensities at two different wavelengths for the analyte-free and analyte-bound chemosensor. The dynamic range and the sensitivity of the chemosensor to the analyte concentration are determined with the help of this parameter.^[143]

In a study, Akkaya and Coskun introduced a new strategy in ratiometric chemosensor design. In this study they demonstrated a chemosensor in which energy transfer process is achieved with BODIPY fluorophore units and also the variation of EET is exhibited with adjusting the interchromophoric distance between the donor BODIPY fluorophore and acceptor BODIPY fluorophore. Metal binding to the designed chemosensor always causes a blue shift in the absorption spectrum and also this shift lies behind an increase in the energy transfer between the acceptor and donor fluorophore. In order to obtain a remarkable and selective cation binding dithiaazacrown-substituted is chosen as a binding unit for Hg(II) cation. The emission response of **19** to Hg(II) ions is shown in Figure 20. Clearly, Hg(II) binding (K_d in THF was determined to be 4.5×10^{-7} M) causes a spectral shift in the absorbance of the longer wavelength dye, due to increased spectral overlap between the energy donor and the acceptor, which enhances the emission peak was observed.^[144]

a)



b)

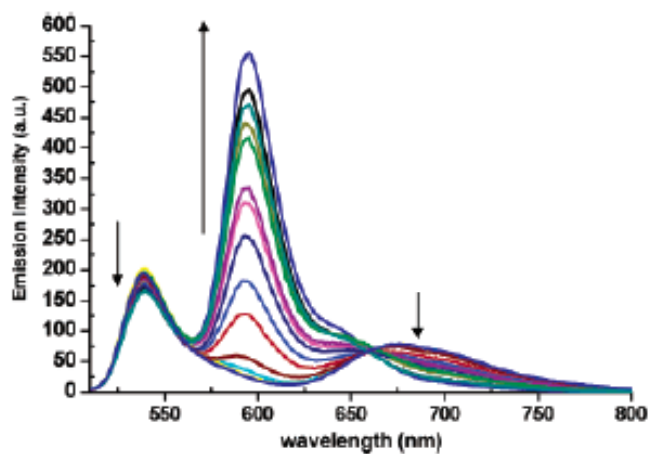


Figure 20 a) Structure of the compound **19**. **b)** The emission response of the dye **19** in THF (1.0 μM) to an increasing concentration (0-25 μM) of Hg(II) ions. A small decrease in the intensity at 540 nm is indicative of larger EET.

1.4 BODIPY

Although known for almost a century, in the area of biology, chemistry and physics, the importance of fluorescence dyes is increasing with time. Recent developments in these arena have also boosted interest in the development of new emissive dyes. Among the large variety of known fluorescent dyes, 4,4-difluoro-4-bora-3a-aza-4a-aza-s-indacene (abbreviated as BODIPY) is the most functional and versatile dye. thus, BODIPY dye gained great popularity by the chemists, biochemists and physicists in the last two decades. The first member of this class of compound was reported by Treibs and Kreuzer in 1968. Thousands of fluorescent probes are known but it is observed that until the end of the 1980s little attention was given to this dye. Then, the potential use of this dye for biological labeling was recognized^[145] and several new Bodipy-based dyes were designed and indeed commercialized for biological labeling. As a consequence, Bodipy came to be known to the biochemist and biologist as a photostable substitute for fluorescein, and the number of papers and patents started to escalate in the mid 1990s.

1.4.1 The nomenclature of BODIPY

The nomenclature of the Bodipy dye is not as expected as IUPAC numbering system, so this leads to some confusion when it is encoded as the dipyrromethenes core. However, The terms β - α positions, and *meso*- are used in just the same way for both systems.

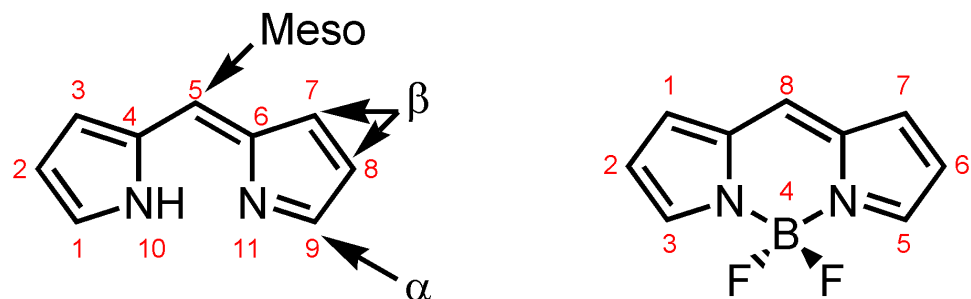


Figure 21 Structural representation of numbering of BODIPY core

1.4.2 The fundamental properties of BODIPY

BODIPY dyes were first discovered in 1968 by Treibs and Kreuzer.^[146] BODIPY **20**, which has no substituents, has not been reported in the literature. This may be because of synthetic difficulties obtaining this compound related to the fact that none of the pyrrole-based carbons are blocked from electrophilic attack. Synthesis of the corresponding dipyrromethene precursor has been reported, but this compound is unstable and decomposes above -30 to -40 °C.^[147] The symmetrical, dimethyl-substituted compound **21** has been prepared^[148] and could be considered as a reference to which other simple alkylated BODIPYs can be compared. The symmetrically substituted systems **22** and **23** have apparently not been reported, reflecting synthetic limitations for even some simple BODIPY systems. However, the unsymmetrically substituted BODIPYs **24** and **25** have been prepared. There are relatively minor differences in the reported absorption maxima, fluorescence emission maxima, and quantum yields of these compounds, and these should not be over-interpreted

because small calibration errors are common in these types of experiments. However, when the symmetrically-, tetra-, hexa-, and hepta-alkylated systems **24**, **25**, and **26** are included in the comparison, then an unambiguous trend toward red-shifted absorption and emission maxima with increased substitution becomes apparent. Alkylation or arylation at the *meso* position has no special effect on the absorption and emission wavelengths (compare **21** with **30**, and **29** with **31**) even though this substitution position is structurally unique. However, the quantum yield of the *meso*-phenyl compound **28** is appreciably less than the more substituted analogue **29**. Such differences are widely attributed to 1,7-substituents preventing free rotation of the phenyl group reducing loss of energy from the excited states via non-irradiative molecular motions. Consistent with this, introduction of *ortho*-substituents on the phenyl ring has been observed to increase quantum yields, and similar explanations have been invoked.

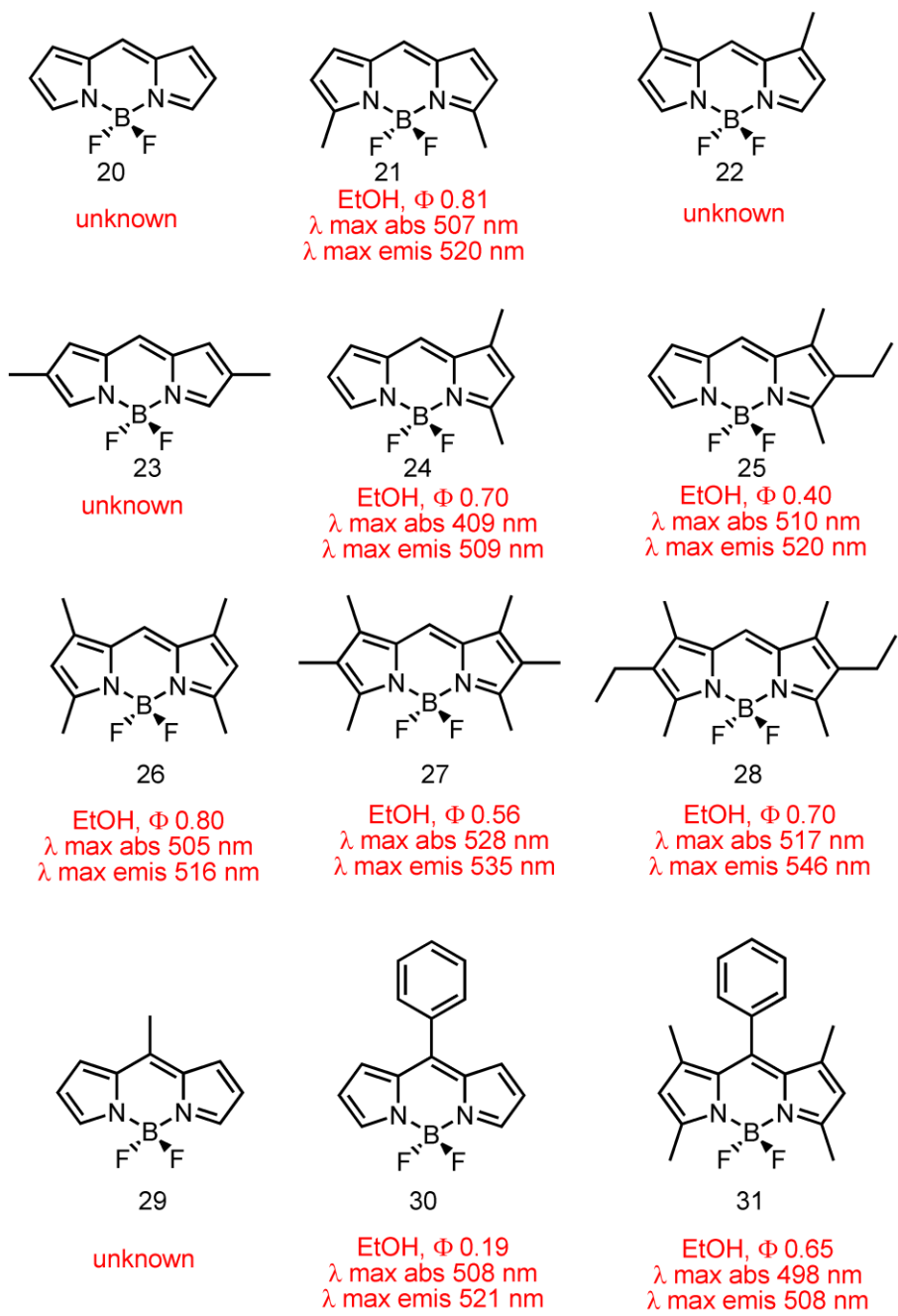


Figure 22 BODIPY cores

1.4.3 Synthesis of BODIPY

The synthesis of BODIPY core is arising mainly from the pyrrole condensation reaction which is also used for the originally synthesis of the porphyrin. BODIPY core is mainly obtained in three units, two pyrrole unit is attached to each other with a methene bridge. A highly electrophilic carbonyl compound such as aldehyde, acyl chloride or acid anhydride, is used to form the methene bridge. This synthetic procedure continues with the addition of a tert-amine such as Et_3N , and $\text{BF}_3 \cdot \text{OEt}_2$.

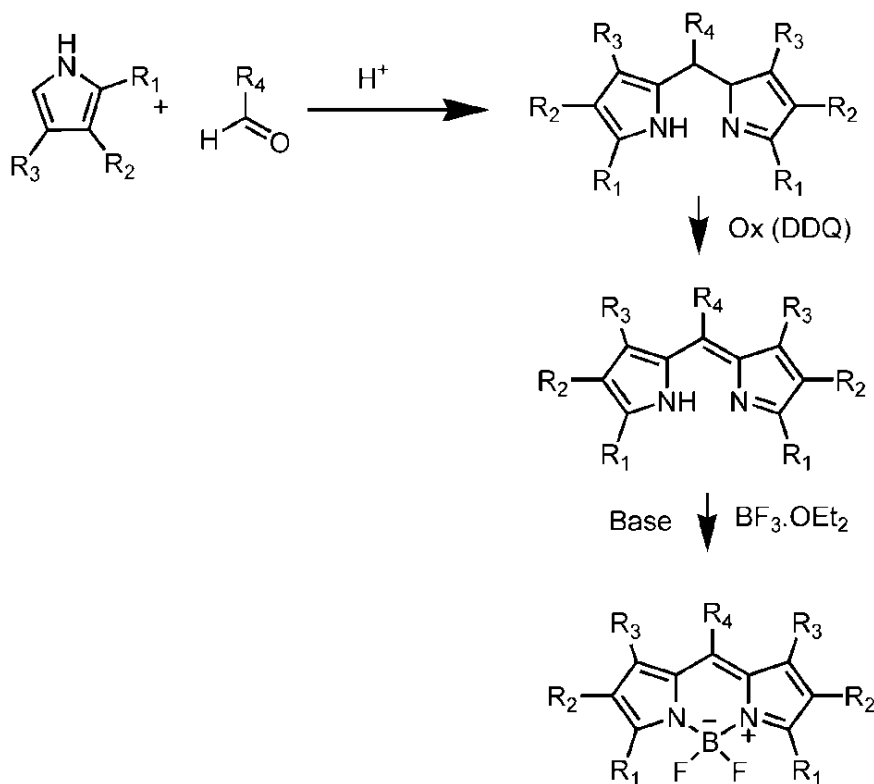


Figure 23 Synthetic pathway for BODIPY

1.4.4 The chemistry of BODIPY

1.4.4.1 Electrophilic Substitution

Treibs and Kreuzer first realized that BODIPY dyes which are free of substituents at the 2,6-positions readily undergo electrophilic substitution reactions in the presence of chlorosulfonic acid.^[146] This high level of reactivity was exploited later by Boyer and co-workers to synthesize water-soluble analogues.^[149] Other electrophiles can be introduced with the same way, thereby providing a facile route to the isolation of Bodipy dyes bearing bromine^[150] or iodine groups^[151] that are then available for further synthetic modification.

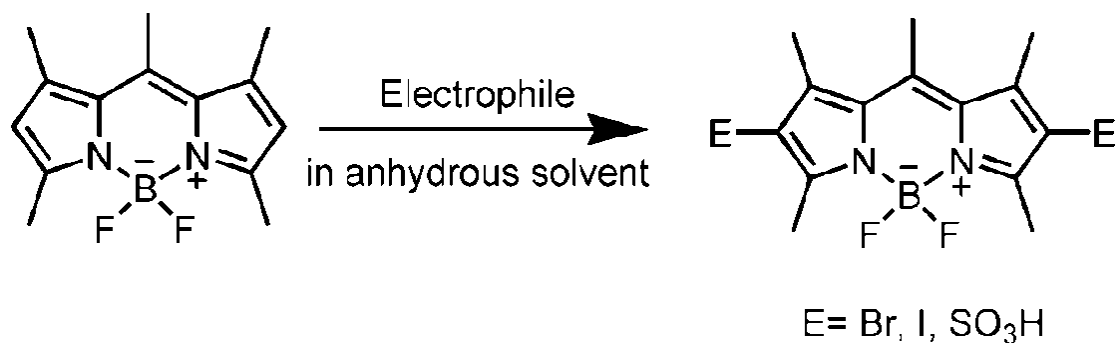


Figure 24 General procedure for electrophilic substitution reaction on BODIPY core

1.4.4.2 Active Methyl Groups (Knoevenagel reaction)

Methyl groups on BODIPY core at the 3,5- positions are suitable position for the modification of the dye because of their nucleophilic character. These methyl groups can be deprotonated under basic conditions. The resultant intermediates will readily add to an aromatic aldehyde, thereby generating a styryl group (Figure 25).^[152] This synthetic procedure has been used to extend the degree of π -electron conjugation and has the effect of introducing a pronounced bathochromic shift to both absorption and fluorescence spectral maxima.

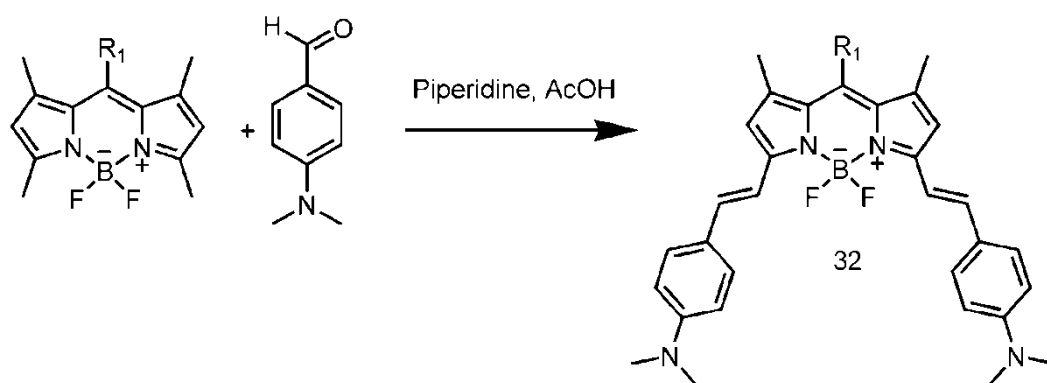


Figure 25 Modification of BODIPY core on 3, 5 positions.

1.4.5 Optical Properties

One of the features of BODIPY dyes is that it is possible to easily modify their molecular backbone, which provides further opportunities to vary their optical properties and to provide recognition sites for a variety of analytes. These dyes have sharp bands in the absorption spectra (half-widths typically being around 25–35 nm), large molar absorption coefficients (typically being in the region of 40000 to 110 000m⁻¹ cm⁻¹), high fluorescence quantum yields (normally between 60 and 90%), reasonably long excited singlet-state lifetimes (these being around 1 to 10 ns), excellent chemical and photochemical stability in both solution and solid states, and versatile charge-transfer properties. The good solubility of these dyes in most common solvents (excluding water) should also be noted.

1.4.5.1 Photoinduced electron transfer on BODIPY core

Modifications to meso-substituted aromatic compound on the BODIPY can acts as an electron donor or an electron acceptor depending on their oxidation potential relative to the excited state of the BODIPY core. In these systematic approach several dyes based on BODIPY core have been sensitized for many different applications.

If electron transfer occurs fluorescence is diminished, in this situation fluorescent group acting as an electron acceptor, this is called as reductive PET or a-PET (“a” for acceptor). However, if the energy states are such that the

excited-state of the fluorescent group can donate electrons to the substituents LUMO, then oxidative-PET, d-PET, occurs (“d” for donor).

Both events are accompanied by a quenching of the fluorophore emission. There are many examples of the first type, in many instances the fluorescence is “turned off” in the absence of the analyte (e.g., cation). When the analyte is added, PET is inhibited and a large enhancement of fluorescence is observed (“off-on” switch). In recent years, Nagano and co-workers applied reductive PET to a BODIPY core. In this work the low fluorescence of the diamine was explained in terms of reductive PET. When nitric oxide converts the diamine into the benzotriazole **33**, then reductive PET does *not* occur and fluorescence is observed. Figure 26 illustrates the synthesis of the probe and the oxidized product.

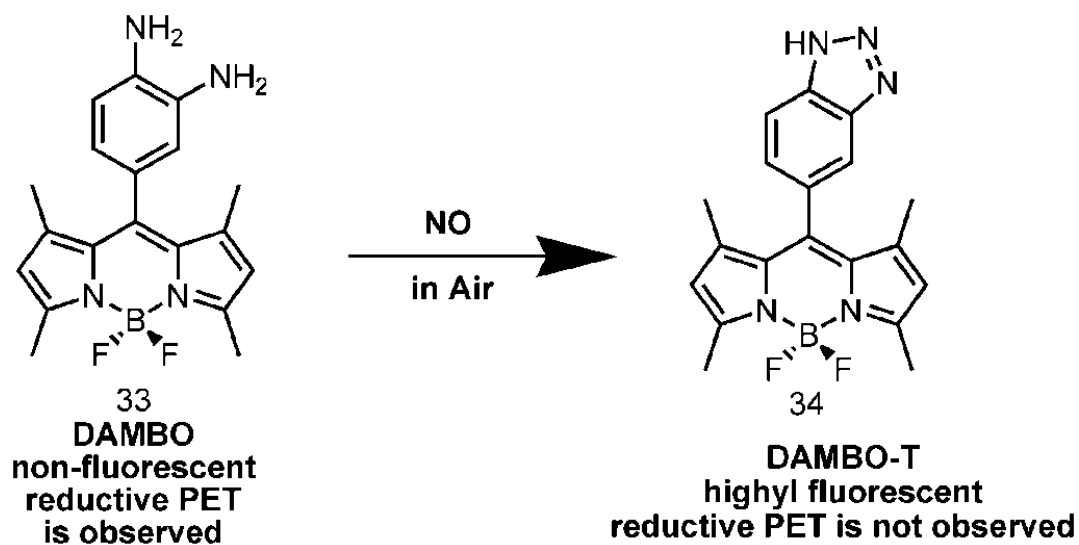


Figure 26 Formation of reductive PET with oxidation of diamine to triazole on BODIPY core

Although, oxidative PET is well-known but rarely utilized in sensing applications, Akkaya and co-workers showed that oxidative PET^[153] is also applicable to the well-known BODIPY core like their novel strategies in other application. In this study bipyridyl-fluorophore conjugation was supplied. The binding of the cation quenches the fluorescence of the receptor-fluorophore. Quenching is most likely caused by the favorable energetics of the electron transfer to the LUMO of the bipyridyl-metal complex, since the metal binding to the bipyridyl moiety lowers both HOMO and LUMO energy levels of the ligand, compared to the metal-free state. They showed that addition of Zn²⁺ causes remarkable quenching on the fluorophore, **35**, and also they claim that oxidative PET appears to be a viable alternative to the reductive PET in developing novel fluorescent chemosensors for ions and small molecules.

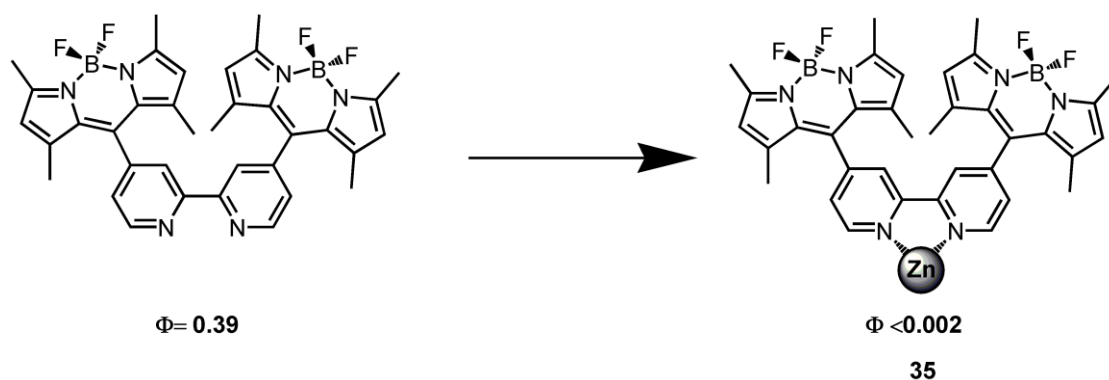


Figure 27 Coordination of Zn²⁺ to ionophore core causes oxidative PET

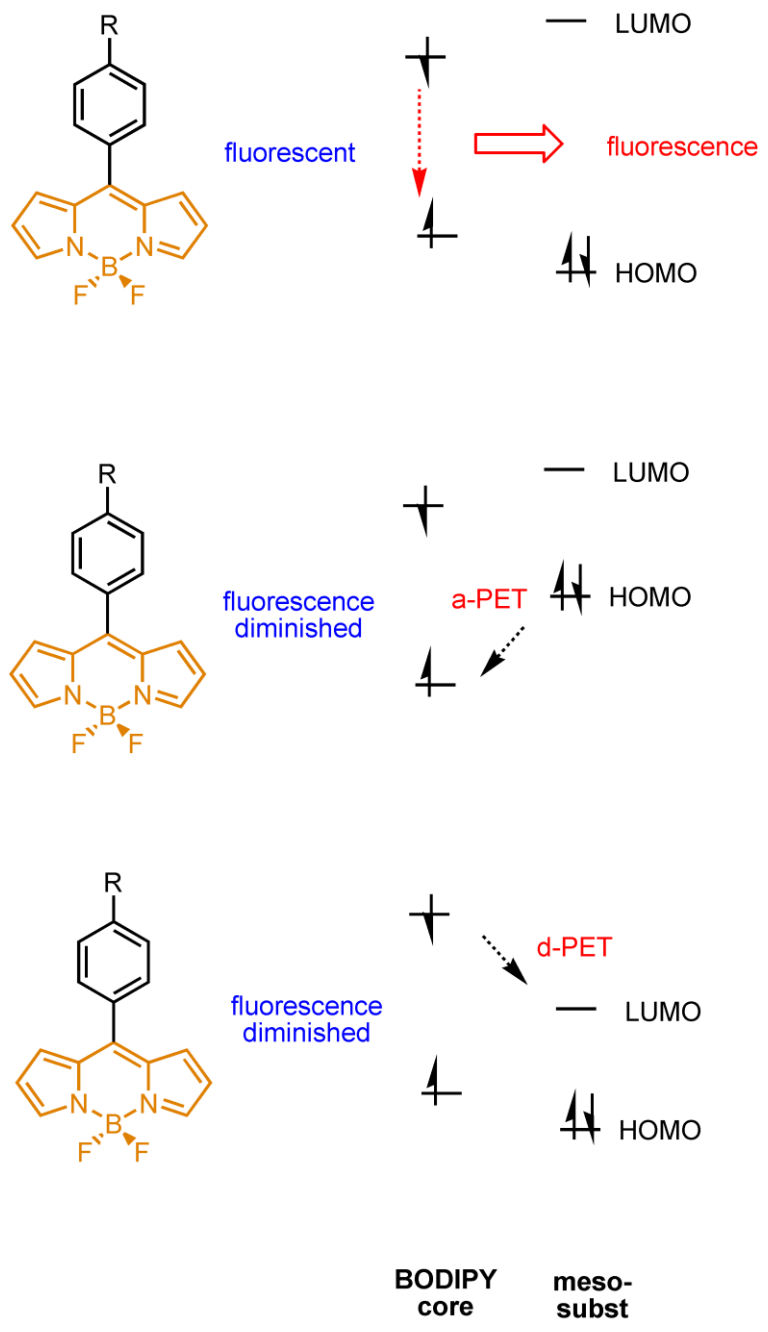


Figure 28 Molecular orbital representation of a-PET and d-PET on BODIPY core

1.4.5.2 ICT on BODIPY core

The internal charge transfer (ICT) mechanism^[154] has been widely exploited for ions sensing,^[155] molecular switching,^[156] and fluorescent labeling^[157] due to the advantages of spectral shifts and quantitative detection. When a fluorophore contains an electron-donating group (often an amino group) conjugated to an electron-withdrawing group, it undergoes intramolecular charge transfer (ICT) from the donor to the acceptor upon excitation by light. The consequence of the ICT is a red shifted emission. Many fluoroionophores have been designed by employing the interaction of cations with the electron donating group. After being bound to a cation, the electron donating group loses its donating ability, so the ICT ceases and a blue shift appears, which is often used for the fluorescent ratiometric determination of the cations. Fluorescence quantum yields always change in the processes. In a study, Peng and co-workers synthesized a fluorophore in which boradiazaindacene (BODIPY) was chosen as the fluorophore because it absorbs and emits in the visible region with high quantum yield, large extinction coefficient, and good photostability^[158] and *N,N*-bis(pyridin-2-ylmethyl)benzenamine as Cd²⁺ receptor, **36**, (and ICT donor). A vinyl group between the receptor and the BODIPY fluorophore can induce longer wavelengths in absorption and fluorescence spectra modification of methyl groups at 3, 5 position on the BODIPY core create the desired red shifted emission on the fluorophore as mentioned. In the literature there are so many example for ICT modulated BODIPY by Akkaya and Rurack. So any modification on these part of the core can also be precursor of the new type of the dyes for different applications.

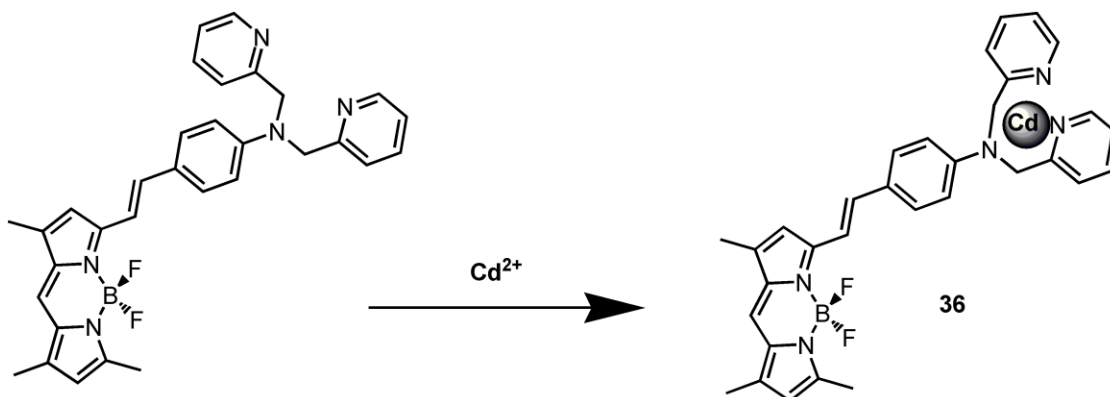


Figure 29 BODIPY based fluorophore designed with the advantages of the strategy of ICT process for cation analysis.

1.4.5.3 Both ICT and PET mechanism on the same BODIPY core

As mentioned before, there are really interesting examples for application in literature for BODIPY dye (it is obviously versatile fluorophore). One of them was published by Akkaya and co-workers.^[156] They designed a BODIPY, **37**, based fluorophore in which both ICT and PET mechanisms are operational within a single BODIPY core to form an example in logic-gate subjected fluorophore arena. In this study, they demonstrated that a single molecule with very large differentials of emission intensity, can carry out an arithmetic operation (subtraction) at the molecular level.

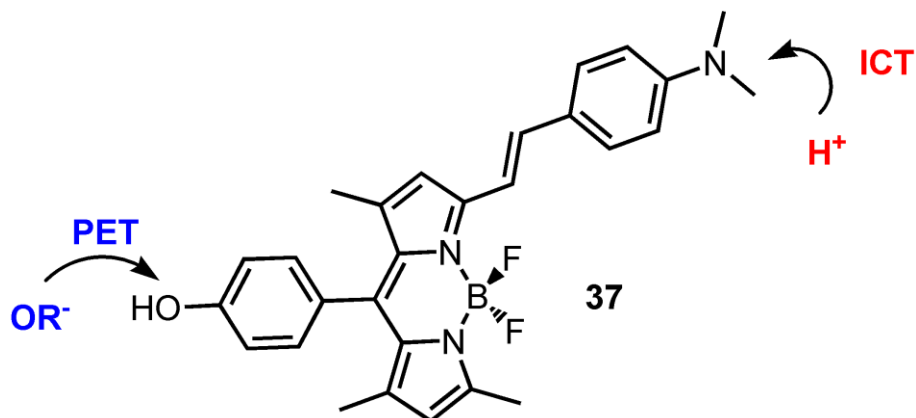


Figure 30 Representation of ICT and PET on BODIPY core

In another study, BODIPY was designed as a cation sensor, published by Yuliang *et.al.* ^[142] They achieved the synthesis of a fluorophore, **38**, comprise BODIPY as a fluorophore center and a crown ether which has specific recognize ability to Hg^{2+} cation. In this work they mentioned that their strategy takes advantage of both PET and ICT processes on a single molecule. There are two binding sites one decoupled from the BODIPY chromophore and the one conjugated to the BODIPY system.

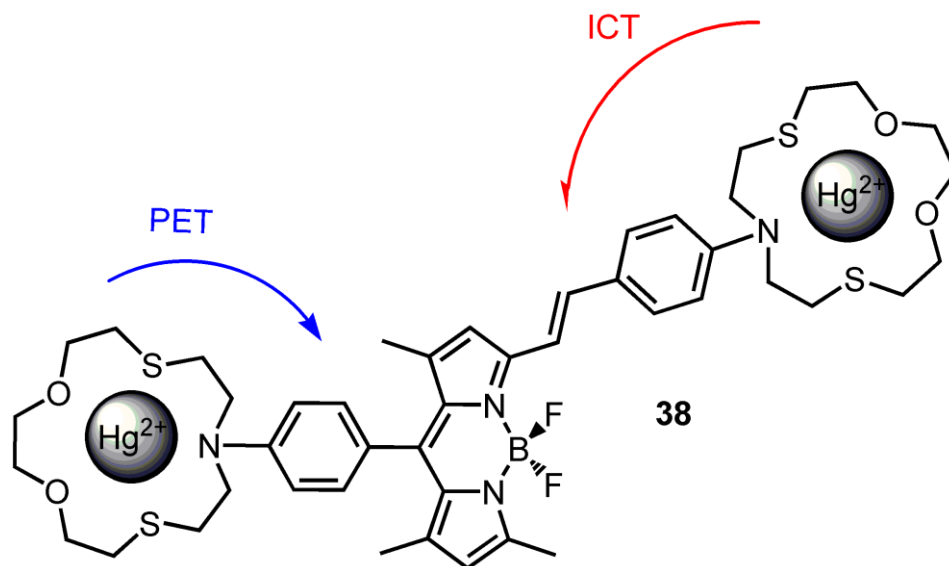


Figure 31 BODIPY, as a cation sensor, with two coordination site with strategies ICT and PET.

1.4.5.4 FRET (Fluorescence resonance energy transfer) on BODIPY core

A common problem found with organic dyes is that the Stokes' shift is too small for optimum use in flow cytometry and fluorescence microscopy. To circumvent this problem a strategy is developed, in this mechanism two fluorescent entities is joined in the same molecule to give a "cassette". One of these, the *donor*, may collect radiation efficiently at the excitation wavelength and pass this energy to the second fluorescent moiety that emits it at a longer wavelength. If the mechanism of energy transfer is through space, then this

system might be called a throughspace energy transfer cassette. Through-space energy transfer cassettes are typically used to artificially enhance the Stokes' shift of a probe. Through-space energy transfer efficiencies depend on several factors, including (i) spectral overlap of the donor emission with the acceptor absorbance, (ii) distance between the donor and the acceptor, (iii) the orientation factors, and (iv) the effectiveness of alternative de-excitation modes. As the BODIPY dye is suitable for many applications, with their high quantum yields (typically 0.6-1.0) and large extinction coefficients ($60\,000$ - $80\,000\text{ M}^{-1}\text{ cm}^{-1}$) properties it is shown that these dyes are also applicable to this kind of studies. In one study of Akkaya, they draw attention to this point and a dendritic light harvesting system was introduced to literature in which four BODIPY donors and a perylene-3,4,9,10-tetracarboxylic diimide (PDI) acceptor was constructed via click chemistry.^[159] Its UV spectrum is equal to the sum of the donor and acceptor components indicating they are not electronically perturbing each other. The extinction coefficients of dye at 526 nm (BODIPY, λ_{max}) and 582 nm (PDI, λ_{max}) are $240\,000$ and $45\,000\text{ M}^{-1}\text{ cm}^{-1}$, respectively; hence, the donor absorption is huge simply because four BODIPY units are involved.^[159] No green fluorescence emission from BODIPY was observed upon excitation at 526 nm, indicating efficient energy transfer (99%). On the basis of the energy transfer efficiency, the authors of this work calculated a Förster critical radius of 47 Å.^[159] In this work they showed that antenna effect is remarkable and comparable with the best cases.

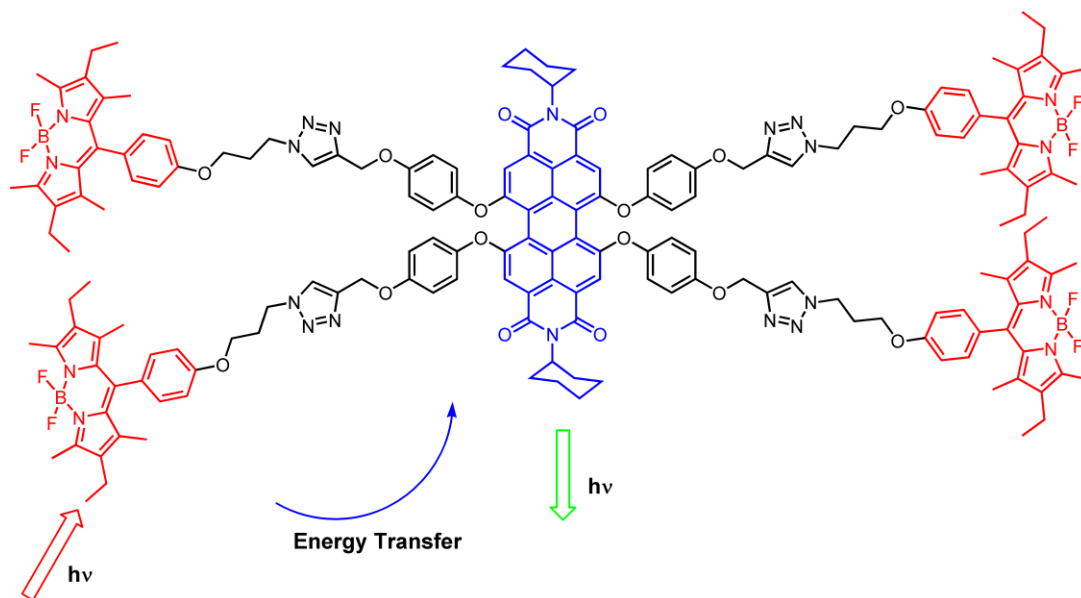


Figure 32 Structure of cassette where an FRET is observed from BODIPYs to PDI core

1.4.5.5 NEAR-IR BODIPY Dyes

As mentioned before 3- and 5-methyl BODIPY-substituents are acidic enough to participate in Knoevenagel reactions. Thus, styryl-BODIPY derivatives can be obtained by condensation of 3,5-dimethyl- BODIPYs with aromatic aldehydes. Several different approaches are created that shift the emission wavelength of the BODIPY-based fluorophore towards lower energy. A relatively facile method involves extending the degree of π conjugation running through the central core. For example, distyryl- boradiazaindacenes have been prepared from the corresponding 3,5-dimethyl derivatives and the resulting dyes show pronounced charge-transfer character, with much reduced fluorescence

quantum yields in polar solvents. ^[160] Water-soluble dyes, **39**, were subsequently obtained by functionalization with oligo(ethyleneglycol) residues in Akkaya laboratory. ^[35] These latter materials show good permeability into intact biological cells and tumor-targeting characteristics that make them interesting candidates for sensitizers in photodynamic therapy and in many strategies about the modification of the BODIPY they showed that there is no limitations for the straightforward functionalization of the BODIPY dyes through Knoevenagel reactions of the moderately acidic methyl substituents It is evident that appropriate functionalization of the distryl-BODIPY dyes, **40** and **41**, would yield near-IR emitting fluorescent probes for pH and other ions simply by judicious selection of the reacting aldehyde and thus the styryl substituent.

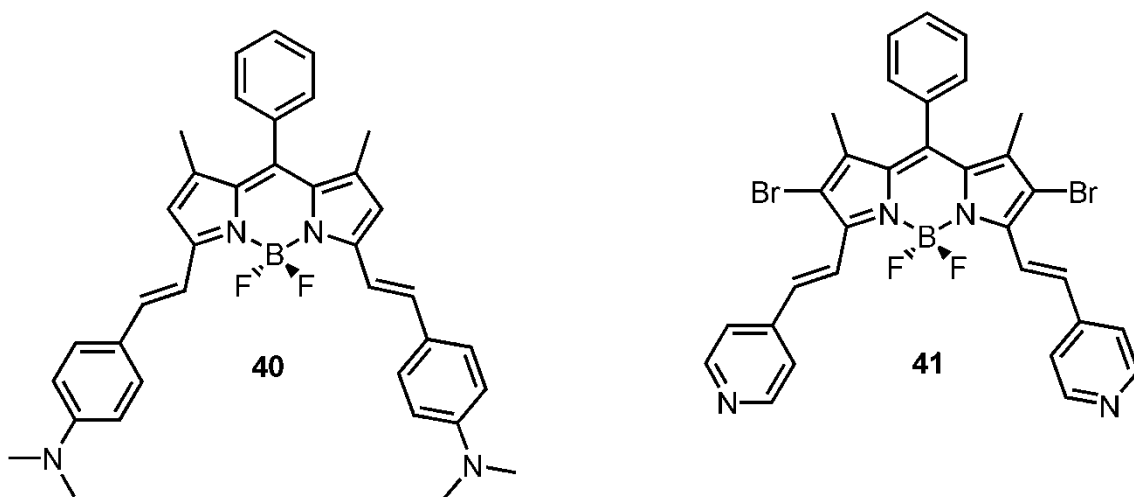
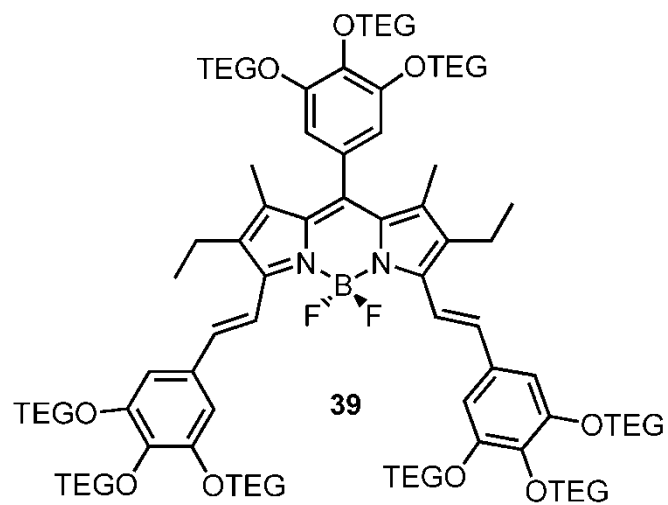


Figure 33 BODIPY based Near-IR dyes

CHAPTER 2

EXPERIMENTAL

All chemicals and solvents purchased from Aldrich were used without further purification. ^1H NMR and ^{13}C NMR spectra were recorded using a Bruker DPX-400 in CDCl_3 or DMSO-D_6 with TMS as internal reference. Absorption spectrometry was performed using a Varian spectrophotometer. Steady state fluorescence measurements were conducted using a Varian Eclipse spectrofluorometer. Column chromatography of all products was performed using Merck Silica Gel 60 (particle size: 0.040–0.063 mm, 230–400 mesh ASTM). Reactions were monitored by thin layer chromatography using fluorescent coated aluminum sheets. Solvents used for spectroscopy experiments were spectrophotometric grade. Mass spectrometry measurements were done at the Ohio State University Mass Spectrometry and Proteomics Facility, Columbus, Ohio, U.S.A.

2.1 Synthesis of Zn (II) selective Chemosensor

2.1.1 Synthesis of ethyl 3, 4, 5-trihydroxybenzoate (43)

3, 4, 5- trihydroxy benzoic acid (5.00 g, 29.4 mmol), **42**, was dissolved in 30 mL EtOH. 1 mL of 96% H₂SO₄ was carefully added in 10 min and the reaction mixture was refluxed overnight. The crude product was chromatographed on silica gel and eluted with chloroform-isopropanol 7:3 (v/v) to yield 3.20 g solid compound 10. Yield was 55%. Without further purification **43** was used through next step.

¹H NMR (CDCl₃): δ (ppm) 6.95 (s, 2H, Ar-H), 4.20 (q, 2H, *J*=7.0 Hz, -CH₂), 1.25 (t, 3H, *J*=7.0 Hz, CH₃).

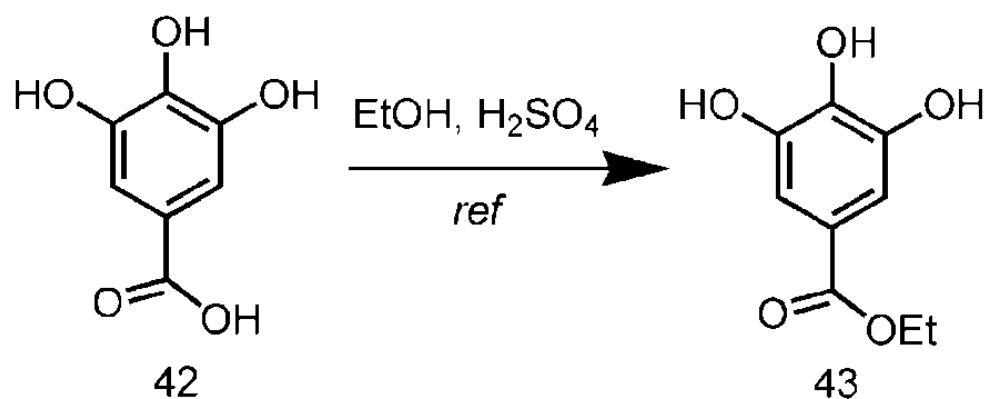


Figure 34 The synthesis of ethyl 3,4,5-trihydroxybenzoate

2.1.2 Synthesis of triethylene glycol methyl ether tosylate

Triethylene methyl ether, **44**, (3.00 g, 15.0 mmol) and 5 mL of Et₃N was dissolved in 150 mL of CH₂Cl₂. In a dropwise manner TosCl (3.20 g, 15.0 mmol) was added to the mixture. The reaction was completed after mixing one day at room temperature. The desired product was then collected with column chromatography in which the eluent was CHCl₃ to yield 3.32 g **45** in a liquid form. Yield 81%.^[161]

¹H NMR (CDCl₃): δ (ppm) 7.55 (d, 2H, *J* = 8.0 Hz, Ar-H), 7.15 (d, 2H, *J* = 8.0 Hz, Ar-H), 4.00 (m, 2H, CH₂), 3.60-3.30 (m, 10H), 3.20 (s, 3H, CH₃), 2.30 (s, 3H, CH₃).

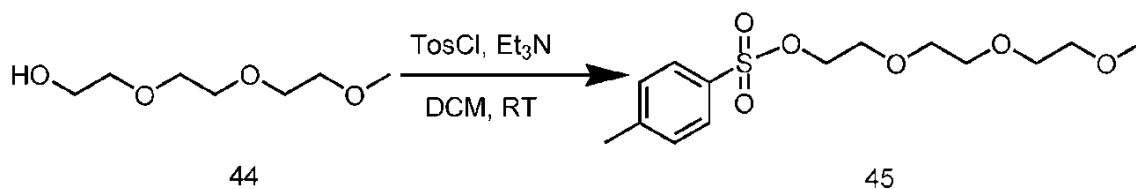


Figure 35 The synthesis of compound **45**

2.1.3 Synthesis of compound 46

A suspension of **43** (3.00 g, 15.0 mmol), **45** (12.4 g, 45.0 mmol), K_2CO_3 (8.10 g, 45.0 mmol) and catalyt amount of 18-crown-6 in 200 ml acetone was refluxed overnight. Acetone was removed by evaporation, and the residue was redissolved in $CHCl_3$ and extracted with distilled water three times. The organic phase was taken and solvent was removed by evaporation. The expected product was taken without any further purification as brown oil (8.50 g, 92%).
 1H NMR ($CDCl_3$): δ (ppm) 7.20 (s, 2H, Ar-H), 4.40- 3.10 (m, 45 H), 2.30 (q, 2H, $J=7.0$ Hz, $-CH_2$), 1.30 (t, 3H, $J=7.0$ Hz, CH_3).

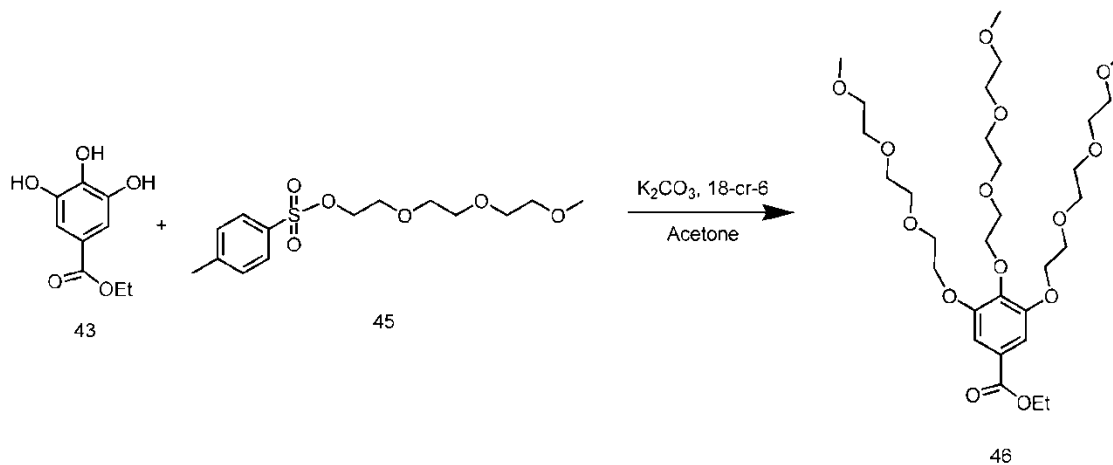


Figure 36 Synthesis of the compound **46**

2.1.4 Synthesis of the compound 47

An excess amount of 2.0 g LiAlH_4 was dissolved in dry 20 ml of THF and **44** (8.00 g, 12.5 mmol) was added to the reaction mixture in a dropwise manner in 30 min. After reaction was completed which was monitored with TLC the excess amount of LiAlH_4 was killed with cold water. The crude reaction was filtered and washed with methanol. The solvent then was removed by evaporation and **47** was taken as an only product. (7.40 g, 100%)

$^1\text{H NMR}$ (CDCl_3): δ (ppm) 7.30 (s, 1H, -OH), 6.60 (s, 2H, Ar-H), 4.55 (s, 2H, - CH_2), 4.30- 3.30 (m, 45H).

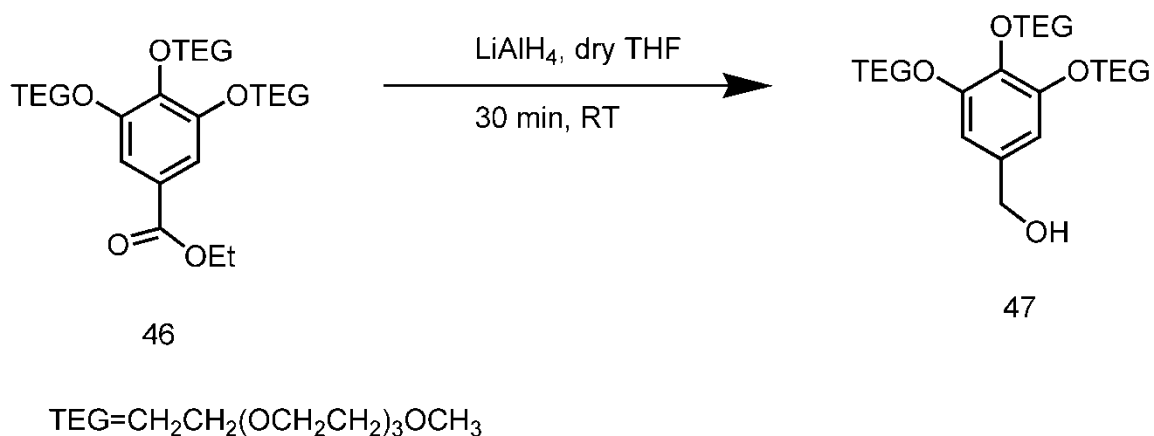


Figure 37 Synthesis of compound **47**

2.1.5 Synthesis of compound 48

Compound **47** (7.00 g, 11.8 mmol) and excess amount of pyridinium chloro chromate (PCC) (5.00 g) were dissolved in CH₂Cl₂. The reaction was monitored by TLC and when complete consumption of **47** was seen the reaction was completed. Crude reaction was extracted with basic aqueous solution one times, then three times with acidic aqueous solution. The organic phase was collected and solvent removed by evaporation. **48** was taken as only product after workup steps (6.90 g, 100%)

¹H NMR (400 MHz, CDCl₃): δ (ppm) 9.80 (s, 1H), 7.10 (s, 2H, Ar-H), 4.30- 3.30 (m, 45H)

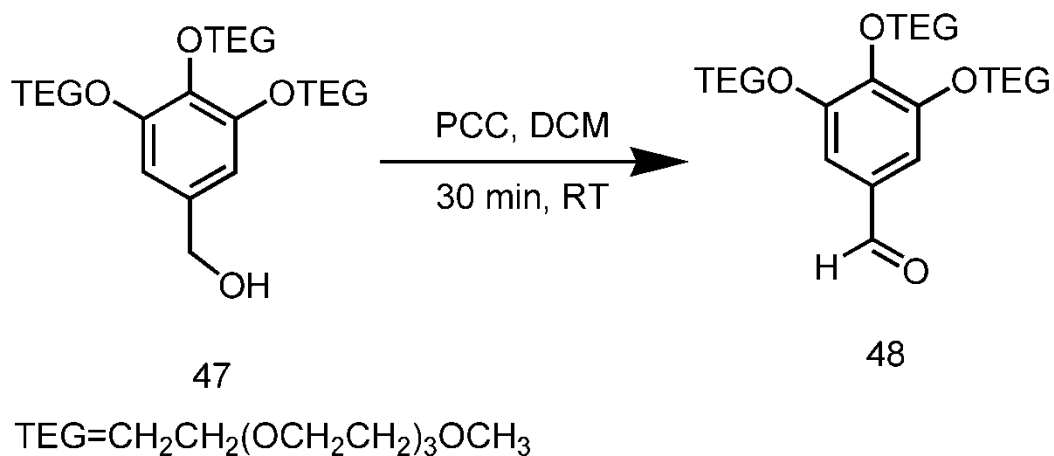


Figure 38 Synthesis of the compound **48**

2.1.6 4,4-difluoro-8-[3,4,5-tris(2-(2 (2methoxyethoxy) ethoxy) ethoxy)]benzaldehyde-2,6-diethyl-1,3,5tetramethyl -4-bora-3a,4a-diaza-s-indacene (50)

3,4,5-tris(2-(2-(2-methoxyethoxy)ethoxy)ethoxy)benzaldehyde (**48**) (0.34 mmol, 200 mg) and 2,4-dimethyl-3-ethyl pyrrole (**49**) (0.68 mmol, 84.0 mg) were dissolved in CH₂Cl₂ (250 mL) purged with argon in a 100 mL flask. 1 drop of TFA was added and the mixture was stirred at room temperature for 3 hrs. When TLC showed consumption of the aldehyde was complete, a solution of 166 mg (0.68 mmol) of DDQ (Tetrachloro-1,4-benzoquinone) in CH₂Cl₂ was added. After 3 h, Et₃N (3 ml) and BF₃.OEt₂ (3 ml) were added. Immediately after the addition of BF₃.OEt₂ bright yellow fluorescence was observed. Crude product washed three times with water, dried over Na₂SO₄ and concentrated in vacuo. Then crude product purified by silica gel column chromatography using CHCl₃/CH₃OH (99/1, v/v). The pale green fraction which has bright yellow fluorescence was collected. Orange solid (0.147 mmol, 120 mg, 43 %).

¹H NMR (400 MHz, CDCl₃) δ: 6.48 (s, 2H, Ar-H), 4.15 (t, *J*= 5.0 Hz, 2H), 4.06 (t, *J*= 5.0 Hz, 4H), 3.76 (t, *J*= 4.9 Hz, 4H), 3.70- 3.42 (m, 26H), 3.30 (s, 3H, -CH₃), 3.27 (s, 6H), 2.48 (s, 6H, -CH₃), 2.24 (q, *J*=7.6 Hz, 2H, -CH₂), 1.46 (s, 6H, -CH₃), 0.92 (t, *J*=7.6 Hz, 3H, CH₃)

¹³C NMR (100 MHz, CDCl₃) δ 153.7, 153.6, 139.7, 139.0, 138.2, 132.7, 130.7, 130.6, 108.0, 72.7, 72.0, 71.9, 70.9, 70.7, 70.6, 70.5, 69.7, 69.2, 59.0, 29.6, 17.0, 14.5, 11.6

ESI-HRMS calcd for M+Na 889.4809, found 889.4808, Δ= 0.1 ppm

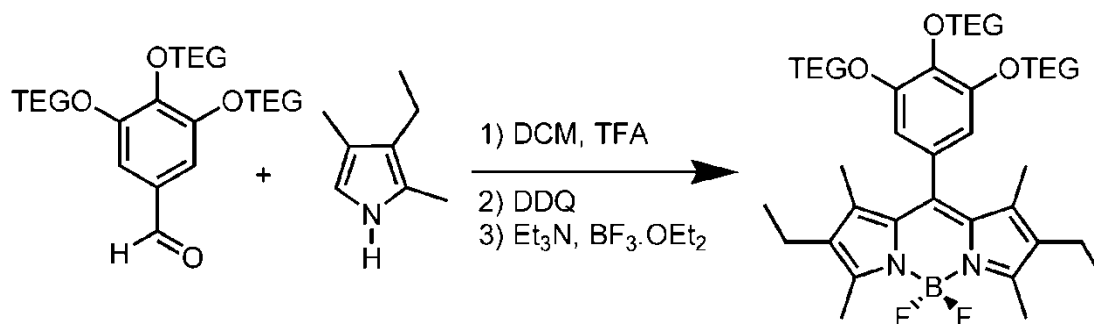


Figure 39 Synthesis of the BODIPY, **50**

2.1.7 N,N-Bis(pyridine-2-ylmethyl) aniline (**53**)

2-Picolyl chloride hydrochloride, **51**, (27.45 mmol, 4.5 g) and aniline, **52**, (9.15 mmol, 850 mg) were refluxed in 100 mL CH₃CN. Solvent was evaporated under reduced pressure and extracted with NaHCO₃ solution and organic phase was collected. Solvent was evaporated and compound **53** was purified by column chromatography with an eluent, CH₃OH; CHCl₃ (95; 5 v/v). Brown crystal compound (8.0 mmol, 2.20 g, 87%) ^[162]

¹H NMR (400 MHz, CDCl₃) δ: 8.47 (d, *J*=4.0 Hz, 2H), 7.50-7.47 (m, 2H), 7.16 (d, *J*=7.6 Hz, 2H), 7.07- 7.03 (m, 4H), 6.62- 6.60 (m, 3H), 4.70 (s, 4H, -CH₂)

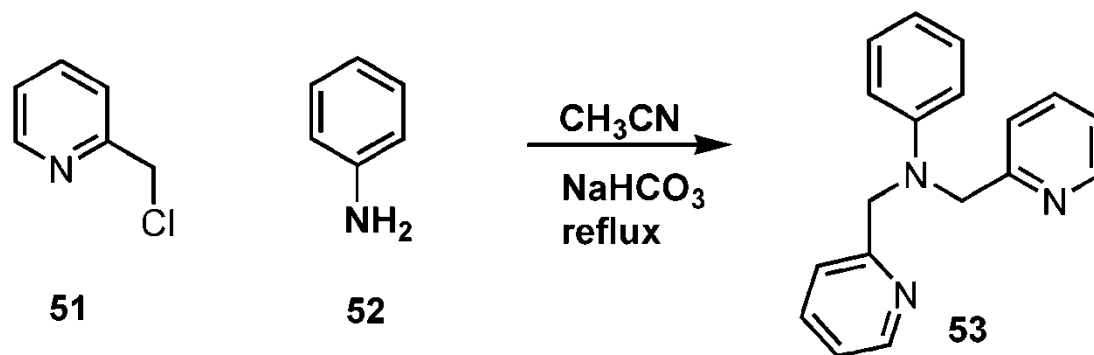


Figure 40 Synthesis of the compound, **53**

2.1.8 4-(bis(pyridin-2-ylmethyl)amino)benzaldehyde

To a cooled (5 °C) solution of freshly distilled anhydrous DMF (25 mL) was added POCl₃ (615 mg, 4 mmol) within 5 min. The mixture was stirred for 30 min, then **53** (1.0 g, 3.30 mmol) was added and the resulting mixture was heated for 3h at 80 °C. The mixture was hydrolyzed by slow addition of ice-cold water and then neutralized with 5 M NaOH. The product was extracted with CHCl₃ and washed with water and dried with Na₂SO₄. After evaporation of the solvent in vacuo, the product was purified by column chromatography eluting with hexane acetone (2:1) to afforded the aldehyde **54** in 80 % yield, as a viscous liquid: 810 mg.^[162]

¹H NMR (400 MHz, CDCl₃) δ: 9.60 (s, 1H, Al-H), 8.50 (d, 2H), 7.55 (m, 4H), 7.10 (m, 4H), 6.70 (d, 2H), 4.80 (s, 4H, -CH₂).

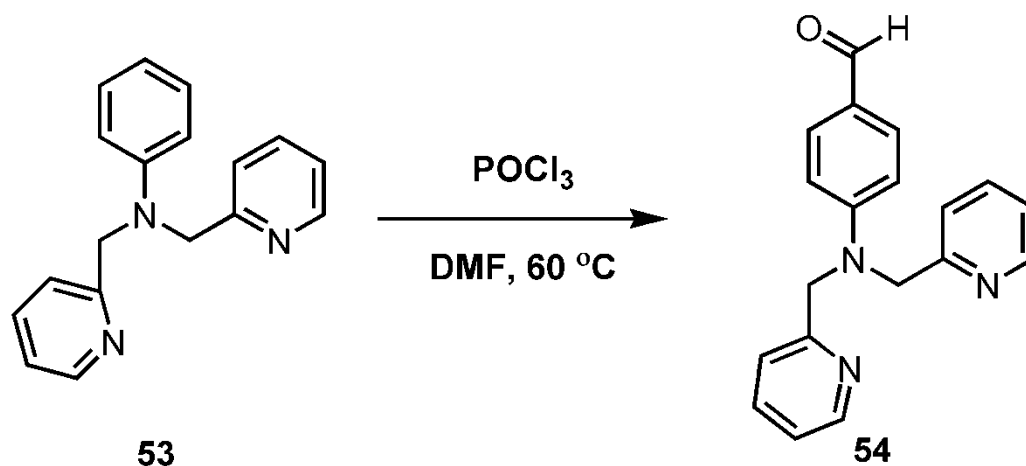


Figure 41 The synthesis of the compound **54**

2.1.9 Monostyryl functionalization of the BODIPY dye, **55**

Compound **48** (0.093 mmol, 90 mg) and **50** (0.186 mmol, 110.2 mg) were refluxed in a mixture of toluene (20 mL), glacial acetic acid (1.5 mL), and piperidine (2 mL). Any water formed during the reaction, was removed azeotropically by heating overnight in a Dean-Stark apparatus. Solvents were removed under reduced pressure, and the crude product was then purified by silica gel column chromatography using $\text{CHCl}_3/\text{CH}_3\text{OH}$ (95/5, v/v). The blue colored fraction was collected then the solvent was removed under reduced pressure to yield compound **55** (0.0186 mmol, 39.5 mg, 21%). Used without purification.

ESI-HRMS calcd for $\text{M}+\text{Na}$ 1463.7739, found 1463.7784, $\Delta = 1.0$ ppm

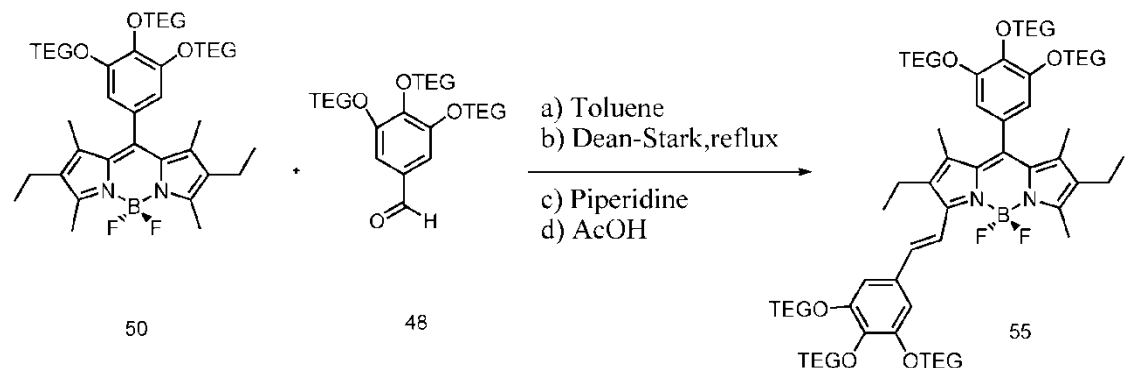


Figure 42 Synthesis of mono-styryl-BODIPY, **55**

2.1.10 Synthesis of the target distyryl-bodipy, **56**

Compound **55** (0.0625 mmol, 90 mg) and **54** (0.0625 mmol, 19.2 mg) were refluxed in a mixture of benzene (20 mL), glacial acetic acid (1.5 mL), and piperidine (2 mL). Any water formed during the reaction, was removed azeotropically by heating overnight in a Dean-Stark apparatus. Solvents were removed under reduced pressure, and the crude product was then purified by silica gel column chromatography using $\text{CHCl}_3/\text{CH}_3\text{OH}$ (95/10, v/v). The green colored fraction was collected then the solvent was removed under reduced pressure to yield compound **56** (0.0186 mmol, 32.5 mg, 32%).

^1H NMR (400 MHz, CDCl_3) δ : 8.52 (d, $J=4.3$ Hz, 2H, Ar-H), 7.58 (t, $J=7.6$ Hz, 2H, Ar-H), 7.55 (d, $J=16.5$ Hz, 2H, ethylene H), 7.37 (d, $J=8.4$ Hz, 2H, Ar-H), 7.20-7.07 (m, 4 H, Ar-H), 7.01 (d, $J=16.5$ Hz, 2H, ethylene H), 6.77 (s, 2H, Ar-H), 6.67 (d, $J=8.4$ Hz, 2H, Ar-H), 6.50 (s, 2H, Ar-H), 4.80 (s, 4H, $-\text{CH}_2$), 4.20-

4.02 (m, 10H), 3.80-3.23 (m, 80 H), 2.50 (q, $J=7.4$ Hz, 4H, $-\text{CH}_2$), 1.48 (s, 6H, $-\text{CH}_3$), 1.08 (t, $J=7.4$ Hz, 6H, $-\text{CH}_3$)

^{13}C NMR (100 MHz, CDCl_3) δ : 157.2, 152.6, 151.8, 151.3, 148.7, 147.8, 147.6, 138.4, 138.0, 136.0, 135.9, 133.6, 133.1, 132.3, 131.5, 130.1, 128.1, 125.6, 124.3, 121.3, 120.0, 118.9, 115.0, 111.7, 109.0, 107.5, 71.8, 71.5, 71.0, 70.9, 69.9, 69.8, 69.6, 69.5, 68.5, 68.3, 68.2, 57.9, 56.2, 30.9, 28.6, 28.3, 21.7, 17.4, 17.3, 13.3, 13.1, 12.9, 10.5, 10.4.

ESI-HRMS calcd for $\text{M}+\text{Na}$ 1748.9065, found 1748.9050, $\Delta=0.9$ ppm

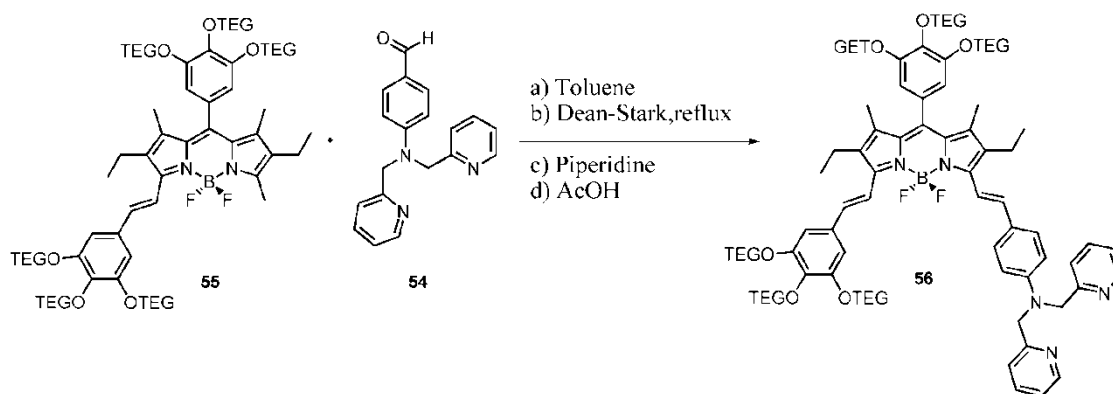


Figure 43 Synthesis of di-styryl-BODIPY, **56**

2.2 Syntesis of Hg(II) selective double-chealated chemosensor

2.2.1 Synthesis of N,N-bis(bromoethyl)aniline, 58

(Phenylazanediy) diethanol, **57**, (5.0 g, 27.5 mmol) was dissolved in 5 ml CH_2Cl_2 and cooled to 0 °C in ice-bath. To this solution PBr_3 (7 mL, 85.3 mmol) was added in a excess amount with a dropwise manner for a one-hour. The reaction was over after 20 hour. Then excess amount of PBr_3 was neutralized with K_2CO_3 solution and extracted three times with CH_2Cl_2 . The solvent was removed under reduced pressure and the product was purified with column chromatography to yield brown solid (4.2 g, yield 60%) in which the eluent was CHCl_3 .^[144]

^1H NMR (400 MHz, CDCl_3) δ 7.22 (t, $J=8$ Hz, 2H, Ar-H), 6.79 (t, $J=7.2$ Hz, 1H, Ar-H), 6.59 (d, $J=8.4$ Hz, 2H, Ar-H), 3.72 (t, $J=7.6$ Hz, 4H, $-\text{CH}_2$), 3.36 (t, $J=7.6$, 4H, $-\text{CH}_2$).

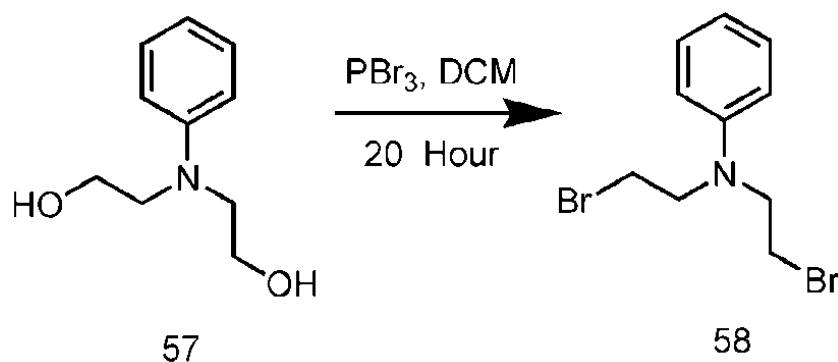


Figure 44 Synthesis of the compound **58**

2.2.2 Synthesis of 10-phenyl-1,4-dioxa-7,13-dithia-10-azacyclopentadecane

Cs_2CO_3 (1.4 g, 4.28 mmol) was added to 200 mL dry THF and mixed for a one-hour. To this solution a mixture of N,N-bis(bromoethyl)aniline (1.63 mmol, 500 mg) and 2,2'-(ethane 1,2diylbis(oxy)) diethanethiol (1.63 mmol, 297 mg) was added dropwise in 3 hours. The reaction was refluxed for 3 days. The final compound was filtered and filtrate was concentrated in vacuo. Finally, the product, **60**, was purified by silica gel chromatography (2:1 Hexane/EtOAc) and eluent was removed under reduced vacuum to yield an orange oily compound (400 mg, yield 75 %).^[144]

^1H NMR (400 MHz, CDCl_3) δ : 7.19 (t, $J=8.0$ Hz, 2H, Ar-H), 6.62-6.57 (m, 3H, Ar-H), 3.72 (t, $J=5.2$ Hz, 4H, $-\text{CH}_2$), 3.57-3.53 (m, 8H, $-\text{CH}_2$), 2.82 (t, $J=7.6$ Hz, 4H, $-\text{CH}_2$), 2.69 (t, $J=5.2$ Hz, 4H, $-\text{CH}_2$).

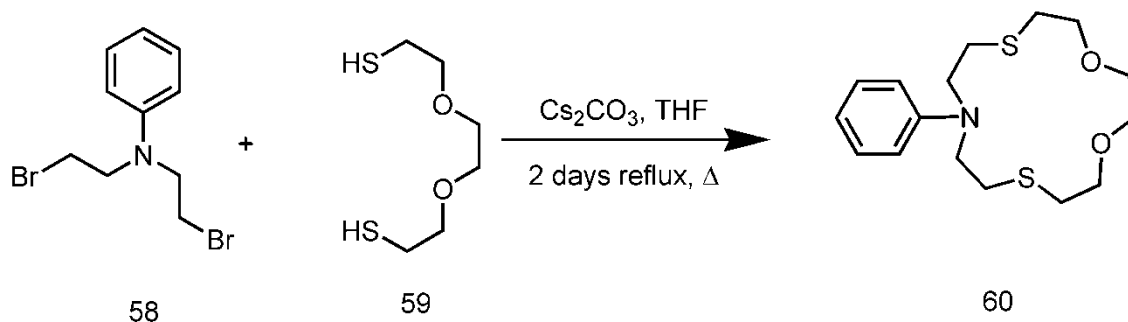


Figure 45 The synthesis of crown ether moiety, **60**

2.2.3 Synthesis of 4-(1,4-dioxa-7,13-dithia-10-azacyclopentadecan-10-yl) benzaldehyde

10 ml of dry DMF was cooled to 0 °C and POCl₃ (1.2mmol, 0.120 mL) was added within 5 minutes to this cooled solution. The mixture was stirred for 30 minute in ice-bath then 10-phenyl-1,4-dioxa-7,13-dithia-10-azacyclopentadecane (0.92 mmol, 300 mg) was added and the resulting mixture was heated for 3h at 80°C under argon. After a dark brownish colored was seen the reaction was over and cooled to room temperature. The mixture then was hydrolized by slow addition of ice-cold water and then neutralized with 5M NaOH. The product was extracted with diethyl ether. It was concentrated under vacuum and the product was purified with a column chromatography (3:1 Hexane/EtOAc) to yield the desired compound, **61**, as a brownish glasslike crystal (310 mg, 95%).^[144]

¹H NMR (400 MHz, CDCl₃) δ; 9.80 (s, 1H, *Al*-H), 7.70 (d, *J*=8.01 Hz, 2H, *Ar*-H), 6.62 (d, *J*=8.01 Hz, 2H, *Ar*-H), 3.73 (t, *J*=5.05 Hz, 4H, -CH₂), 3.60 (m, 8H, -CH₂), 2.84 (t, *J*=5.1 Hz, 4H, -CH₂), 2.69 (t, *J*=5.04 Hz, 4H, -CH₂).

¹³C NMR (100 MHz, CDCl₃) δ; 190.9, 153.2, 134.4, 126.2, 114.2, 76.4, 70.2, 53.7, 32.2, 29.5

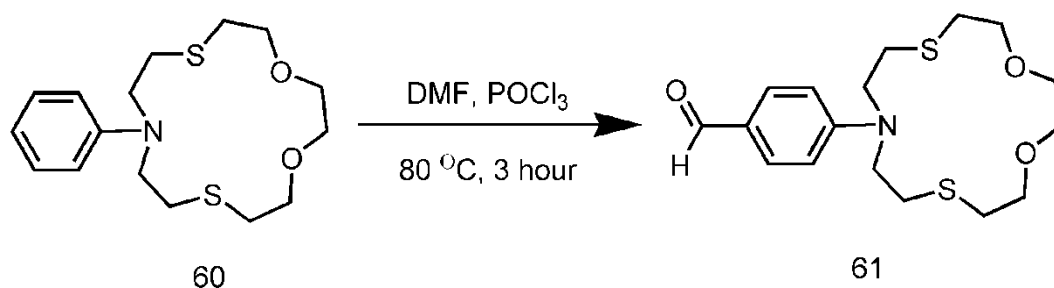


Figure 46 Vilsmeier reaction of the compound **61**

2.2.4 Synthesis of 2,6-diethyl-4,4-difluoro-1,3,5,7-tetramethyl-8-(4-*tert*-butylphenyl)-4-bora-3a,4a-diaza-s-indacene

4-*tert*-butyl benzaldehyde, **62**, (6.2 mmol, 1.0 mL) and 3-ethyl- 2,4-dimethyl pyrrole, **49**, (12.4 mmol, 1.70 mL) were dissolved in CH₂Cl₂ degassed with argon for an hour and TFA (trifluoroacetic acid) was added (2-3 drops). When TLC analysis indicated consumption of the aldehyde, a solution of 500 mg (3.1 mmol) of DDQ (Tetrachloro-1,4-benzoquinone) in CH₂Cl₂ was added as an oxidizing agent. After 3 hour Et₃N (5 mL) and BF₃.OEt₂ (5 mL) were added. Crude product was washed with water 3 times and dried over Na₂SO₄ and concentrated in vacuum. The product, **63**, was purified by silica gel column chromatography (eluent was CHCl₃) to collect the bright yellow fluorescent compound. Orange solid (260 mg, 10%).

¹H NMR (400 MHz, CDCl₃) δ; 7.39 (d, *J*=8.1 Hz, 2H, *Ar*-H), 7.11 (d, *J*=8.1 Hz, 2H, *Ar*-H), 2.40 (s, 6H, CH₃), 2.22 (q, *J*=7.8 Hz, 4H, -CH₂), 1.29 (s, 9H, CH₃), 1.18 (s, 6H, CH₃), 0.9 (t, *J*=7.7 Hz, 6H, CH₃).

¹³C NMR (100 MHz, CDCl₃) δ; 153.2, 152.2, 140.4, 138.2, 132.2, 130.0, 126.4, 124.0, 34.2, 30.9, 16.7, 16.5, 14.0, 11.9, 11.0

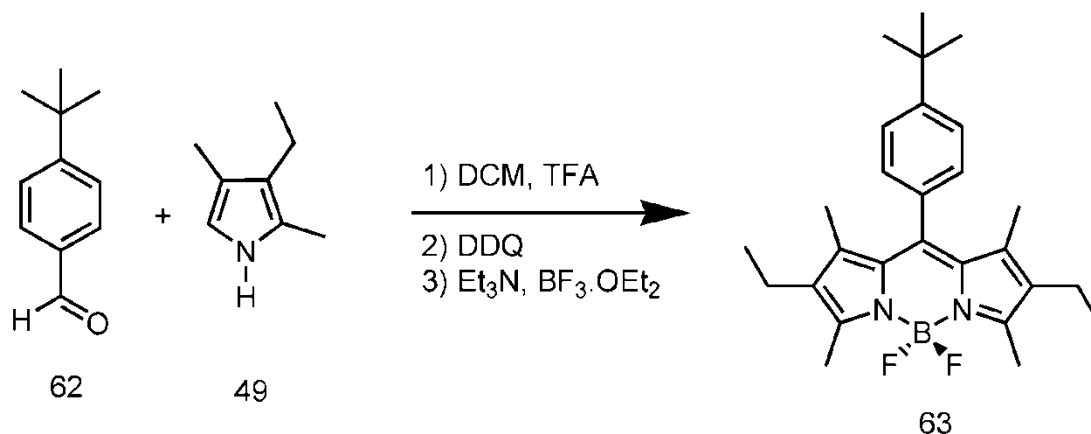


Figure 47 Synthesis of BODIPY, **63**.

2.2.5 Synthesis of distyryl BODIPY, **64**

Compound **63** (0.25 mmol, 110 mg) and compound **61** (0.50 mmol, 184 mg) were dissolved in dried 50 mL of benzene. To this solution 0.5 mL glacial acetic acid and 0.5 mL piperidine added then heated to reflux for one day. Any water formed during the condensation reaction was removed azeotropically by heating overnight in a Dean-Stark apparatus. Solvent was removed and the product was concentrated. Column chromatography was done for the purification of the green product with a eluent CHCl₃. The green fraction was isolated. (55 mg, 20%)

¹H NMR (400 MHz, CDCl₃) δ: 7.54 (d, *J*=16.0 Hz, 2H), 7.45 (d, *J*=8.0 Hz, 4H, *Ar*-H), 7.40 (d, *J*=8.0 Hz, 2H, *Ar*-H), 7.13 (d, *J*=8.0 Hz, 2H, *Ar*-H), 7.19 (d, *J*=16.0 Hz, 2H), 6.61 (d, *J*=8.0 Hz, 4H, *Ar*-H), 3.75 (t, *J*=5.0 Hz, 8H, -CH₂), 3.64-3.60 (m, 8H), 3.58 (s, 8H), 2.88-2.84 (m, 8H), 2.70 (t, *J*=5 Hz, 8H), 2.53 (q, *J*=7.4 Hz, 4H) 1.30 (s, 9H), 1.23 (s, 6H), 1.07 (t, *J*=7.4 Hz, 6H).

^{13}C NMR (100 MHz, CDCl_3) δ : 152.2, 150.3, 147.2, 138.1, 136.9, 135.5, 133.4, 133.2, 133.0, 129.0, 128.5, 126.1, 125.6, 116.1, 111.9, 74.2, 70.7, 52.0, 34.7, 31.4, 31.3, 30.8, 29.6, 18.4, 14.0, 11.6

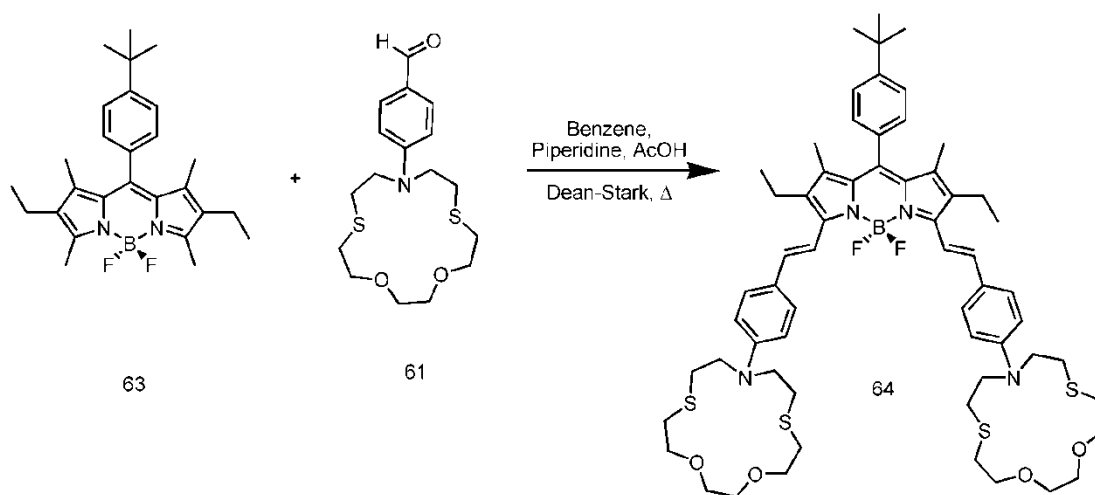


Figure 48 Synthesis of double armed Hg^{2+} selective chemosensor, **64**

2.3 Synthesis of ratiometric FRET based fluorescent chemosensor for Hg(II) cation

2.3.1 Synthesis of 4-(prop-2-ynyloxy)benzaldehyde

1.50 g of K_2CO_3 (7.3 mmol) was added into 100 ml of CH_3CN and then to this solution a mixture of 4-hydroxybenzaldehyde, **65**, (100 mg, 0.82 mmol), and 3-bromoprop-1-yne, **66**, (106 mg, 0.90 mmol) in 5 ml CH_3CN was added in a dropwise manner for an hour. After addition the solution was heated until reflux temperature. After stirring for 2 days at this temperature the solution was filtered and filtrate was concentrated by rotary evaporation under vacuum. The crude product was purified by column chromatography using $CHCl_3$ as the eluent to afford product **67** as a white solid (98.4 mg, 74%).^[159]

1H NMR (400 MHz, $CDCl_3$) δ : 9.84 (s, 1H, Al-H), 7.79 (d, $J=8.8$ Hz, 2H, Ar-H), 7.02 (d, $J=8.8$ Hz, 2H, Ar-H), 4.71 (d, $J=2.4$ Hz, 2H, $-CH_2$), 2.50 (t, $J=2.4$ Hz, 1H, $-CH$).

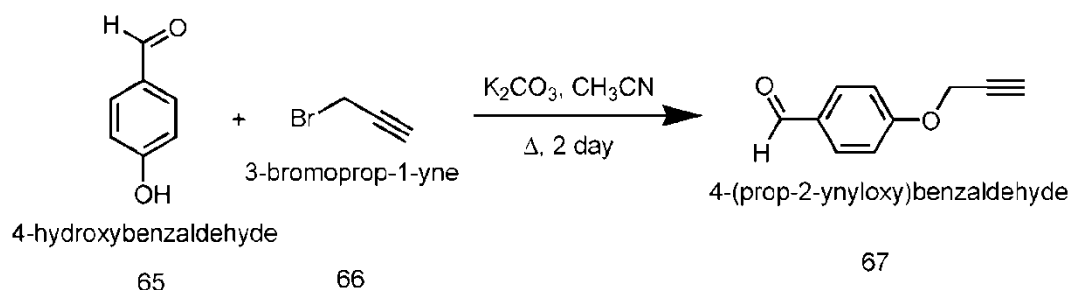


Figure 49 Synthesis of 4-(prop-2-ynyloxy)benzaldehyde, **67**.

2.3.2 Synthesis of 4,4-difluoro-8-(4-(prop-2-ynoxy)phenyl)-1,3,5,7-tetramethyl-4-bora-3a,4a-diaza-s-indacene

To a deoxygenated solution of aldehyde, **67**, (1.25 mmol, 200 mg) and 2,4-dimethylpyrrole, **68**, (2.5 mmol, 237 mg) in CH_2Cl_2 (500 mL), TFA (125 mg, 1.1 mmol) was added and the mixture was stirred overnight. The red solution was treated with DDQ (284 mg, 1.25 mmol), stirred for 30 min, then 5 ml of Et_3N and 3 ml of $\text{BF}_3 \cdot \text{Et}_2\text{O}$ were added, and the mixture was stirred at rt for further 40 min. The organic phase was separated, dried (MgSO_4), filtered, and concentrated. The residue was purified by column chromatography (CHCl_3), collecting the first green fluorescent fraction afforded the expected BODIPY dye, **69**, 47 mg (10% yield), orange-red solid.

^1H NMR (400 MHz, CDCl_3) δ : 7.12 (d, $J=8.8$ Hz, 2H, Ar-H), 7.01 (d, $J=8.8$ Hz, 2H, Ar-H), 5.90 (s, 2H, pyrrole-H), 4.68 (d, $J=2.0$ Hz, 2H, $-\text{CH}_2$), 2.52 (d, $J=2.0$ Hz, 1H, CH), 2.48 (s, 6H, $-\text{CH}_3$), 1.35 (s, 6H, $-\text{CH}_3$)

^{13}C NMR (100 MHz, CDCl_3) δ : 158.1, 155.4, 143.1, 141.5, 131.8, 130.4, 129.3, 128.0, 121.2, 115.6, 78.0, 75.9, 56.0, 14.7, 14.6

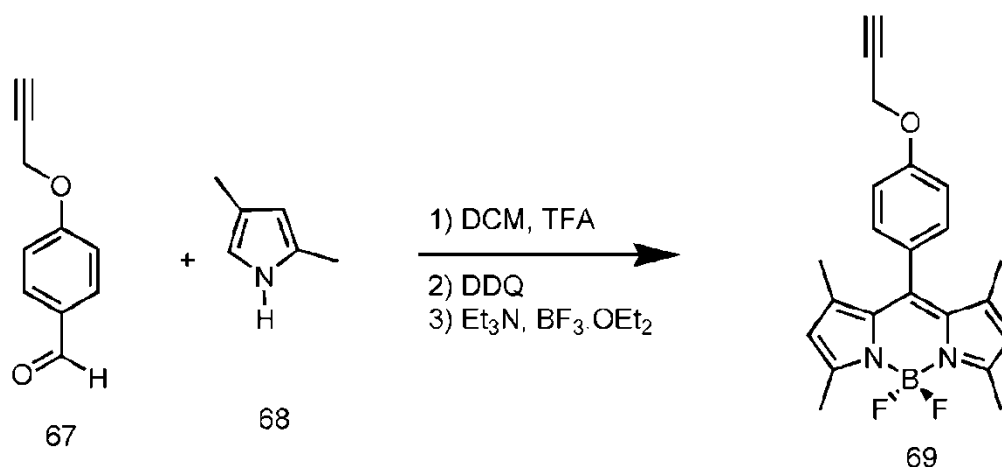


Figure 50 Synthesis of BODIPY dye, **69**.

2.3.3 Synthesis of 4-(6-bromohexyloxy)benzaldehyde, 71

To a solution of K_2CO_3 (200 mg, 1.45 mmol) in 100 ml freshly distilled acetone was added 4-hydroxybenzaldehyde, **65**, (100 mg, 0.82 mmol) and 1,6-dibromo hexane, **70**, (219 mg, 0.90 mmol) and the mixture was stirred at the reflux temperature for 2 days. After removal of the solid part by filtration organic solvent was removed under reduced pressure. The crude product was dissolved in $CHCl_3$ to extract it with water. Organic layer was evaporated and resulting residue chromatographed (3:1 Hexane/EtOAc) to give yellow oil. (94 mg, yield 40%)^[159]

1H NMR (400 MHz, $CDCl_3$) δ : 9.87 (s, 1H, Al-H), 7.82 (d, $J=8.8$ Hz, 2H, Ar-H), 6.98 (d, $J=8.8$ Hz, 2H, Ar-H), 4.03 (t, $J=6.4$ Hz, 2H, $-CH_2$), 3.42 (t, $J=6.8$ Hz, 2H, $-CH_2$), 1.93-1.80 (m, 4H), 1.52-1.49 (m, 4H).

^{13}C NMR (100 MHz, $CDCl_3$) δ : 189.1, 162.5, 130.3, 128.2, 113.1, 66.5, 32.1, 31.0, 27.2, 26.2, 23.6

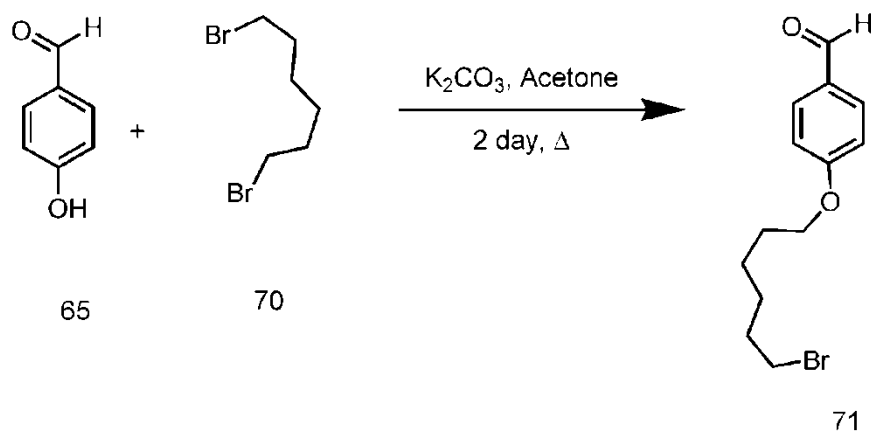


Figure 51 Structural representation of the production of compound 71

2.3.4 Synthesis of 4-(6-azidohexyloxy)benzaldehyde, **72**

4-(6-bromohexyloxy)benzaldehyde, **71**, (80 mg, 0.32 mmol) and NaN₃ (24 mg, 0.37 mmol) was added to DMSO and stirred vigorously. This suspension was then heated to 80 °C and stirred at this temperature for 3 hours. When TLC analysis showed complete consumption of the starting material the reaction was cooled to room temperature and then the crude product was poured onto brine solution and extracted three times with CHCl₃. The organic layer was removed by rotary evaporator. And the residue was purified with column chromatography, EtOAc as an eluent, to give the product, **72**, as a brown oil. (75 mg, 95% yield) ^[159]

¹H NMR (400 MHz, CDCl₃) δ: 9.78 (s, 1H, Al-H), 7.74 (d, *J*=8.8 Hz, 2H, Ar-H), 6.90 (d, *J*=8.8 Hz, 2H, Ar-H), 3.95 (t, *J*=6.4 Hz, 2H, -CH₂), 3.20 (t, *J*=6.8 Hz, 2H, -CH₂), 1.78-1.71 (m, 2H), 1.59-1.52 (m, 2H), 1.47-1.33 (m, 4H)

¹³C NMR (100 MHz, CDCl₃) δ: 190.7, 164.1, 131.9, 129.8, 114.7, 68.1, 51.3, 28.9, 28.7, 26.4, 25.6.

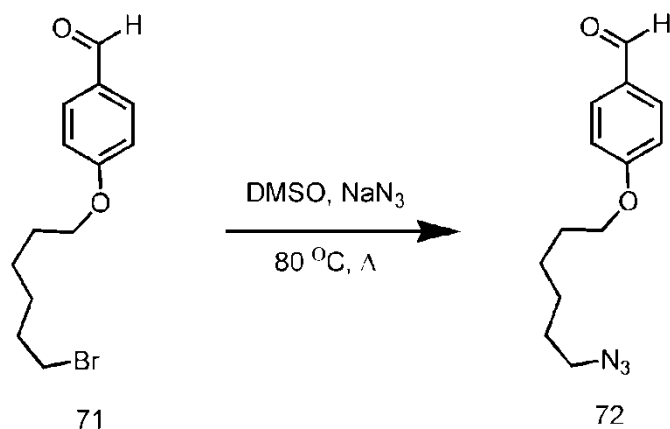


Figure 52 Synthesis of 4-(6-azidohexyloxy)benzaldehyde, **72**

2.3.5 Synthesis of Mono-styryl BODIPY (Blue-BODIPY), **73**

Tert-Butyl Bodipy, **63**, (200 mg, 0.46 mmol), compound **61** (160 mg, 0.46 mmol), were refluxed in a mixture of benzene (20 mL), glacial acetic acid (0.5 mL) and piperidine (1.0 mL). Any water formed during the reaction was removed azeotropically by heating overnight in a Dean–Stark apparatus. Crude product was then concentrated under vacuum, and purified by silica gel column chromatography (CHCl₃). The blue colored fraction was collected and the solvent was removed under reduced pressure to yield the bright red fluorescent compound **73** (35 mg, 10%).

¹H NMR (400 MHz, CDCl₃) δ; 7.49 (d, *J*=16.4 Hz, 1H), 7.43-7.40 (m, 4H, Ar-H), 7.12 (d, *J*=8.4 Hz, 2H, Ar-H), 7.08 (d, *J*=16.4 Hz, 1H), 6.57 (d, *J*=8.8 Hz, 2H, Ar-H), 3.74 (t, *J*=4.8 Hz, 4H, -CH₂), 3.63-3.58 (m, 8H), 2.84 (t, *J*=8.0 Hz, 4H, -CH₂), 2.71 (t, *J*=4.8 Hz, 4H, -CH₂), 2.50 (q, *J*=7.2 Hz, 2H, -CH₂), 2.23 (q, *J*=7.6 Hz, 2H, -CH₂), 1.50 (s, 3H, -CH₃), 1.30 (s, 9H, -C(CH₃)₃), 1.23 (s, 3H, -CH₃), 1.21 (s, 3H, -CH₃), 1.06 (t, *J*=7.2 Hz, 3H, -CH₃), 0.91 (t, *J*=7.6 Hz, 3H, -CH₃).

¹³C NMR (100 MHz, CDCl₃) δ; 153.2, 137.7, 137.4, 136.6, 135.2, 134.7, 132.1, 131.8, 131.0, 130.5, 128.0, 127.9, 127.6, 125.3, 115.6, 114.9, 111.7, 74.2, 71.7, 51.1, 35.2, 31.4, 31.3, 29.6, 18.4, 16.3, 13.6, 13.0, 11.6, 10.6, 10.3.

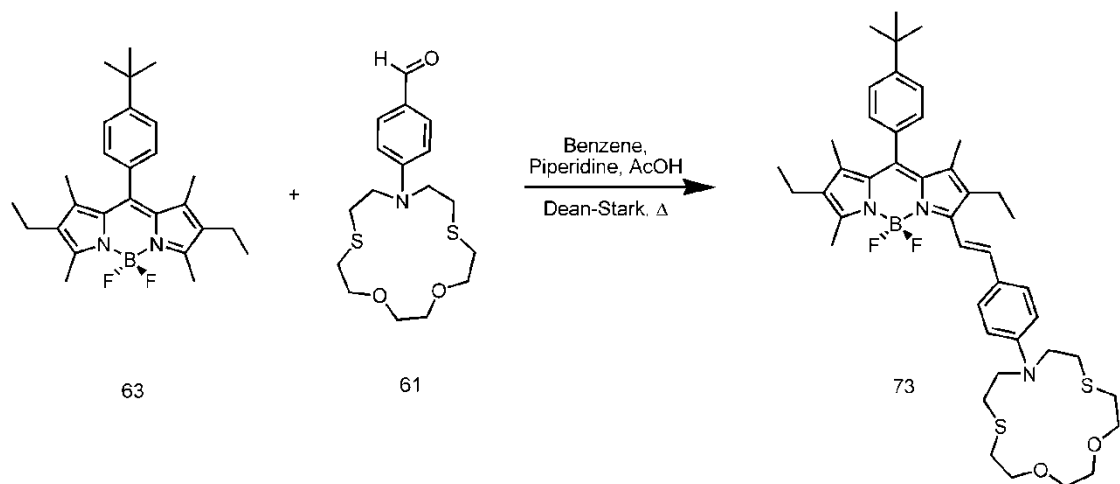


Figure 53 Synthesis of mono-styryl BODIPY, **73**.

2.3.6 Synthesis of di-styryl BODIPY, **74**

To a freshly distilled benzene Mono-styryl-BODIPY, **73**, (blue-BODIPY) (25 mg, 0.032 mmol) and 4-(6-azidohexyloxy)benzaldehyde, **72**, (16 mg, 0.064 mmol) were added. After vigorously stirring glacial acetic acid (0.5 mL), piperidine (1.0 mL) was added to this solution, heated to reflux temperature and kept at this temperature until TLC observation showed complete consumption of the blue BODIPY and formation of the green red fluorescent di-styryl BODIPY. At this point organic layer was removed under reduced pressure and the crude product re-dissolved in CHCl_3 and extracted three times with brine solution. The organic layer was removed finally residue was purified with column chromatography, CHCl_3 as an eluent. The red fluorescent compound was isolated, **74**. (24 mg, 75% yield).

^1H NMR (400 MHz, CDCl_3) δ : 7.60 (d, $J=16.4$ Hz, 1H), 7.55 (d, $J=16.8$ Hz, 1H), 7.49 (d, $J=8.4$ Hz, 2H, Ar-H), 7.46 (d, $J=8.8$ Hz, 2H, Ar-H), 7.41 (d, $J=8.0$ Hz, 2H, Ar-H), 7.15-7.06 (m, 4H, Ar-H), 6.86 (d, $J=8.8$ Hz, 2H, Ar-H), 6.60 (d, $J=8.8$ Hz, 2H, Ar-H), 3.94 (t, $J=6.4$ Hz, 2H), 3.75 (t, $J=4.8$ Hz, 4H), 3.65-3.59 (m, 8H), 3.21 (t, $J=6.8$ Hz, 2H), 2.88-2.84 (m, 4H), 2.71 (t, $J=4.8$ Hz, 4H), 2.54-2.51 (m, 4H), 1.80-1.72 (m, 2H), 1.63-1.56 (m, 2H), 1.48-1.47 (m, 4H), 1.30 (s, 9H, $-\text{C}(\text{CH}_3)_3$), 1.24 (s, 6H, $-\text{CH}_3$), 1.07 (t, $J=7.6$ Hz, 6H, $-\text{CH}_3$)

^{13}C NMR (100 MHz, CDCl_3) δ : 159.4, 152.1, 151.4, 149.0, 147.4, 139.0, 137.9, 137.5, 136.3, 134.4, 133.6, 133.3, 133.2, 133.0, 132.7, 130.5, 130.0, 129.2, 128.6, 128.3, 125.9, 125.7, 118.4, 115.9, 114.7, 111.9, 74.3, 70.8, 67.9, 52.0, 51.4, 34.8, 31.4, 31.3, 29.6, 29.2, 28.8, 26.6, 25.7, 18.5, 18.4, 14.1, 14.0, 11.4, 11.3.

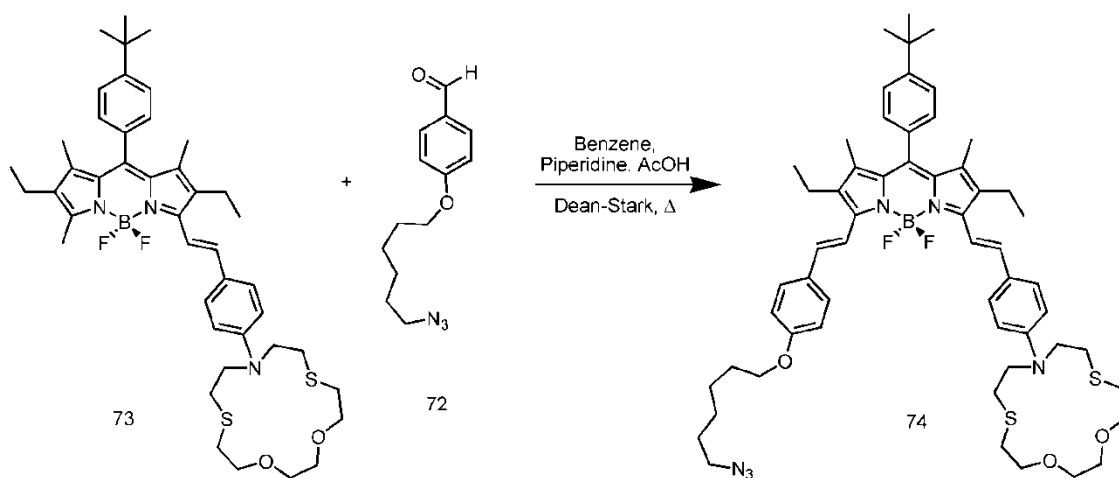


Figure 54 Structural representation of the synthesis of the compound, **74**.

2.3.7 Synthesis of the targeted Di-styryl BODIPY, 75

To a freshly distilled THF, 1.0 equiv of BODIPY-acetylene (9.01 mg, 0.023 mmol) and 1.1 equiv. of di styryl-BODIPY-N₃ (24 mg, 0.024 mmol) was added. Then TEA (10–30 mol% per triple bond) was added to this mixture, and stirred for 5 min, 10-30 mol% per triple bond of sodium ascorbate was added, followed by 5–15 mol% of CuSO₄·5H₂O per triple bond. (A stock solution of sodium ascorbate and CuSO₄·5H₂O in water was prepared in concentration 100 mg/mL) The THF/H₂O ratio must be 1/1 (v/v). The heterogeneous mixture was stirred vigorously until TLC analysis indicated complete consumption of the starting material. The reaction mixture was diluted with water and extracted with CH₂Cl₂. The combined organic layers were dried with Na₂SO₄, and concentrated in vacuo. Purification by column chromatography (CHCl₃, as an eluent) gave the desired product. (13.6 mg, 90% yield)

¹H NMR (400 MHz, CDCl₃) δ; 7.61 (d, *J*=16.8 Hz, 1H, ethylene-H), 7.58 (s, 1H, triazole-H), 7.53 (d, *J*=16.8 Hz, 1H, ethylene-H), 7.50-7.40 (m, 6H, Ar-H), 7.15-7.01 (m, 8H, Ar-H), 6.84 (d, *J*=8.8 Hz, 2H, Ar-H), 6.59 (d, *J*=8.8 Hz, 2H, Ar-H), 5.89 (s, 2H, pyrrole-H), 5.16 (s, 2H, methylene-H), 3.94 (t, *J*=6.4 Hz, 2H, -CH₂), 3.74 (t, *J*=4.8 Hz, 4H, -CH₂), 3.67-3.57 (m, 8H), 3.47-3.45 (m, 1H), 3.42-3.40 (m, 1H), 2.87-2.83 (m, 4H), 2.70 (t, *J*=4.8 Hz, 4H), 2.47 (s, 6H, -CH₃), 2.55-2.51 (m, 4H), 1.95-1.88 (m, 2H), 1.76-1.70 (m, 2H), 1.54-1.46 (m, 4H), 1.34 (s, 6H, -CH₃), 1.31 (s, 9H, -CH₃), 1.24 (s, 6H, -CH₃), 1.07 (t, *J*=7.6 Hz, 3H, -CH₃), 1.07 (t, *J*=7.6 Hz, 3H, -CH₃).

¹³C NMR (100 MHz, CDCl₃) δ; 159.3, 158.9, 155.3, 152.2, 151.6, 148.9, 147.5, 143.6, 143.1, 141.6, 139.1, 137.9, 137.6, 136.4, 134.3, 133.7, 133.3, 133.2, 133.0, 132.7, 131.8, 130.6, 130.4, 129.3, 129.2, 128.6, 128.4, 127.6, 127.5, 126.3, 126.0, 125.0, 123.5, 123.2, 122.6, 121.6, 121.2, 118.5, 114.8, 114.6,

111.9, 74.3, 71.7, 71.0, 70.7, 67.7, 62.1, 61.9, 52.0, 50.4, 34.8, 31.9, 31.7, 31.4, 31.3, 30.2, 29.7, 29.6, 29.4, 28.9, 14.5, 14.1, 14.0, 13.9.

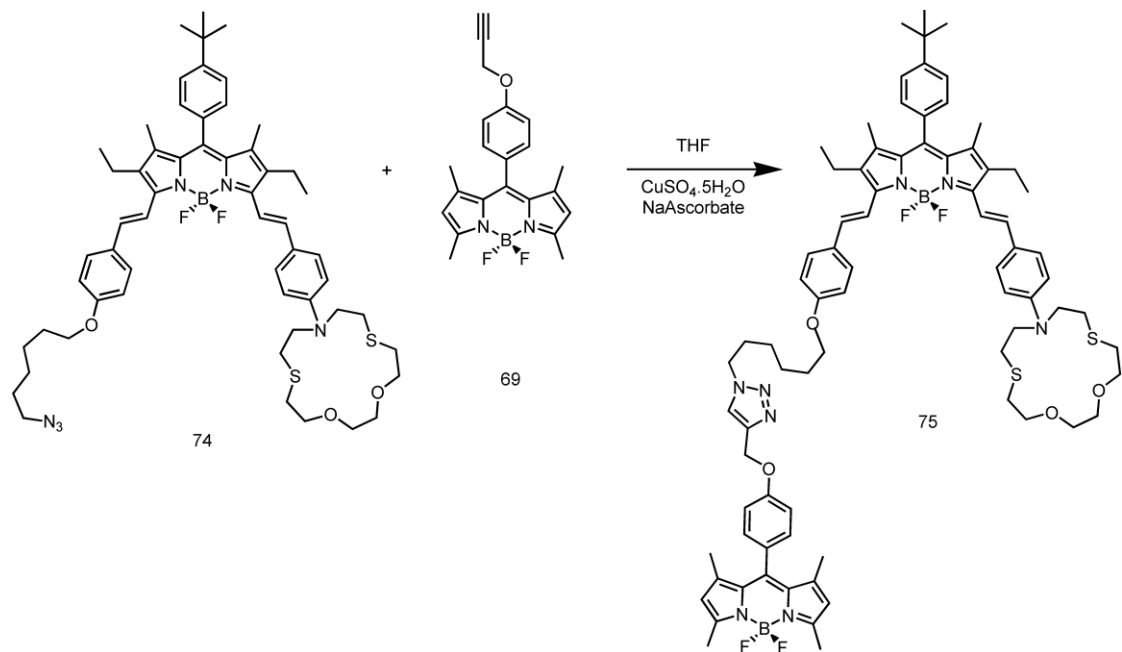


Figure 55 Synthesis of the targeted di-styryl BODIPY, **75**.

CHAPTER 3

RESULTS AND DISCUSSION

3.1 A Sensitive and Selective Ratiometric Near IR Fluorescent Probe for Zinc Ions Based on the Distyryl-Bodipy Fluorophore^[161], 56

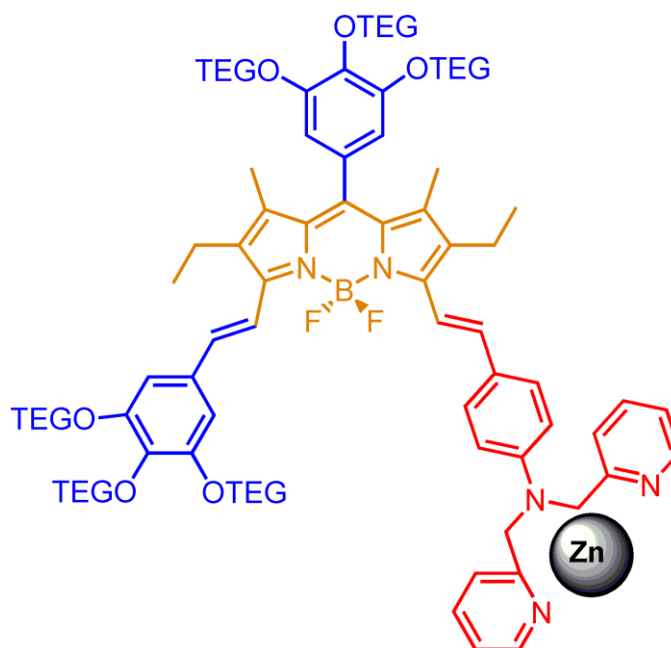


Figure 56 Representation of the modulated BODIPY fluorophore as a Zn²⁺ selective chemosensor

Recently in the literature, various Zn^{2+} selective fluorescent probes have been presented. However, for most of them, water solubility is limited, which necessitate the usage of various solvent mixtures for characterization. This fact, together with the requirement for shorter wavelength excitation, hinders biological applications. In this study we aimed to synthesize a ratiometric fluorescent sensor for Zn^{2+} cation. The well-known versatile dye, BODIPY, is chosen as a fluorescent probe. It is intended to achieve an applicable dye by which, all the limitations for biological applications are eliminated. These limitations and the answers to these limitations can be summarized as;

- i. Unfortunately, for most of Zn^{2+} selective dyes, water solubility is limited and some solutions are suggested to overcome this obstacle such as usage of solvent mixture for characterization. However, biological applications can not be carried out with such solvent mixtures. This limitation is passed over with the use of TEG (triethyleneglycol) groups (blue moieties on Figure 56). This group supply fully water solubility for our designed fluorophore. The TEG groups are placed on a gallic acid derived, 3, 4, 5 trihydroxyphenyl unit. There are two TEG linked gallate unit on the targeted fluorophore, one on the 8 position of the BODIPY, and one placed as a styryl group with the condensation of the methyl group at the position of 3 on the BODIPY core. It is observed that six TEG groups are enough to make this molecule compatible with water. Water solubility limitation is overcome with these groups and it can be said that, a water soluble fluorescent dye is synthesized. Water solubility is shown in both absorption and emission spectra studies. In both studies, dye is prepared in 5:95 ethanol-aqueous buffer solutions. Metals are chosen as their chloride salts for spectral studies.

- ii. Second limitation is selectivity and sensitivity, that are indispensable properties of any fluorescent dyes. In this study, dipicolylamine (DPA)(red moiety in figure 56), a well-known Zn^{2+} selective ligand, is chosen as metal chelator. This cheate, coordinated to BODIPY core as second styryl group, results from the condensation of methyl group on the position of 5 on BODIPY core.
- iii. Emission in the red end of the visible spectrum is another criteria for biological applications. Di-styryl BODIPY dyes are illustrated as red emitting dyes when excited at appropriate wavelength. As illustrated before, this targeted distyryl BODIPY dyes are synthesized with stepwise condensation of methyl groups at 3, 5 positions of the BODIPY core. The key step of this work is the double condensation with different functional groups, leading us to obtain a near-IR emitting dye. The presence of red-emission is proved in both absorption and emission spectra.

With these considerations we set out compound **56** and charecterized with 1H and ^{13}C NMR and HRMS.

The absorption spectrum displays a broad peak centered at 680 nm, and the molar extinction coefficient is $72\ 000\ M^{-1}cm^{-1}$ at this wavelength. Gradually addition of Zn^{2+} was observed in absorption spectrum as a 15 nm blue shift and the color turned from green to blue as shown in figure 58. No change in color and absorption maxima was observed with addition of the other selected cations to this targeted fluorescent dye. (Figure 57)

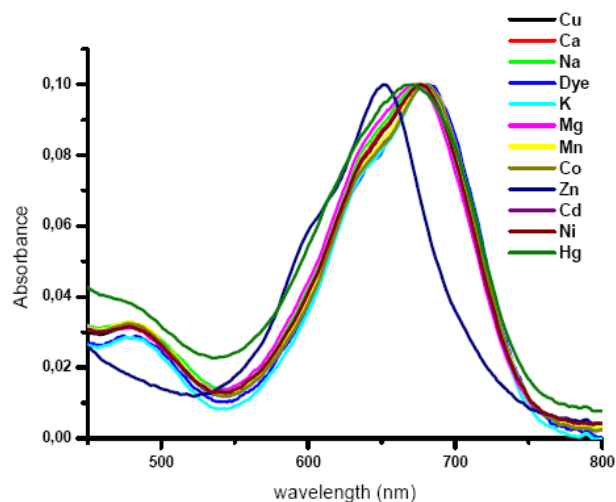


Figure 57 Absorbance change of the dye **56** ($2.5 \mu\text{M}$) in response to different metal ions ($5.0 \mu\text{M}$) in aqueous solutions. The solutions are buffered with 0.1 M HEPES pH 7.2 . 5% EtOH was added as cosolvent.

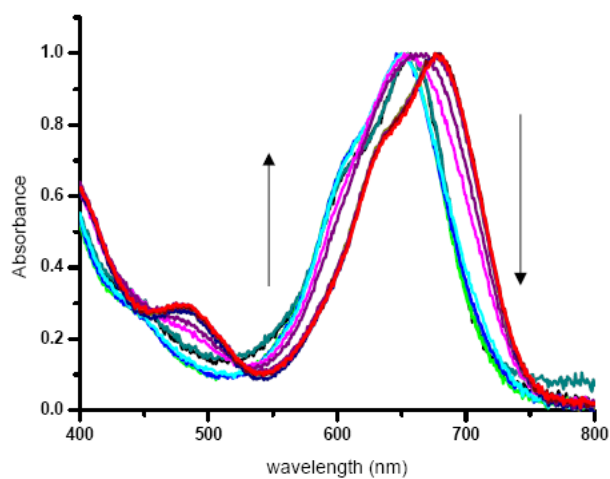


Figure 58 The change in absorption spectrum of the dye ($2.5 \mu\text{M}$) as a function of increasing Zn(II) concentration. Concentration of Zn(II) is varied between 0 to $100 \mu\text{M}$.

The emission spectrum obtained in aqueous buffer solution (5% ethanol was added as a cosolvent) shows a peak centered at 726 nm (Figure 59). Gradual addition of Zn(II) ions to this solution results in a blue shift to 675 nm with a concomitant increase in emission intensity. This clearly shows that the coordination of Zn(II) ions effectively blocks excited-state charge transfer from the dipicolylphenyl group. Hill plot analysis of the data obtained in the titration of **56** with Zn(II) yielded a 1:1 stoichiometry (slope= 0.97) with a dissociation constant (K_d) of 2.0×10^{-5} M (Figure 60). The fluorescence emission of the Zn(II) complex is bright red, whereas weaker intensity emission of the free chemosensor is hardly visible since it is at the red end of the visible spectrum, extending to near IR. Not surprisingly, the dipicolylamine ligand imparts remarkable metal ion selectivity onto this chemosensor (Figure 61). The chemosensor **56** generates the largest signal in the presence of Zn(II) ions, but Hg(II) and Cd(II) also show some response. Fortunately, in biological media (unlike environmental samples), these three ions rarely compete, and our data show that most likely biological interferants such as Ca(II), K(I), Na(I), and Mg(II) have no effect on the emission spectrum. The results of a competition experiment between Zn(II) and selected metal ions is shown in Figure 62. Digital photographs (Figure 63) of the aqueous solutions of the chemosensor with added Zn(II) clearly show very large enhancement of the red emission under UV illumination at 360 nm, with no perceivable changes in the presence of other biologically relevant ions.

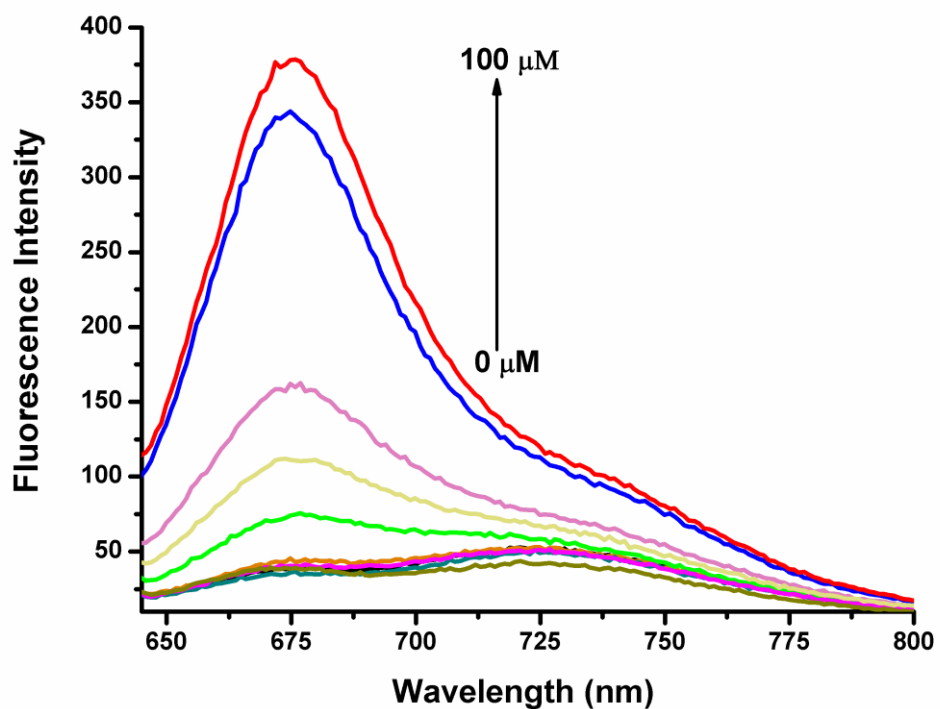


Figure 59 Change in the emission spectrum of the Dye (2.5 μM) in response to increasing concentrations of Zn(II) in ethanol-water mixture (%5 in ethanol). Zinc concentrations were varied in the following order: 0, 0.25, 0.5, 1, 2, 5, 10, 20, 50, 100 μM. Excitation was at 630 nm, with slit widths of 5 nm.

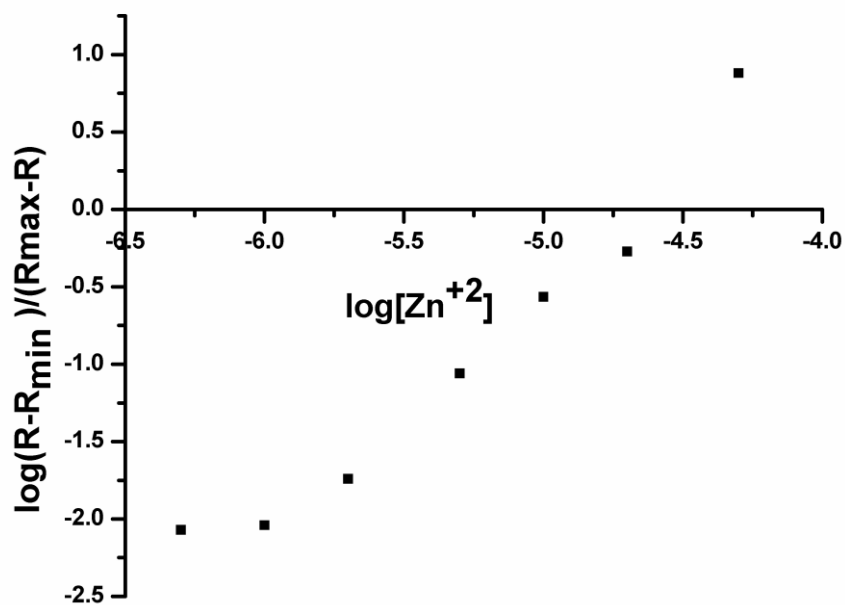


Figure 60 Fluorescence intensity ratio (F_{675}/F_{730}) of **56** versus increasing concentration of $\log [\text{Zn}^{2+}]$. The concentration of **56** was 2.5 μM . Hill plot analysis yielded to 1:1 stoichiometry with a slope 0.97.

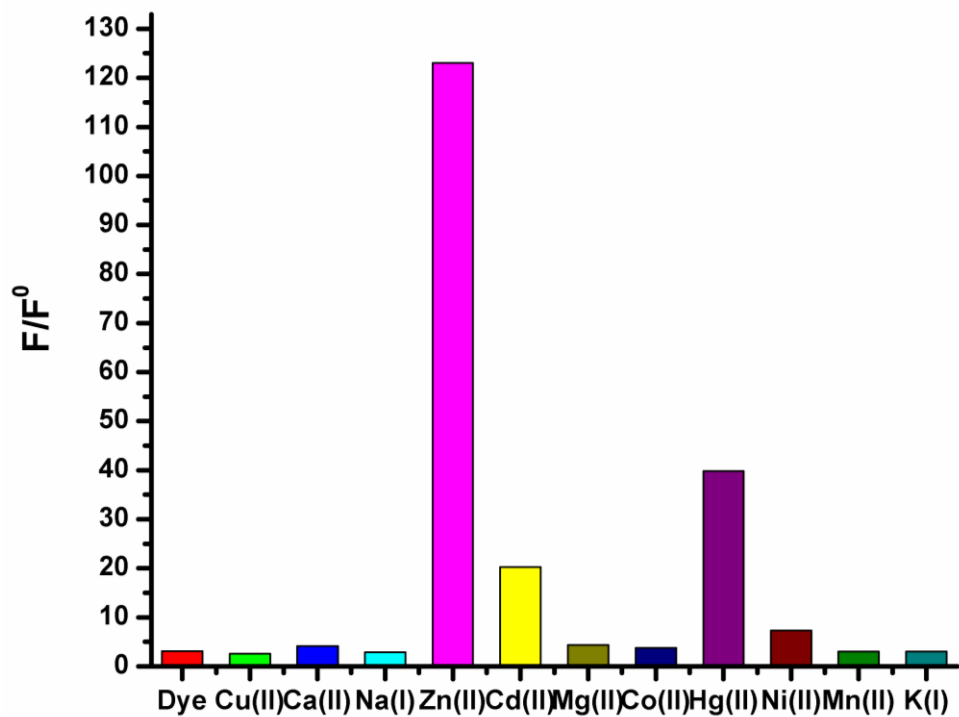


Figure 61 Normalized emission intensities at 680 nm (the emission intensity of the free dye= 1) of the chemosensor ($1.2 \mu\text{M}$) in the presence of selected metal ions (1.0 mM). Excitation was done at 630 nm with 5 nm slit widths. Solvent: ethanol-aqueous buffer mixture (5% in ethanol, HEPES 0.1 M, pH= 7.2).

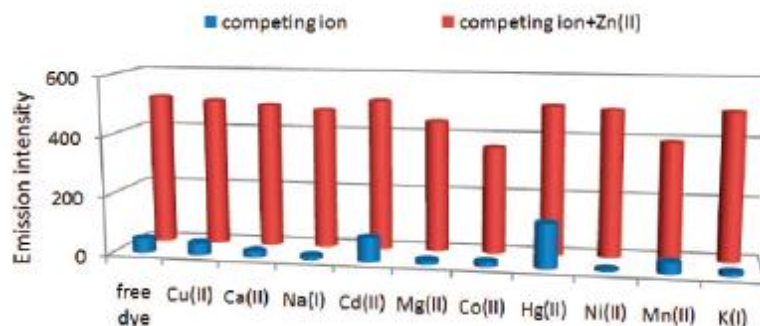


Figure 62 Results of the competition experiments between Zn (II) and selected metal ions. The free dye **56** (chemosensor) concentrations were set at 2.5 μM . Excitation was at 630 nm; emission intensity values at 680 nm were collected; and all metal ions were added at 200 μM concentration. Solvent: ethanol-aqueous buffer mixture (5% in ethanol, HEPES 0.1 M, pH=7.2).

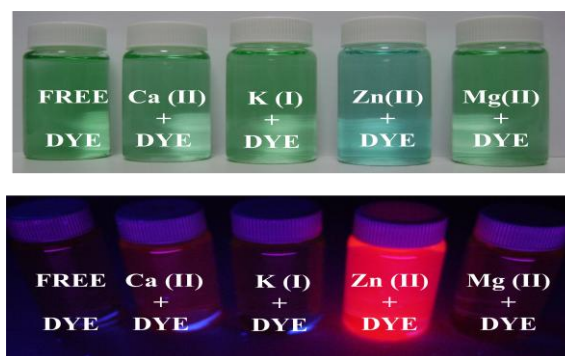


Figure 63 Digital photographs of the chemosensor solutions (5.0 μM) in the presence of different metal ions at 100 μM concentration. The upper plate is taken under ambient light, and the bottom one under UV illumination at 360 nm. Solvent: ethanol-aqueous buffer mixture (5% in ethanol, HEPES 0.1 M, pH= 7.2).

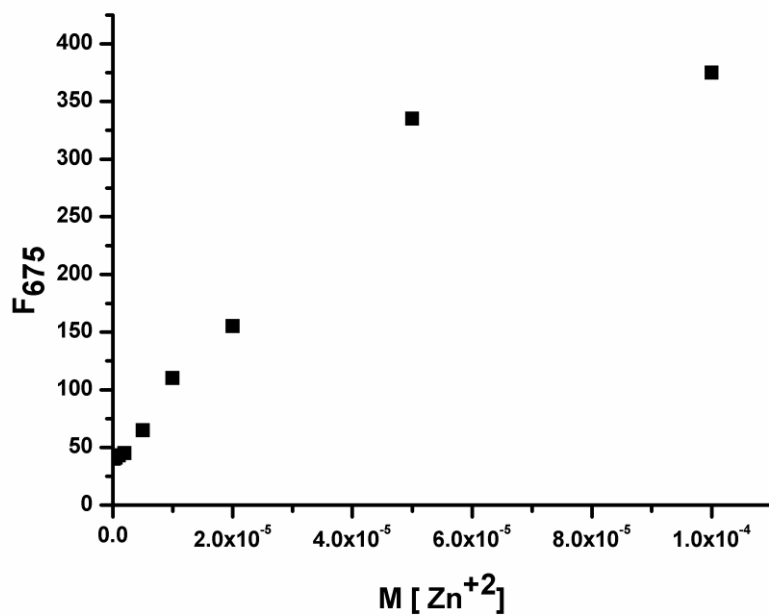


Figure 64 Curve of fluorescence intensity at 675 nm of the dye versus increasing concentration of Zn²⁺. The concentration of the dye was 5.0 μM. Dissociation constant was calculated as 2.0×10^{-5} M

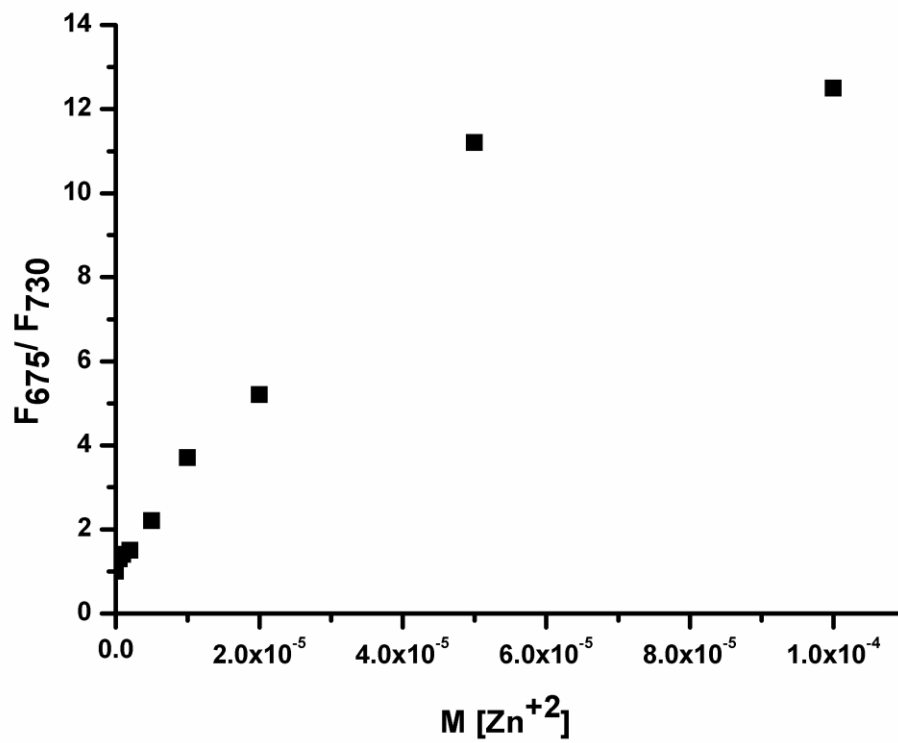


Figure 65 Curve of fluorescence ratio of the dye at 675 nm and 730 nm (5.0 μM) versus increasing concentration of Zn^{2+} .

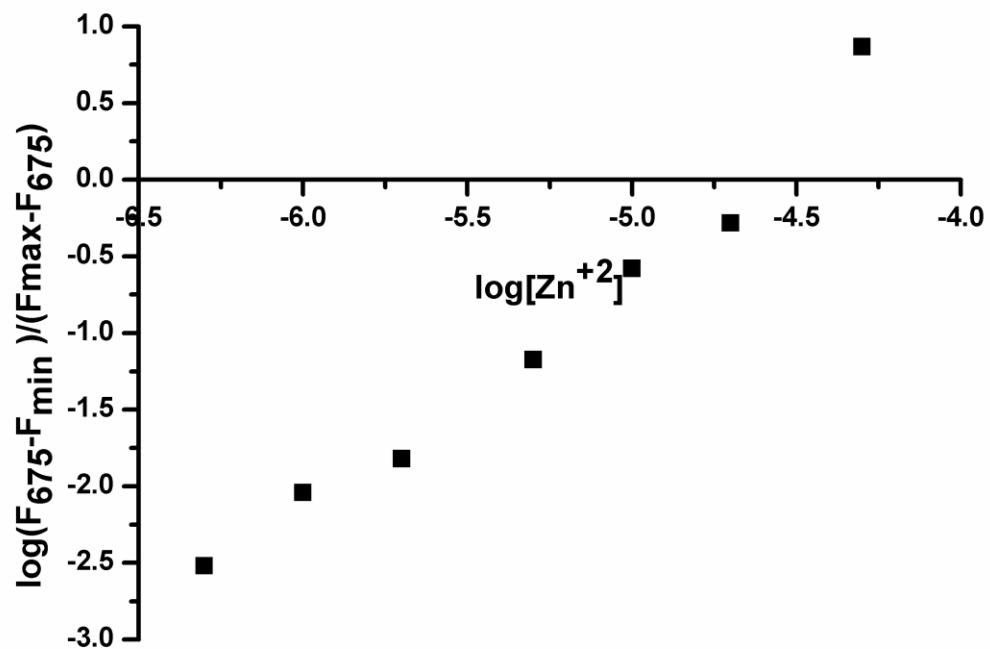


Figure 66 Logarithmic values for the fluorescence intensity of dye at 675 nm versus $\log [Zn^{2+}]$. Hill coefficients (0.938) fits with 1:1 coordination of dye- Zn^{2+}

3.2 Double Chealated Near-IR Di-Styryl BODIPY Based Ratiometric Fluorescent Chemosensor For Hg(II) (64)

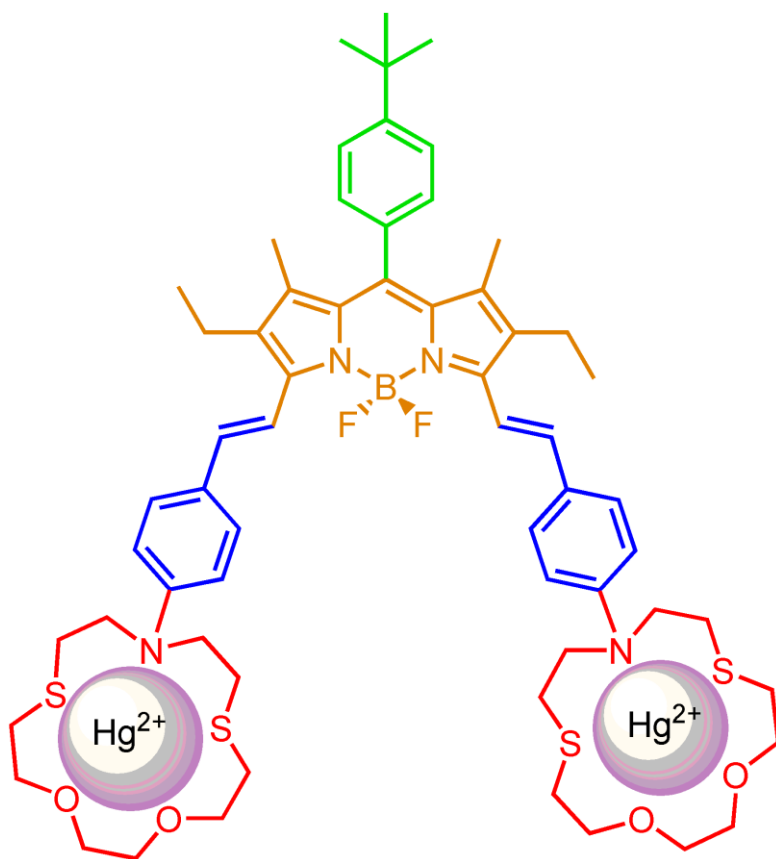


Figure 67 Structural representation of chemosensor **64** as a mercury selective fluorophore

This work aims to synthesize a novel double chealated fluorescent sensor, **64**, with high selectivity for mercury cation over the other known metals. We have chosen BODIPY unit as a fluorophore (orange moiety in figure 67)

since boradiazaindacene based fluorophores proved to have tremendous potential as a chemosensor with versatile modification on the core and also with the property of red shift in absorption and emission spectra. Extended conjugation at methyl groups at 3, 5 positions and conjugation of dialkylamino substituents on the BODIPY core was achieved, leading to the longer wavelengths in the red region of the visible site for BODIPY fluorophore. Our modeling consists of two chelating substituents on BODIPY core for mercury cation sensing (red moiety in figure 67). Hg^{2+} is a soft acid and use of soft donor atoms at receptor units results in good selectivity for Hg^{2+} , thus the well-known Hg^{2+} selective ligand, dithia-dioxa-aza macrocycle is chosen as a receptor. We have also gained the advantages of ICT mechanism with these substituents. ICT process gives a rise to two distinct absorption and emission wavelengths. A ratiometric chemosensor design is presented with the formation of these two distinct wavelengths. Coordination of cation to nitrogen donor atom of the dithia-dioxa-aza unit blocks ICT process to the BODIPY fluorophore, following a spectral shift on absorption and emission spectra of the fluorophore.

To synthesize our target fluorophore, p-tert-butyl-BODIPY was prepared according to the procedure as reported in experimental chapter. Vilsmeier-Haack reaction is used to provide aldehyde unit of the dithia-dioxa-aza macrocycle. Finally designed fluorophore was synthesized with the condensation reaction at methyl groups, at 3, 5, position of BODIPY core. Later, full characterization of the dye with both $^1\text{H-NMR}$ and $^{13}\text{C-NMR}$ analysis, absorption and emission studies were done with an appropriate solvent, THF.

Absorption spectrum of the compound was acquired in THF and shows a peak at 720 nm. The addition of $\text{Hg}(\text{ClO}_4)_2$ to a solution of the dye in THF caused the appearance of a new band at 630 nm and a simultaneous disappearance of the band at 720 nm (Figure 68). This new band is blue-shifted by 90 nm and is observable as a color change from green to blue (can de

detected with naked-eye). Meanwhile addition of any metal ions other than Hg^{2+} , cause no change at the absorption maxima (shown in Figure 68).

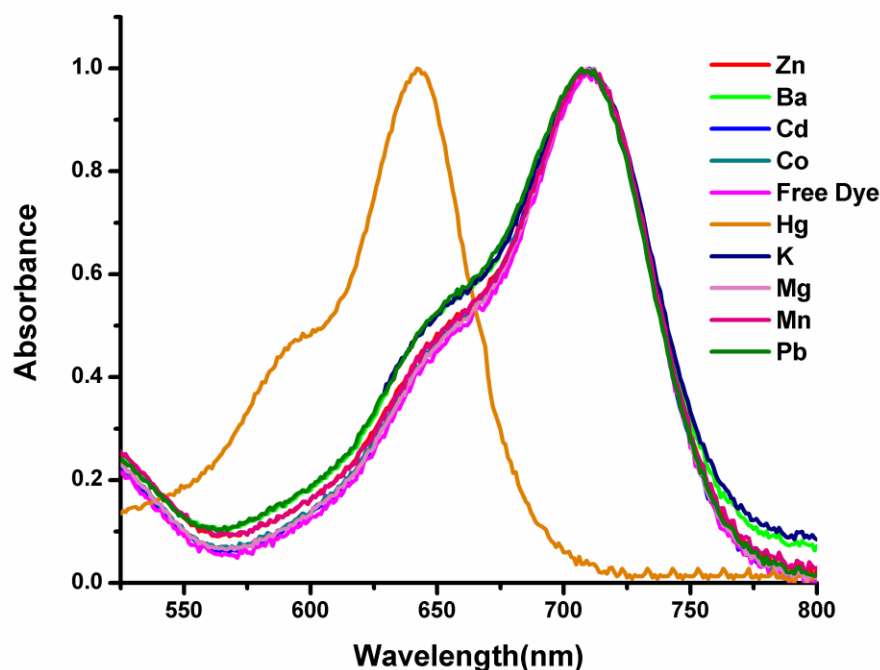


Figure 68 Normalized absorption spectra of di-styryl BODIPY (1.5 μM) in the presence of different cations (10.0 μM) in THF.

Fluorescence spectrum was also performed with this highly mercury selective dye in THF. ICT process on the designed fluorophore from crown unit to the BODIPY core is leading to strong fluorescence quenching. The emission spectrum of free dye displays no band. The coordination of the Hg^{2+} to the receptors resulted in the reduction of the electron-donating ability of the two amino groups conjugated to the BODIPY core, the receptor showed a 90 nm blue shift of fluorescence emission (Figure 69). Due to the selectivity of the

receptor, the other metal ions other than Hg^{2+} showed no change in emission spectra neck and crop in absorption spectra (Figure 70). Presence of these metal ions also did not affect the coordination of Hg^{2+} to the fluorophore (showed in figure 71). This visible change in fluorescence emission for Hg^{2+} coordination to double-chealated BODIPY core is observable by the naked eye under UV-light.

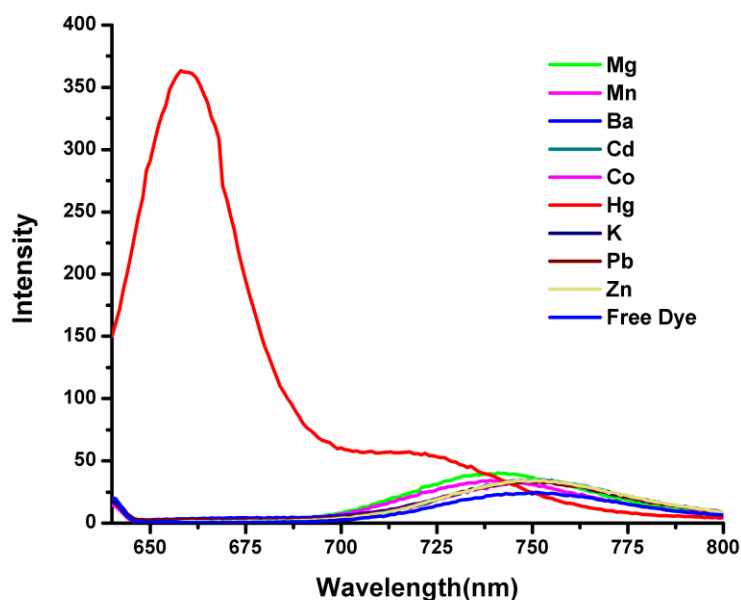


Figure 69 Change in the emission spectrum of di-styryl BODIPY (1.5 μM) in response to the different cation with a cation concentration 10.0 μM in THF. Excitation wavelength was 640 nm with a slit width 2.5 nm.

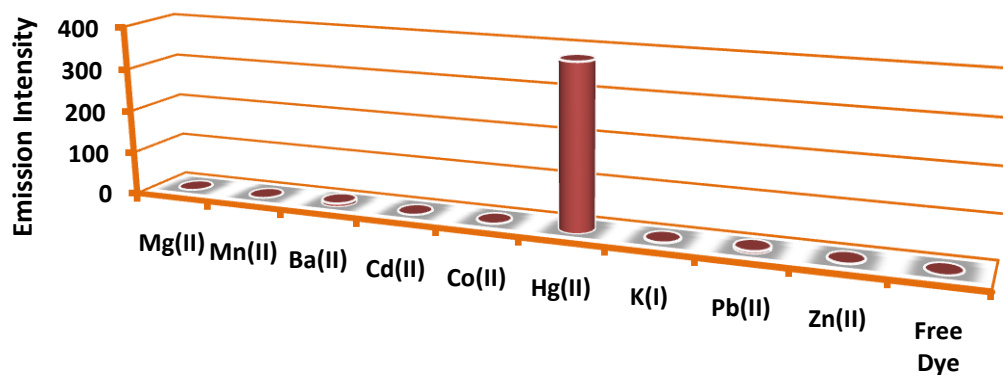


Figure 70 Fluorescence response of di-styryl BODIPY (1.5 μM) to various cations (10.0 μM) in THF. Excitation was done at 640 nm with a slit width 2.5 nm.

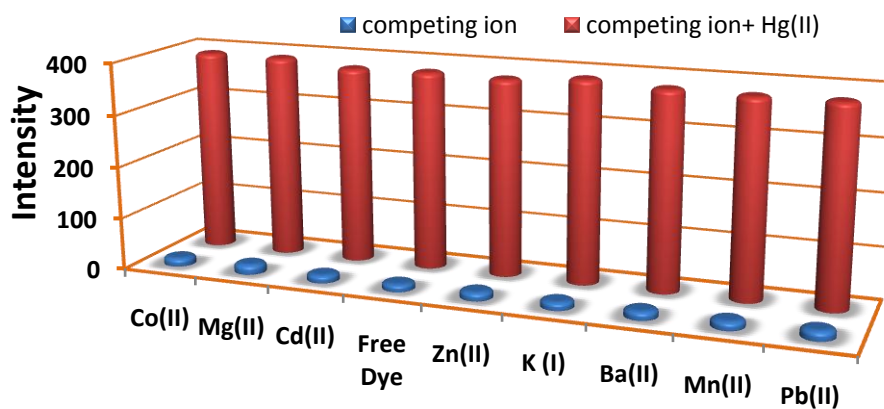


Figure 71 The fluorescence intensity response of di-styryl BODIPY (1.5 μM) with 20 μM metal followed by 10 μM Hg^{+2} in THF. Excitation wavelength was 640 nm with a slit width 2.5 nm.

Titration experiment was also conducted in order to observe ratiometric analysis and also to calculate binding constant (K_d) of the fluorophore with Hg^{2+} . The ion-free fluorophore shows an absorption maximum at 720 nm. Gradual addition of Hg^{2+} alters the absorption maximum of the dye to 640 nm and shows an isosbestic point at 665 nm, illustrating that Hg^{2+} was caught by the dithia-dioxa-aza crown macrocycle (Figure 72). At the same time the green color of the dye turns to blue.

Metal-free form of the compound **64** is non-fluorescent, however complexation of Hg^{2+} with dye results in a drastic increase in intensity of fluorescence. When excitation was done at 640 nm, a significant blue shift with the gradual increasing of Hg^{2+} ion concentration is observed (shifting from 750 nm to 660 nm).

Dissociation constants were also calculated with titration experiment (Figure 74). Sigmodial curves in both figures 74 and 75 indicate that, dissociation constants are 1.8×10^{-6} and $2.4 \times 10^{-6} M$, respectively. Hill coefficient confirms both fluorescence response as 1:2 (dye: metal) complexation is the result as expected. (Figure 76) (Details in auxiliary section)

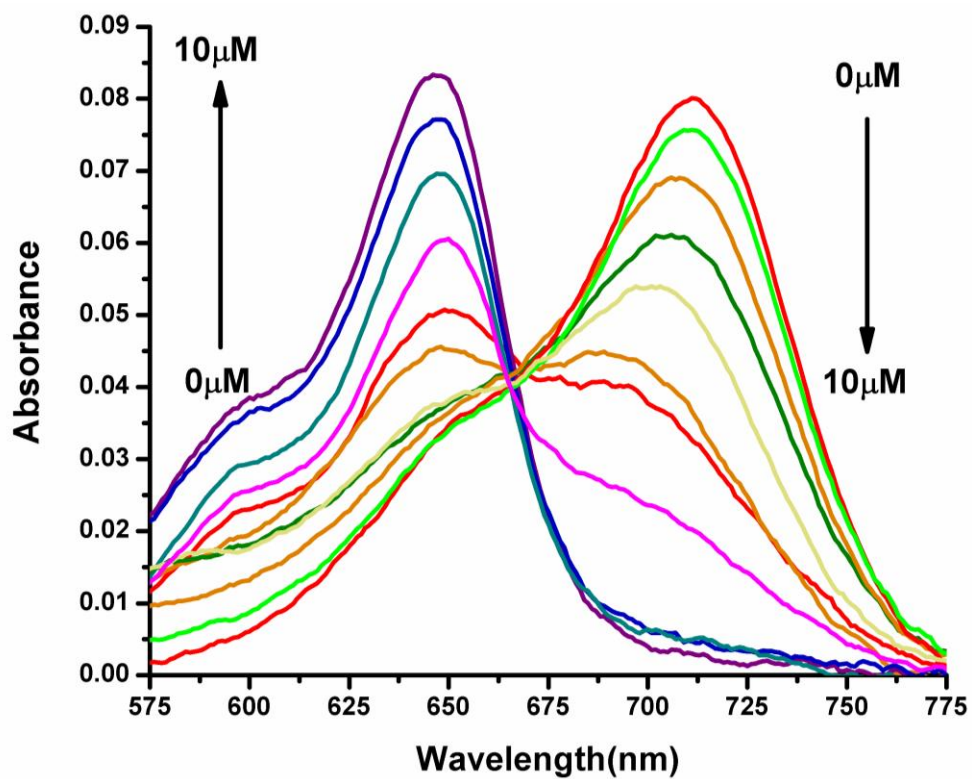


Figure 72 Absorption spectra of di-styryl BODIPY (1.5 μM) in the presence of increasing concentration of Hg²⁺ (cation concentrations; 0, 0.5, 0.75, 1.0, 1.5, 2.0, 2.5, 4.0, 5.0, 7.5, 10 μM) in THF solution

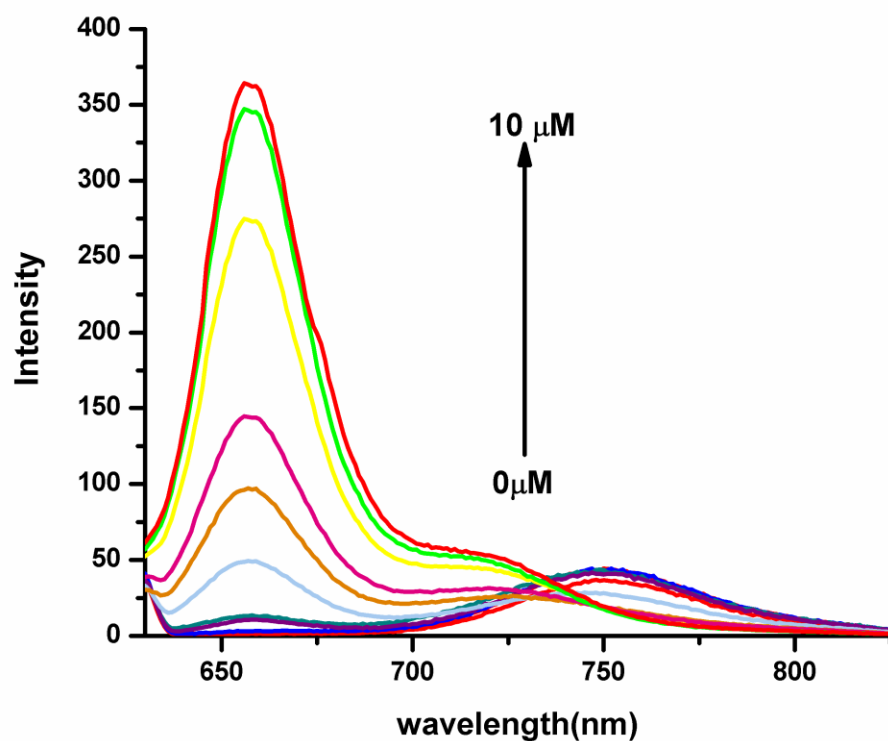


Figure 73 Emission spectrum of the chemosensor, di-styryl BODIPY (1.5 μM), at increasing concentration of the Hg²⁺ (cation concentrations; 0, 0.5, 0.75, 1.0, 1.5, 2.0, 2.5, 4.0, 5.0, 7.5, 10 μM). Excitation wavelength was 630 nm with a slit width 2.5 nm.

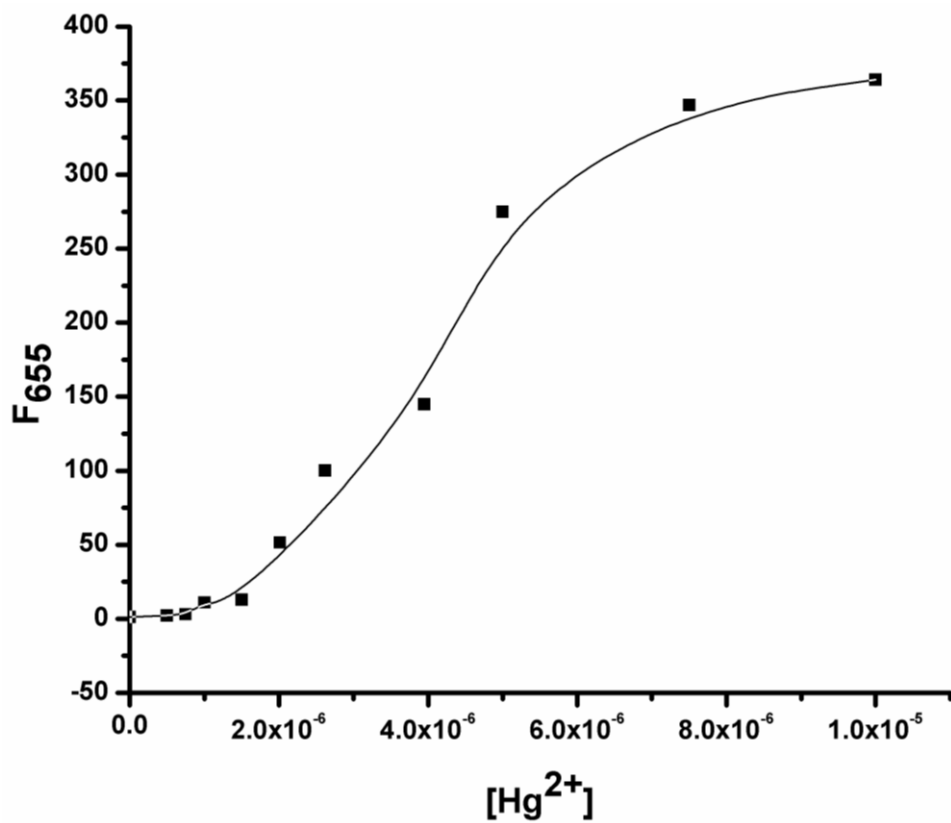


Figure 74 Curve of fluorescence intensity at 655 nm of the dye versus increasing concentration of Hg²⁺. The concentration of the dye was 1.5 μM. dissociation constant was calculated as 1.8 × 10⁻⁶ M.

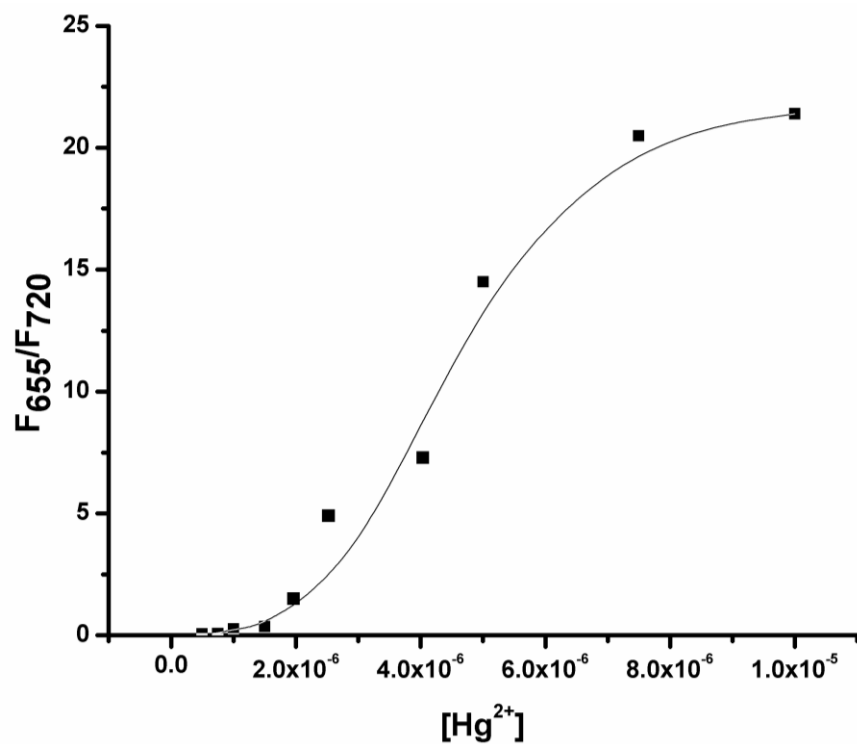


Figure 75 Curve of fluorescence ratio of the dye (1.5 μM) versus increasing concentration of Hg^{2+} . The dissociation constant was calculated as $2.4 \times 10^{-6} \text{M}$.

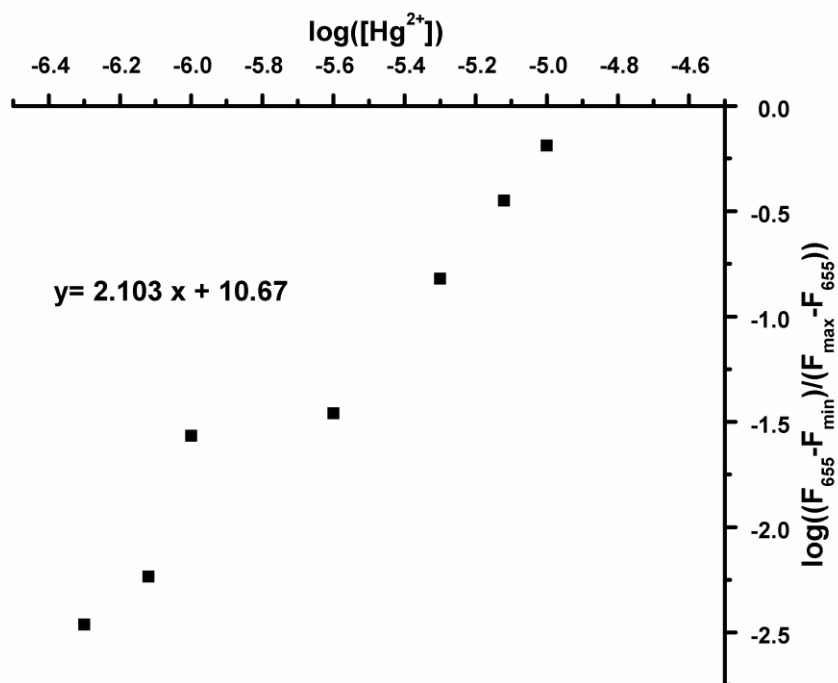


Figure 76 Logarithmic value for the fluorescence intensity of dye at 655 nm versus $\log [\text{Hg}^{2+}]$. Hill coefficients (2.1038) fits with 1:2 coordination of dye- Hg^{2+}

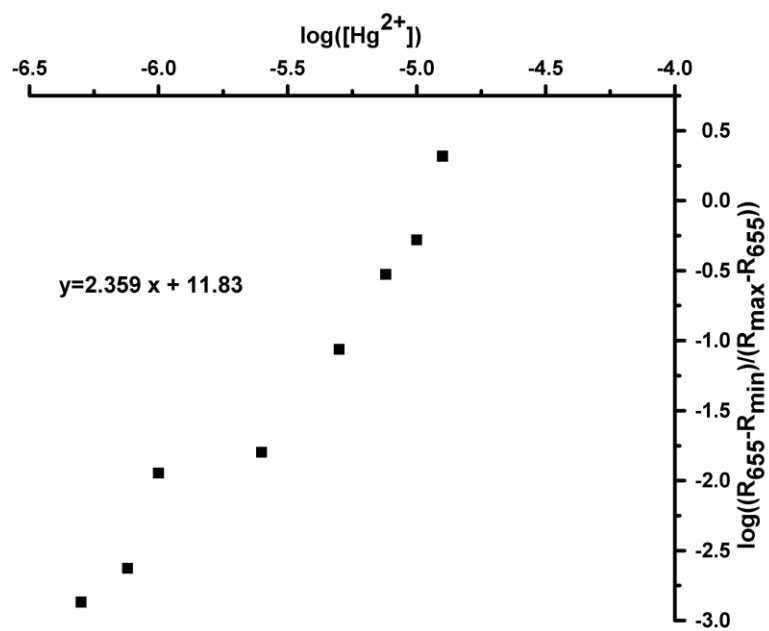


Figure 77 Logarithmic value for the fluorescence intensity ratio of dye at 655 and 720 nm versus $\log [Hg^{2+}]$. Hill coefficients (2.3598) fits with 1:2 coordination of dye- Hg^{2+} .

3.3 Ratiometric Analysis Of Hg(II) With Near-IR Fluorescent Chemosensor via Energy-Transfer System, 75

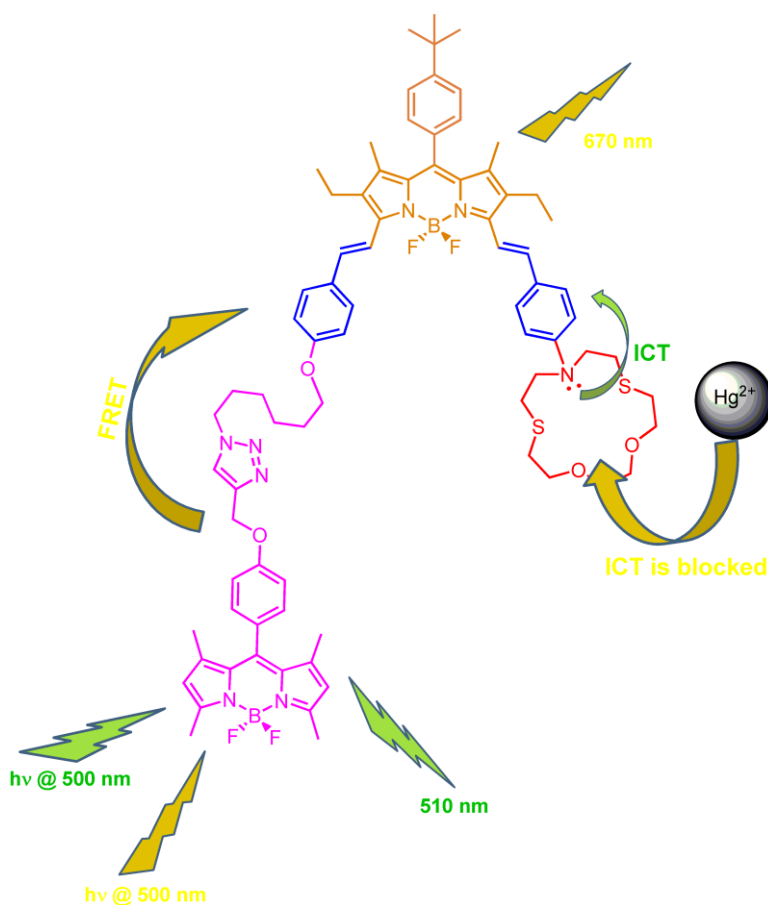


Figure 78 Structural representation of working scheme for Hg²⁺ selective FRET based near-IR BODIPY dye, 75. Green color indicates the process where no interaction exists between dye and metal cation. Yellow color represents the process where an interaction is provided between dye and metal.

In this work we present the synthesis, characterization and spectral studies of a novel Hg^{2+} selective chemosensor. A diverse strategy is used to afford this chemosensor. This modulating chemosensor consists of two fluorophore and a selective ligand. This two fluorophore are based on BODIPY unit in consideration of its photophysical properties such as large Stokes shift, sharp absorption and emission spectrum, high extinction coefficients and also versatile modification. One, on the trunk, is enhanced with extended conjugation at methyl groups which are next to BF_2 bridge unit on the BODIPY core with stepwise reactions with distinctive aldehyde to yield a near-IR dye. One arm on this main core comprise dithia-dioxa-mono aza crown-ether moiety (represented as red color in figure 78) which has specific recognition ability to the Hg^{2+} ion. ICT process was presented with this extended conjugation. Moreover, second arm is extended with a different aldehyde to yield near-IR dye and to yield more reactions on the core. 4-(6-azidohexyloxy)benzaldehyde has chosen to achieve the desired product for the second arm modification. Second fluorophore is synthesized with standard BODIPY procedure, in which 4-(prop-2-ynoxy)benzaldehyde and 2,4-dimethyl pyrrole are used as reactants, and attached to the main BODIPY core through the second arm with click chemistry in appropriate conditions and yielded completely to the product (represented as purple color in figure 78). The combination of these two fluorophore is presented to achieve energy transfer process from shorter wavelength absorption, corresponds to the second dye (assigned as a purple color in figure 78), to longer wavelength absorption dye, corresponds to first dye (represented as orange color in figure 78). The connection of these two fluorescent probes are achieved with a long carbon chain thus a Förster type energy transfer is presented. This energy transfer and ICT process results in a ratiometric

fluorescent chemosensor with large Stokes shift result in three different wavelength observation.

The characterization of the products were presented in both ^1H - and ^{13}C NMR spectrum. The characterization is also strengthened with mass spectrum. Triazole proton and trans coupled ethylene protons of the targeted dye are easily assigned in ^1H -NMR spectrum. The evidence of energy transfer and sensitivity and selectivity to Hg^{2+} cation is reinforced with absorption and emission spectrum in THF.

The absorption spectra of the compound show two distinct maxima at 490 nm and 690 nm. The shorter absorption wavelength at 490 nm corresponds to the donor fluorescent probe, second fluorophore, meanwhile the longer wavelength at 690 nm harmonize to the acceptor fluorescent probe, numbered as 1 (Figure 79).

When metal ion conjugates to the metal chelator, the electron density of dithia-dioxa-mono aza crown-ether chelator is decreased, thus electron donating ability of the amine in the chelating moiety is decreased. Consequently, ICT process from donor to acceptor is interrupted with coordination of Hg^{2+} to the metal chelator. This indication is established with absorption spectrum in which the absorption maxima of the first dye shifts to the blue ~ 40 nm with coordination of Hg^{2+} to the metal chelator and significant color change from green to blue could be observed easily by naked eye (Figure 79). No changes are observed at absorption maxima of the second fluorophore in whole analysis and also addition of metals, except than Hg^{2+} in THF, do not change the absorption maxima of the first fluorophore as illustrated in figure 79.

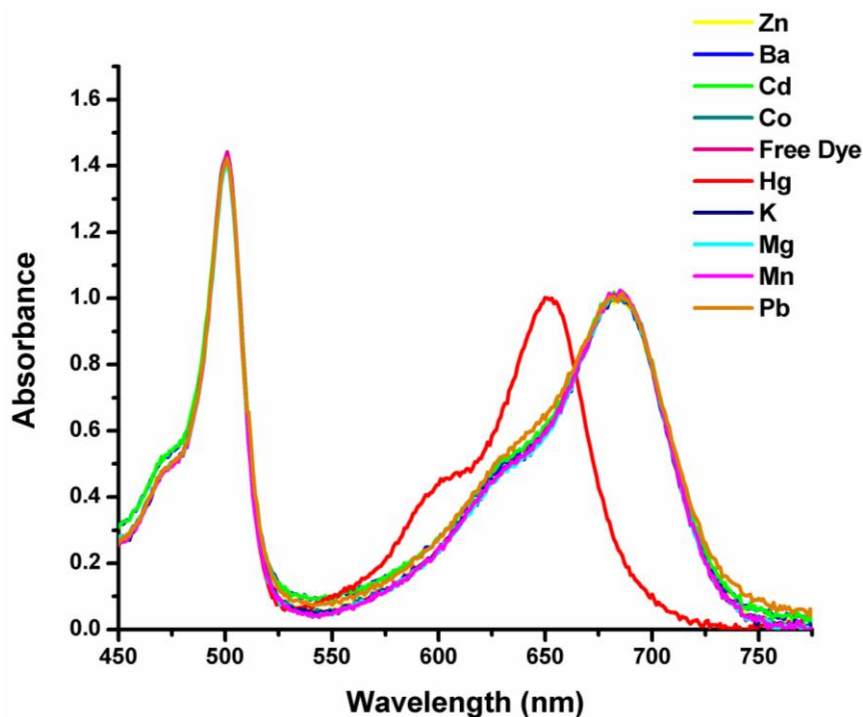


Figure 79 Absorption spectra of the dye **75** (1,5 μM) in the presence of some selected metal cations (20 μM) in THF.

The fluorescent spectral properties of dye were also investigated in THF solution. Free ionophore showed characteristic emission peaks of BODIPY at 510 nm and 730 nm for second and first dye, respectively, when excitation was done at 500 nm. Meanwhile free dye numbered as 1 displayed very weak fluorescence because of very low energy transfer from donor dye results in absence of a well overlapping between emission wavelength of the donor and absorption wavelength of the acceptor dye. Fluorescent measurements of dye with various metal ions displayed excellent selectivity for Hg^{2+} as shown in figure 80. Energy transfer process from donor to acceptor is enhanced with addition of Hg^{2+} . It is observed as a decrease in intensity of the second dye at

510 nm with increase in intensity of the first dye with a new fluorescence emission maxima at 660 nm, following the intensity of the fluorescent peak at 730 nm decreases. Other metal ions do not induce any changes in the fluorescence spectrum of this well-designed dye.

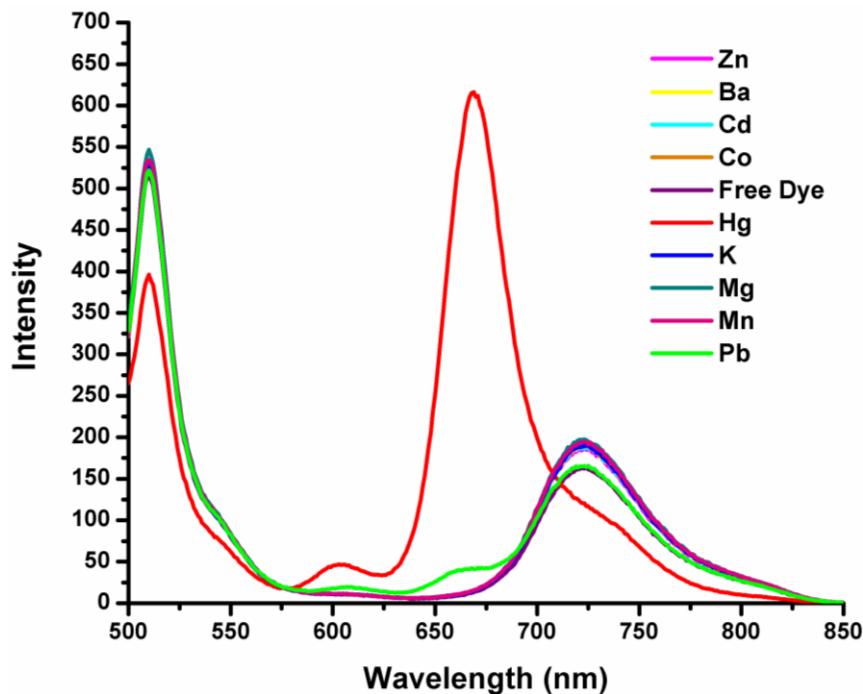


Figure 80 Fluorescence spectrum of the dye (1.5 μM) with various cation (10.0 μM). Excitation was done at 500 nm with a slit width 5.0 nm.

The interaction of Hg^{2+} and dye is also performed by measuring the fluorescence ratio at 670 nm and 510 nm, respectively. This facts distinctly indicates that an intramolecular FRET is increasing with the coordination of Hg^{2+} cation to receptor moiety. Coordination of Hg^{2+} to the receptor increase the fluorescence ratio of the dye at 670 nm (corresponds to first dye) and 510 nm

(corresponds to second dye) from 0.029 to 1.54 by 54-fold enhancement (figure 81).

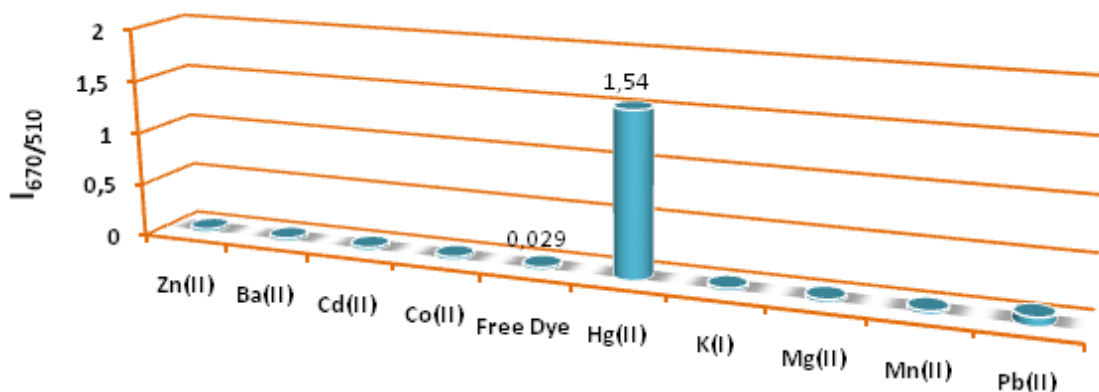


Figure 81 Fluorescence intensity ratio at 670 nm and 510 nm of the dye with responds to metal interaction in THF solution.

An other measurement performed by the fluorescence ratio of the dye at 670 nm and 720 nm, respectively. It is obviously performed that fluorescence wavelength of the first dye is shifted to 670 nm with a decrease in the emission intensity at 720 nm following the coordination of the Hg^{2+} cation with respect to the metal-free dye. No changes was observed with the addition of metals other than Hg^{2+} . In the presence of Hg^{2+} , the ratio of emission intensity ratio at 670 nm and 720 nm ($I_{670/720}$) varied from 0.092 to 5.08, corresponding to a 55-fold enhancement.

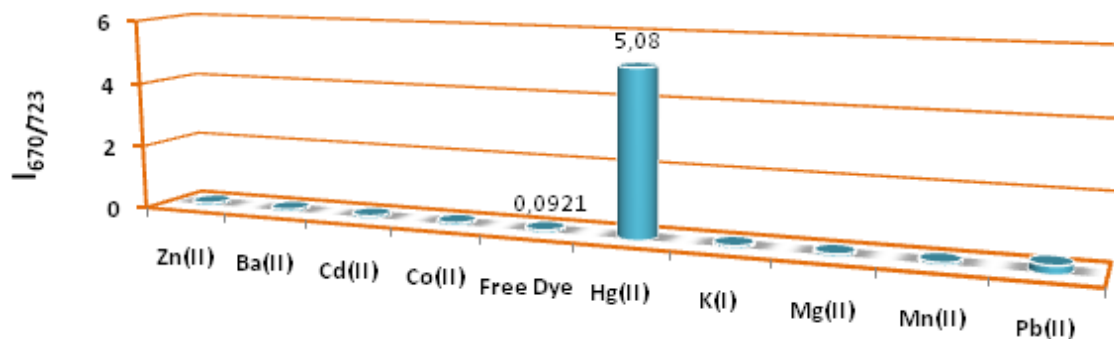


Figure 82 Fluorescence ratio of the dye at 670 nm and 723 nm corresponds to metal cation interactions.

Fluorescence response of the dye in the presence of Hg^{2+} ($10 \mu\text{M}$) with competing cation ($20 \mu\text{M}$) is presented in Figure 83. Consequently, the fluorescence intensity of the dye is unaffected and it is obviously observed that presence of any metal other than Hg^{2+} is not influence the coordination of this cation to the receptor moiety.

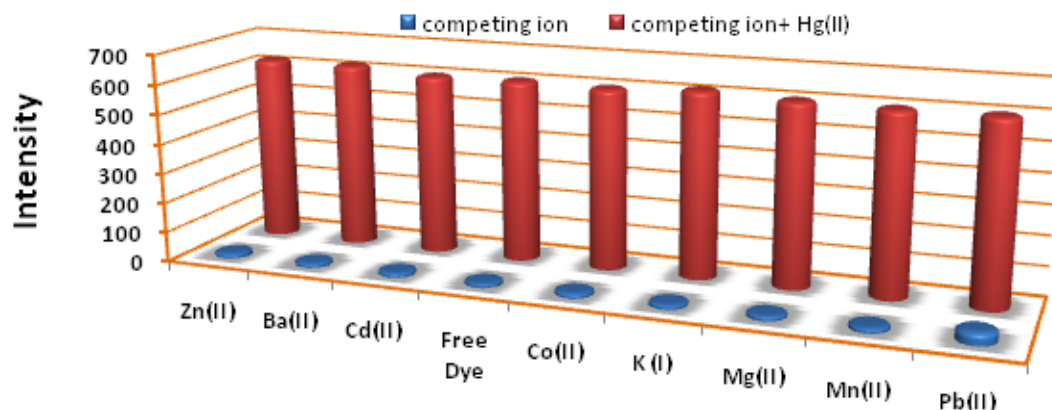


Figure 83 Results of the competition experiments between Hg(II) and selected metal ions. The free dye **75** (chemosensor) concentration was set at $1.5 \mu\text{M}$, the concentration of the competing cation 100 mM and concentration of Hg^{2+} was 10 Mm . Excitation was at 500 nm with a slit width 5.0 nm .

Gradual addition of metal ion ($0 \mu\text{M}$ to $15 \mu\text{M}$), (Figure 84) to the dye solution was performed and it is observed that the absorption band of the near-IR emitting dye is shifted from 690 nm to 650 nm . The band at 690 nm is decreasing with increasing metal ion concentration, which is leading to a new band centered at 650 nm as a result of coordination of mercury cation to receptor moiety, with an isosbestic point at 670 nm . In whole analysis of the absorbance studies with this dye, as expected, no change was observed on the absorption maxima of the second dye on the main core of the dye as illustrated in Figure 84. The absorbance maximum at 500 nm remains firm whatever the nature of the cations added to the dye solution in whole analysis.

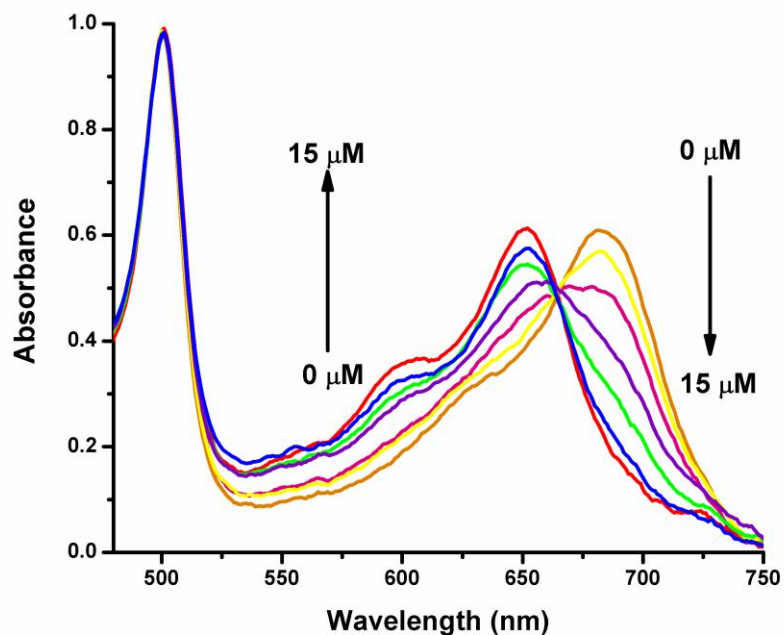


Figure 84 Absorption spectrum of the dye **75** ($1.5 \mu\text{M}$) with increasing concentration of Hg^{2+} in THF. Hg^{2+} concentration is varied from 0 to $15 \mu\text{M}$.

Spectral studies for fluorescent measurements due to increasing concentration of mercury from $0 \mu\text{M}$ to $15 \mu\text{M}$ is also performed as shown in figure 85. FRET process is exerted with the excitation wavelength at 500 nm , corresponds to second dye excitation wavelength. When titrated by mercury cation the emission intensity of the metal free form of the dye at 725 nm decreased with the concomitant increase in emission maxima at 670 nm . The emission intensity is 4 fold increasing following addition of Hg^{2+} cation with respect to metal free form of the dye with a hypsochromic shift $\sim 80 \text{ nm}$ when excitation was done at 500 nm . At the same time it is obviously observed that

with the coordination of metal, a decrease in the emission maxima of the second dye and increase in the emission intensity of the first dye is pointed results in the increase in the efficiency of the energy transfer from donor to acceptor.

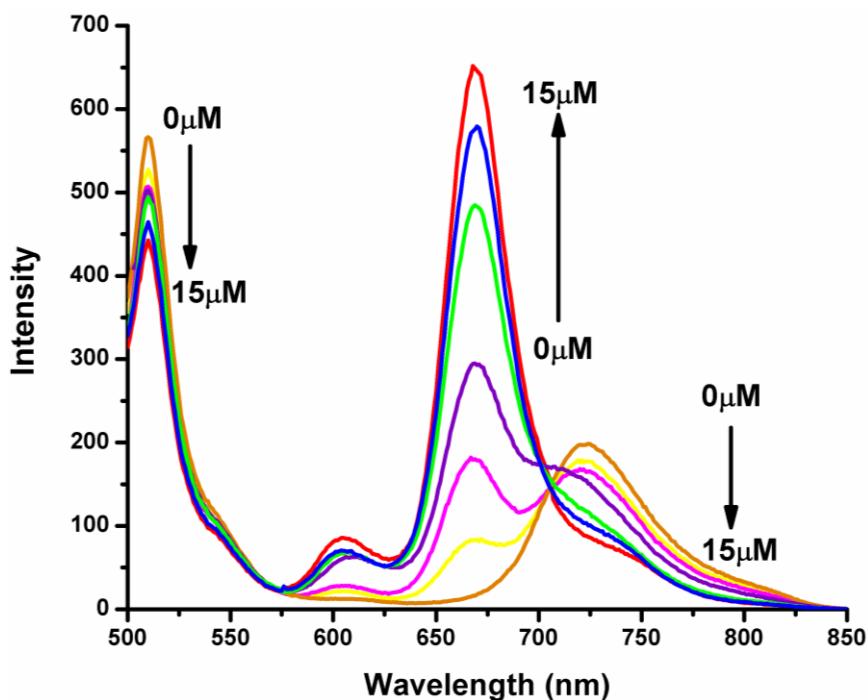


Figure 85 Change in the emission spectrum of the dye in response to the increasing concentration of Hg^{2+} in THF. Cation concentration is varied from 0 to 15 μM . Excitation was done at 500 nm with a slit width 5.0 nm.

To illustrate the energy transfer process a fluorescence study was done. In this study BODIPY dye (mentioned as a second dye), dye **75** and dye+ Hg^{2+} was examined individually with the same concentration, 1.0 μM . It is observed that BODIPY dye has very high fluorescence with respect to dye **75** and dye+ Hg^{2+} . It is obviously seen that coordination of second dye to first dye via

click chemistry relatively affects the emission intensity of the second dye as a result in energy transfer process through the first dye. (Figure 86)

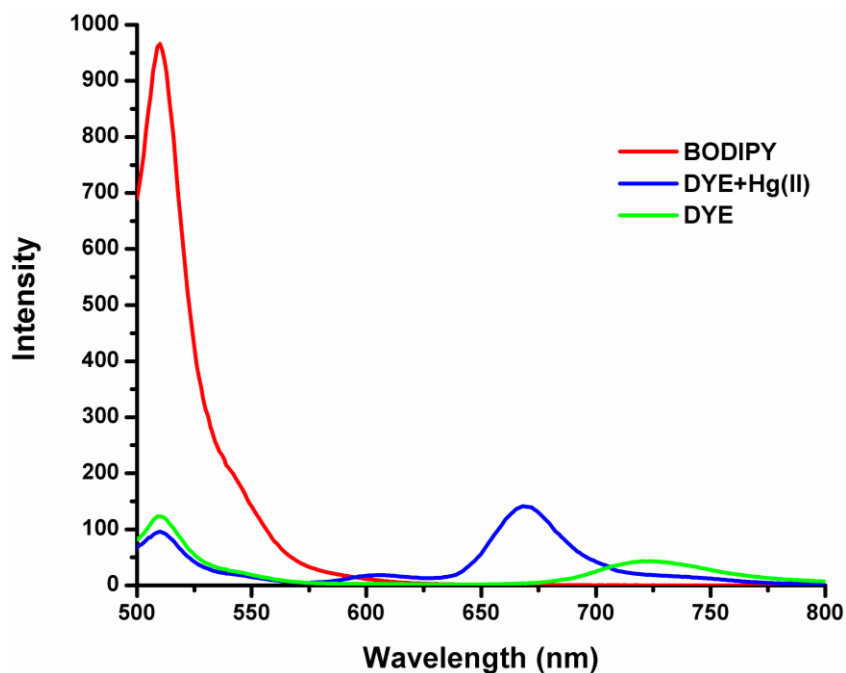


Figure 86 Demonstration of energy transfer with fluorescence intensity of BODIPY, dye **75** and dye+Hg²⁺.

Titration experiment was applied to calculate the dissociation constant and Hill coefficient. Dissociation constant was calculated from figures 89 and 90 and it is 3.1×10^{-6} . Logarithmic graphs present the Hill coefficient of the complexation of dye with metal, 1:1 as expected (figure 87).

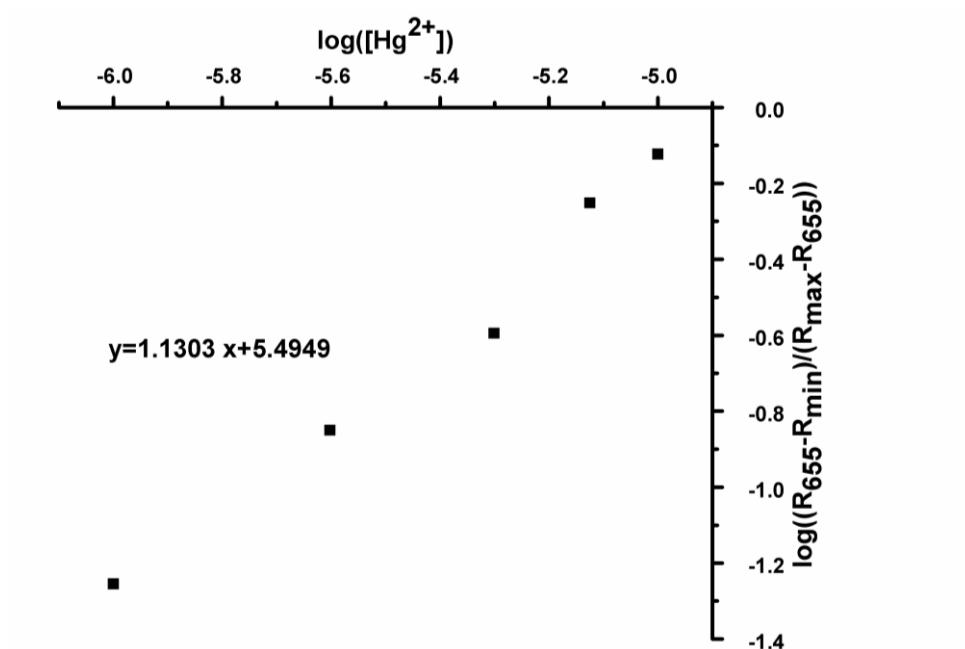


Figure 87 Logarithmic value for the fluorescence intensity ratio of dye 75 at 670 and 725 nm versus $\log[\text{Hg}^{2+}]$. A Hill coefficient (1.13) fits with 1:1 coordination of dye- Hg^{2+}

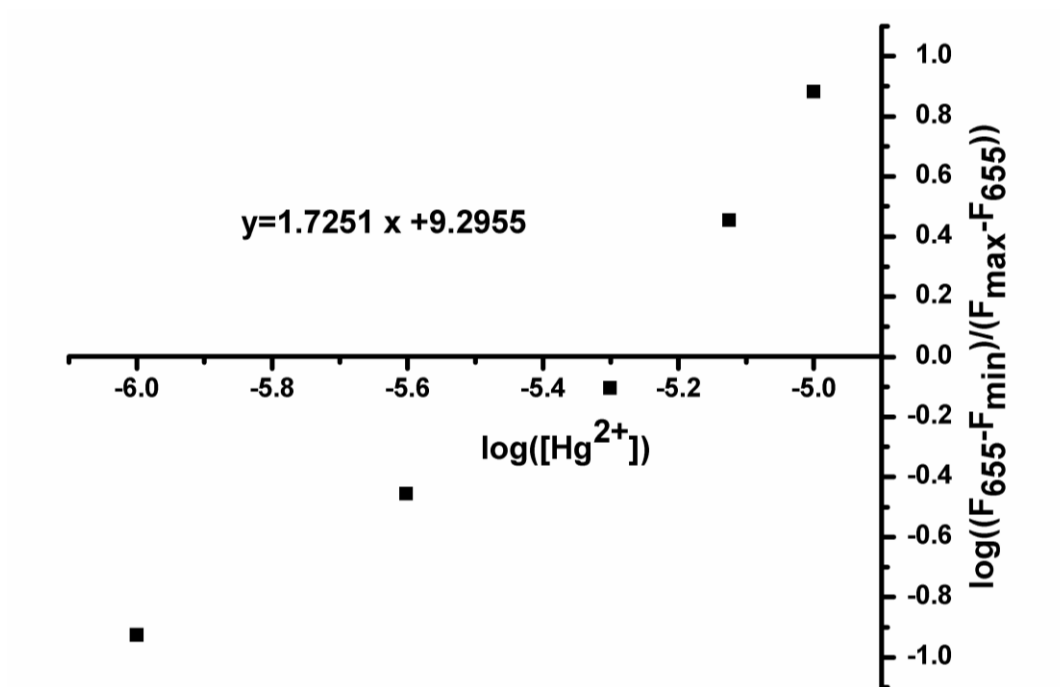


Figure 88 Logarithmic value for the fluorescence intensity of dye **75** at 670 nm versus $\log[Hg^{2+}]$.

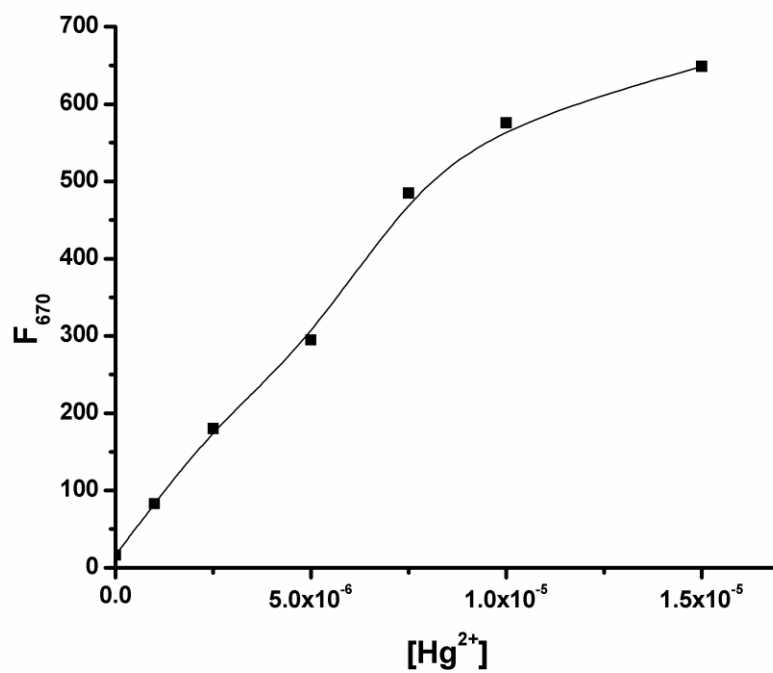


Figure 89 Curve represents the fluorescence intensity of the dye (1.5 μM) at 670 nm versus increasing concentration of Hg^{2+} . The dissociation constant was calculated as 3.1×10^{-6} M.

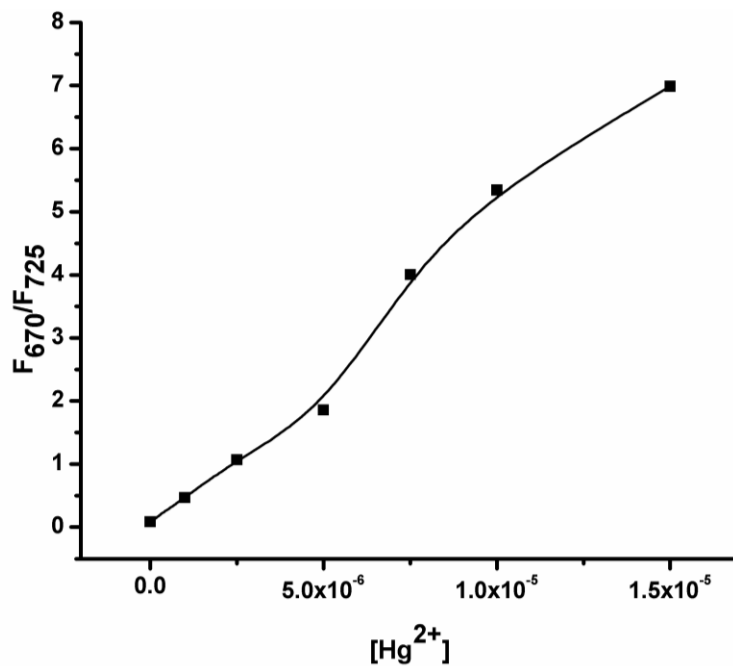


Figure 90 Curve of fluorescence intensity ratio at 670 nm and 725 nm of the dye versus increasing concentration of Hg^{2+} . The concentration of the dye was 1.5 μM . Dissociation constant was calculated as 3.2×10^{-6} .

CHAPTER 4

CONCLUSION

In conclusion, we have demonstrated that versatile BODIPY chemistry allows the synthesis of long wavelength emitting at the methyl groups 3 and 5 positions of the BODIPY core. Thus multiple groups, with same functional groups or distinct functional groups, can be easily placed on the BODIPY core to achieve effective chemosensors.

Considering the zinc selective chemosensor, **56**, two distinct functional groups were placed on the BODIPY core, one part is modulated as receptor moiety for cation and the other part is functionalized for water solubility. This type of BODIPY core has been synthesized for the first time.

Modulation with the same functional group strategy leads us to synthesize a novel chemosensor, **64**. Modulation on double-armed BODIPY dye is first time synthesized and results to a new type of near-IR emitting fluorescent chemosensor. ICT process is easily applied to this new dye.

We have also demonstrated a new type-FRET based fluorescent chemosensor, **75**, for Hg^{2+} that execute well selectivity over the other metal cations with a new strategy on versatile BODIPY core. A remarkable change in two different absorption wavelength and three different emission wavelengths were clearly presented.

A novel biologically important and feasible BODIPY with near-IR emitting wavelength was presented to be a prototype for other applications based on BODIPY core. These innovative strategies based on BODIPY chemistry is expected to lead new practical fluorescent chemosensors in years to come.

REFERENCES

1. Morrison LE, Stols LM. *Biochemistry*, 1993, 32:3095–3104.
2. Gardner SJ, Hewlett DF. *J Forensic Sci*, 2003, 48(6):1–5
3. Gambetta GA, Lagarias JC. *Proc Natl Acad Sci USA*, 2001, 98(19):10566–10571.
4. Heller CA, Henry RA, McLaughlin BA, Bliss DE. *J Chem Eng Data* 1974, 19(3):214–219.
5. Ford GW, Weber WH. *Phys Rep* 1984, 113:195–287.
6. Klonis N, Wang H, Quazi NH, Casey JL, Neumann GM, Hewish DR, Hughes AB, Deady LW, Tilley L. *J Fluoresc* 2001, 11(1):1–11.
7. Chen RF. *Anal Biochem* 1967, 19:374–387.
8. Axelrod D, Hellen EH, Fulbright RM. Vol. 3: *Biochemical applications*, 1992, pp. 289–343. Ed JR Lakowicz. Plenum Press, New York.
9. Lindstrom CD, *Chem. Rev*, 2006, 106 (10), 4281-4300
10. Kavarnos GJ. 1993. *Fundamentals of photoinduced electron transfer*. VCH Publishers, New York.

11. Kumbhakar M, Nath S, Rath MC, Mukherjee T, Pal H. Photochem Photobiol 2004, 74(1):
12. Pal SK, Bhattacharya T, Misra T, Saini RD, Ganguly T. J Phys Chem A 2003, 107:10243– 10249.
13. Knibbe H, Rehm D, Weller A. Ber Bunsenges, 1968, 72(2):257–263.
14. Rubstov IV, Shirota H, Yoshihara K., J. Phys. Chem A, 1999,103:1801–1808.
15. Vos R, Engelborghs Y. Photochem Photobiol 1994, 60(1):24–32.
16. Ricci RW, Nesta JM. J Phys Chem, 1976,80(9): 974–980.
17. Evans RF, Kuntz RR, Volkert WA, Ghiron CA. Photochem Photobiol, 1978, 27: 511-515
18. Vos R, Engelborghs Y. Photochem Photobiol, 1994, 60(1):24–32.
19. Valeur B, Molecular Fluorescence; principles and applicaitons. 298-307
20. Lakowicz J.R. Principles of Fluorescence spectroscopy (Third Edition). 443-445
21. Parkhurst KM, Parkhurst LJ. J Biomed Opt 1996, 1(4):435–441.

22. Förster Th. *Ann Phys (Leipzig)* 1948, 2:55–75.
23. Clegg RM, Wang Ed XF, Herman B. John Wiley & Sons, New York 1996.
24. Cheung HC. *Biopolymers* 1991, 13:1573–1605. 13
25. Fabian J, Zahradnik R, *Angew. Chem., Int. Ed. Engl.* 1989,
26. Frangioni JV, *Curr. Opin. Chem. Biol.*, 2003, 7, 626;
27. Sevick-Muraca E. M, Houston J. P, Gurfinkel M, *Curr. Opin. Chem. Biol.*, 6, 2002, 642;
28. Sun C, Yang J, Li L, Wu X, Liu Y, Liu S, , *J. Chromatogr. B*, 2004, 803, 173;
29. Funovics M, Weissleder R, Tung CH, *Anal. Bioanal. Chem.*, 2003, 377, 956;
30. Haugland RP, *Handbook of Fluorescent Probes and Research Chemicals*, 6th ed, 1996, Molecular Probes, Eugene,
31. Ntziachristos V, Ripoll J, Weissleder R, *Opt. Lett.*, , 2002 27, 333.
32. Sowell J, Strekowski L, Patonay G, *J. Biomed. Opt.*, 2002, 7, 571.
33. Emmelius M, Pawlowski G and Vollmann HW, *Angew. Chem., Int. Ed. Engl.*, 1989, 28, 1445;

34. Fabian J and Zahradnik R, *Angew. Chem., Int. Ed. Engl.*, 1989, 28, 677;
35. Atilgan S, Ekmekci Z, Dogan AL, Guc D, Akkaya EU, *Chem. Commun.* 2006, 4398–4400
36. Gurfinkel M, Ke S, Wen XX, Li C, Sevick-Muraca EM, *Dis. Markers* 2003, 19, 107 –121.
37. Dekker E, Fockens P, *Eur. J. Gastroenterol. Hepatol.* 2005, 17, 803 –808.
38. Ballou B, Ernst L. A, Waggoner A. S, *Curr. Med. Chem.* 2005, 12,795 – 805.
39. Licha K, Olbrich C, *Adv. Drug Delivery Rev.* 2005, 57, 1087 –1108
40. Wang YB, Yang JH, Wu X, Li L, Sun S, Su BY, Zhao ZS, *Anal. Lett.* 2003, 36, 2063 –2094.
41. Jiang P, Guo Z., *Coord. Chem. Rev.* 2004, 248, 205 –229.
42. Lim NC, Freake HC, BrMckner C., *Chem. Eur. J.* 2005, 11, 38–49.
43. Berg JM, Shi Y., *Science* 1996, 271, 1081 –1085.
44. Kleiner D. *Arch. Biochem. Biophys.* 1974, 165 121–125.

45. Frederickson CJ, Suh SW, Silva D, Thompson RB. *J. Nutr.* 2000, 130 1471–1483.
46. Bush AI, *Trends Neurosci.* 2003, 26, 207-214.
47. Suh SW, Jensen KB, Jensen MS, Silva DS, Kesslak PJ, Danscher G, Frederickson CJ, *Brain Res.* 2000, 852, 274-278.
48. Bush AI, *Alzheimer Dis. Assoc. Disord.* 2003, 17, 147-150.
49. Cuajungco MP, Lees GJ. *Neurobiol Dis*, 1997, 4, 137–169.
50. Rosen DR, Siddique T, Patterson D, Figlewicz DA, Sapp P, Hentati A, Donaldson D, Goto J, O'Regan JP, Deng HX, Rahmani Z, Krizus A, Mckenna-Yasek D, Cayabyab A, Gaston SM, Berger R, Tanzi RE, Halperin JJ, Herzfeldt B, Van den Bergh R, Hung WY, Bird T, Deng G, Mulder DW, Smyth C, Laing NG, Soriano E, Pericak-Vance MA, Haines J, Rouleau GA, Gusella JS, Horvitz HR, Brown RHJ. *Nature*, 1993, 362, 59–62.
51. Fukahori M, Itoh M. *Brain Res*, 1990, 529, 16–22.
52. Cole TB, Robbins CA, Wenzel HJ, Schwartzkroin PA, Palmiter RD. *Epilepsy Res*, 2000, 39, 153–169.
53. Troung-Tran AQ, Carter J, Ruffin RE, Zalewski PD, *Biometals* 2001, 14, 315-330.

54. Frederickson CJ, Kasarskis EJ, Ringo D, Frederickson RE, J Neurosci Methods 1987, 20:91-103.
55. Hendrickson KM, Geue JP, Wyness O, Lincoln SF, Ward AD, J Am Chem Soc 2003, 125:3889-3895.
56. Gee KR, Zhou ZL, Qian WJ, Kennedy R, J Am Chem Soc 2002, 124:776-778.
57. Walkup GK, Burdette SC, Lippard SJ, Tsien RY: J Am Chem Soc 2000, 122:5644-5645.
58. Burdette SC, Walkup GK, Springler B, Tsien RY, Lippard SJ: J Am Chem Soc 2001, 123:7831-7841.
59. Maruyama S, Kikuchi K, Hirano T, Urano Y, Nagano T, J. Am. Chem. Soc. 2002, 124, 10 650 – 10651
60. Mei Y, Bentley PA, Bioorg. Med. Chem. Lett. 2006, 16, 3131 –3134.
61. Silva D, Gunaratne HQN, Gunnlaugsson T, Huxley AJM, McCoy CP, Rademacher JT, Rice TE, Chem. Rev. 1997, 97, 1515 –1566.
62. Dongen EMWM, Dekkers LM, Spijker K, Meijer EW, Klomp LWJ, Merkx M, J. Am. Chem. Soc. 2006, 128, 10 754 – 10762.
63. Sclafani JA, Maranto MT, Sisk TM, Van Arman SA, Tetrahedron Lett. 1996, 37, 2193 –2196;

64. Wu DY, Xie LX, Zhang CL, Duan CY, Zhao YG, Guo ZJ, Dalton Trans. 2006, 3528 – 3533.
65. Silva D, Zavaleta A, Baron DE, Allam O, Isidor EV, Kashimura N, Percarpio JM, Tetrahedron Lett. 1997, 38, 2237 –2240.
66. Haugland RP, Handbook of Fluorescent Probes and Research Products, 9th ed., Molecular Probes Inc., Eugene, 2002.
67. Lakowicz JR, Principles of Fluorescence Spectroscopy, 2nd ed. Kluwer Academic/Plenum, New York, 1999.
68. Lim NC, BrMckner C, Chem. Commun. 2004, 1094 –1095;
69. Dilek G, Akkaya EU, Tetrahedron Lett. 2000, 41, 3721 –3724.
70. Maruyama S, Kikuchi K, Hirano T, Urano Y, Nagano T, J. Am.Chem. Soc. 2002, 124, 10 650 – 10651;
71. Kiyose K, Kojima H, Urano Y, Nagano T, J. Am. Chem. Soc. 2006, 128, 6548 –6549.
72. Nendza M, Herbst T, Kussatz C, Gies A, Chemosphere 1997, 35, 1875.
73. Renzoni A, Zino F, Franchi E, Environ. Res., Sect. A 1998, 77, 68.
74. Boening DW, Chemosphere 2000, 40, 1335.

75. Malm O, *Environ. Res., Sect. A* 1998, 77, 73.
76. Mercury Update: Impact of Fish Advisories. EPA Fact Sheet EPA 823-F-01-011; EPA, Office of Water: Washington, DC, 2001.
77. Gustin MS, Coolbaugh, MF, Engle MA, Fitzgerald BC, Keislar RE, Lindberg SE, Nacht DM, Quashnick J, Rytuba JJ, Sladek C, Zhang H, Zehner, RE, *Environ. Geol.* 2003, 43, 339.
78. Chu P, Porcella DB, *Water, Air, Soil Pollut.* 1995, 80, 135.
79. Mason RP, Morel FMM, Hemond HF, *Water, Air, Soil Pollut.* 1995, 80, 775.
80. Celo V, Lean DRS, Scott SL, *Sci. Total Environ.* 2006, 368, 126
81. Mason RP, Reinfelder JR, Morel FMM, *Water, Air, Soil Pollut.* 1995, 80, 915.
82. Harris HH, Pickering IJ, George, G. N. *Science* 2003, 301, 1203.
83. Kraepiel AML, Keller K, Chin HB, Malcolm EG, Morel FMM. *Environ. Sci. Technol.* 2003, 37, 5551.
84. Burger J, Gochfeld M, *Environ. Res.* 2004, 96, 239.

85. Kuwabara JS, Arai Y, Topping BR, Pickering IJ, George GN, Environ. Sci. Technol. 2007, 41, 2745
86. Johnson DW, Lindberg SE, Water, Air, Soil Pollut. 1995, 80, 1069.
87. Forman J, Moline J, Cernichiari E, Sayegh S, Torres, JC, Landrigan MM, Hudson J, Adel HN, Landrigan PJ, Environ. Health Perspect. 2000, 108, 575.
88. Silbergeld EK, Silva IA, Nyland JF, Toxicol. Appl. Pharmacol. 2005, 207-282
89. Forman J, Moline J, Cernichiari E, Sayegh S, Torres JC, Landrigan MM, Hudson J, Adel HN, Landrigan PJ, Environ. Health Perspect. 2000, 108, 575
90. Newby CA, Riley DM, Leal-Almeraz TO, Ethn. Health 2006, 11, 287.
91. Drexler H, Schaller KH, Environ. Res., Sect. A 1998, 77, 124.
92. Factor-Litvak P, Hasselgren G, Jacobs D, Begg M, Kline J, Geier J, Mervish N, Schoenholtz S, Graziano J, Environ. Health Perspect. 2003, 111, 719.
93. Dye BA, Schober SE, Dillon CF, Jones RL, Fryar C, McDowell M, Sinks TH, Occup. Environ. Med. 2005, 62, 368.
94. Magos L, J. Appl. Toxicol. 2001, 21, 1.

95. Pichichero ME, Cernichiari E, Lopreiato J, Treanor J, Lancet 2002, 360, 1737
96. Clarkson TW, Magos L, Myers GJ. New Engl. J. Med. 2003, 349, 1731.
97. Clarkson TW, Magos L, Crit. Rev. Toxicol. 2006, 36, 609.
98. Takeuchi T, Morikawa N, Matsumoto H, Shiraishi Y., Acta Neuropathologica 1962, 2, 40.
99. Harada M, Crit. Rev. Toxicol. 1995, 25, 1.
100. Akagi H, Grandjean P, Takizawa Y, Weihe P, Environ. Res. Sec. A 1998, 77, 98.
101. Eto K, Tokunaga H, Nagashima K, Takeuchi T, Toxicol. Pathol. 2002, 30, 714.
102. Bakir F, Damluji SF, Amin-Zaki L, Murtadha M, Khalidi A, Al-Rawi NY, Tikriti S, Dhahir HI, Clarkson TW, Smith JC, Doherty RA, Science 1973, 181, 230.
103. Amin-Zaki L, Majeed MA, Clarkson TW, Greenwood MR, McKeown-Eyssen GE, Ruedy J, Neims A, Am. J. Epidemiol. 1983, 118, 470.

104. Davidson PW, Myers GJ, Cox C, Shamlaye CF, Marsh DO, Tanner MA, Berlin M, Sloane-Reeves J, Cernichiari E, Choisy O, Choi A, Clarkson TW, Neurotoxicol. 1995, 16. 677.
105. Grandjean P, Weihe P, White RF, Debes F, Environ. Res. Sec. A 1998, 77, 165.
106. Bolger PM, Schwetz BA, New Eng. J. Med. 2002, 347, 1735.
107. Counter SA, Buchanan LH, Toxicol. Appl. Pharmacol. 2004, 198, 209.
108. Kaur P, Aschner M, Syversen T, Neurotoxicol. 2006, 27, 492.
109. Shanker G, Mutkus LA, Walker SJ, Aschner, M. Mol. Brain Res. 2002, 106,
110. Zalups RK, Ahmad S, J. Am. Soc. Nephrol. 2004, 15, 2023.
111. Zalups RK, Lash LH, Toxicol. Appl. Pharmacol. 2006, 214, 88.
112. Kasha M, J. Chem. Phys. 1952, 20, 71.
113. El-Sayed MA, Acc. Chem. Res. 1968, 1, 8.
114. Koziar JC, Cowan DO, Acc. Chem. Res. 1978, 11, 334.
115. Svejda P, Maki AH, Anderson RR, J. Am. Chem. Soc. 1978, 100, 7138.

116. Masuhara H, Shioyama H, Saito T, Hamada K, Yasoshima S, Mataga N, J. Phys. Chem. 1984, 88, 5868.
117. Burrell CN, Bodine MI, Elbjeirami O, Reibenspies JH, Omary MA, Gabbai FP, Inorg. Chem. 2007, 46, 1388.
118. Tsien, R. Y.; Poenie, M. Trends in Biol. Sci. 1986, 11, 450.
119. Costero, A. M.; Andreu, R.; Monrabal, E.; Martínez-Máñez, R.; Sancenón, F.; Soto, J. J. Chem. Soc., Dalton Trans. 2002, 1769. Descalzo, A. B.; Martínez-Máñez, R.; Radeaglia, R.; Rurack, K.; Soto, J. J. Am. Chem. Soc. 2003, 125, 3418.
120. Hennrich, G.; Sonnenschein, H.; Resch-Genger, U. J. Am. Chem. Soc. 1999, 121, 5073.
121. Rurack K, Kollmannsberger M, Resch- Genger U, Daub J, J. Am. Chem. Soc. 2000, 122, 968.
122. Prodi L, Bargossi C, Montalti M, Zaccheroni N, Su N, Bradshaw JS, Izatt RM, Savage PB, J. Am. Chem. Soc. 2000, 122, 6769.
123. Moon SY, Cha NR, Kim YH, Chang SK, J. Org. Chem. 2004, 69, 181.
124. Moon SY, Youn NJ, Park SM, Chang SK, J. Org. Chem. 2005, 70, 2394.
125. Resch U, Rurack K, Bricks JL, Slominski JL, J. Fluorescence 1997, 7, 231.

126. Cha NR, Kim MY, Kim YH, Choe JI, Chang SK, J. Chem. Soc. Perkin Trans. 2 2002, 1193.
127. Rurack K, Resch-Genger U, Bricks J, Spieles M, Chem. Commun. 2000, 2103.
128. Rurack K, Kollmannsberger M, Resch-Genger U, Daub J, J. Am. Chem. Soc. 2000, 122, 968.
129. Kadarkaraisamy M, Sykes AG, Polyhedron 2007, 26, 1323.
130. Rurack K, Resch-Genger U, Bricks JL, Spieles M, Chem. Commun. 2000, 2103.
131. Rurack K, Kollmannsberger M, Resch-Genger U, Daub J, J. Am. Chem. Soc. 2000, 122, 968.
132. Liu B, Tian H, Chem. Commun. 2005, 3156.
133. Wang Z, Zhang D, Zhu D, Anal. Chim. Acta 2005, 549, 10.
134. Kim JS, Choi MG, Song KC, No KT, Ahn S, Chang SK, Org. Lett. 2007, 9, 1129.
135. Feng L, Chen Z, Sensors and Actuators B 2007, 122, 600.
136. Cheung SM, Chang WH, Tetrahedron 2006, 62, 8379.

137. Yuan M, Li Y, Li J, Li C, Liu X, Lv J, Xu J, Liu H, Wang S, Zhu D, *Org. Lett.* 2007, 9, 2313.
138. Wang J, Qian X, Cui J, *J. Org. Chem.* 2006, 71, 4308.
139. Nolan EM, Lippard SJ, *J. Mater. Chem.* 2005, 15, 2778.
140. Nolan EM, Lippard SJ, *J. Am. Chem. Soc.* 2007, 129, 5910.
141. Cheung SM, Chang WH, *Tetrahedron* 2006, 62, 8379.
142. Yuan M, Li Y, Li J, Li C, Liu X, Lv J, Xu J, Liu H, Wang S, Zhu D, *Org. Lett.* 2007, 9, 2313.
143. Gryniewicz G, Poenie M, Tsien RY, *J. Biol. Chem.* 1985, 260, 3440-3450.
144. Coskun A, Akkaya EU, *J. Am. Chem. Soc.*, 2006, 128 (45), pp 14474–14475
145. Haugland RP, in *Handbook of Molecular Probes and Research Products*, Molecular Probes, Inc., Eugene, OR, 9th edn, 2002.
146. Treibs A, Kreuzer F H *Justus Liebigs Ann. Chem.* 1968, 718, 208
147. Van Koeveeringe JA, Lugtenburg, *J. Recl. Trav. Chim. Pays-Bas* 1977, 96, 55.

148. Vos de Wael E, Pardoen JA, Van Koeveringe JA, Lugtenburg, J. Recl. Trav. Chim. Pays-Bas 1977, 96, 306.
149. Boyer JH, Haag AM, Sathyamoorthi G, Soong ML, Thangaraj K, Heteroat. Chem. 1993, 4, 39 – 49.
150. Yogo T, Urano Y, Ishitsuka Y, Maniwa F, Nagano T, J. Am. Chem. Soc. 2005, 127, 12162 – 12163.
151. Rurack K, Kollmannsberger M, Daub J, New J. Chem. 2001, 25, 289.
152. Saki N, Dinc T, Akkaya EU, Tetrahedron 2006, 62, 2721 – 2725.
153. Turfan B, Akkaya EU, Org. Lett. 2002, 4, 2857.
154. de Silva AP, Nimal Gunaratne HQ, Gunnlaugsson T, Huxley AJM, McCoy CP, Rademacher JT, Rice T.E, Chem. Rev. 1997, 97, 1515-1566.
155. Coskun A, Akkaya EU, J. Am. Chem. Soc. 2005, 127, 10464-10465.
156. Coskun A, Deniz E, Akkaya EU, Org. Lett. 2005, 7, 5187-5189.
157. Peng X, Song F, Lu E, Wang Y, Zhou W, Fan J, Gao Y, J. Am. Chem. Soc. 2005, 127, 4170-4171.
158. Karolin J, Johansson LBA, Strandberg L, Ny T, J. Am. Chem. Soc. 1994, 116, 7801-7806.

159. Yilmaz MD, Bozdemir OA, Akkaya EU, *Org. Lett.* 2006, 8, 2871.
160. Dost Z, Atilgan S, Akkaya EU, *Tetrahedron* 2006, 62, 8484 – 8488
161. Atilgan S, Ozdemir T, Akkaya EU, *Org. Lett.*, 2008, 10 (18), pp 4065–4067

APPENDIX A

AUXILIARY

The dissociation constants of the dyes presented in this thesis were studied with the appropriate metal cations with fluorescence intensity ratio in the well matched emission wavelength as illustrated in the figures 64, 65, 74, 75, 89 and 90. These figures obtained with the results in fluorescence intensity values of the titration created by dye and appropriate metal cation. The following equation is used to achieve these graphs.



$$K_s = [ML] / [M] [D]$$

Complexation of metal cation with dye at each concentration represented as, c_M , the fluorescence intensity recorded at two wavelengths (these wavelengths are chosen as where dye is metal free and at the wavelengths where metal is complexed with dye).

$$Y(w_1) = a_{w1} [D] + b_{w1} [MD]$$

$$Y(w_2) = a_{w2} [D] + b_{w2} [MD]$$

The ratiometric measurements consist of R;

$$R = \frac{a_{w1} [D] + b_{w1} [MD]}{a_{w2} [D] + b_{w2} [MD]}$$

For the free dye and fully complexation of dye with metal, the values of R;

$$R_{\min} = \frac{a_{w1}}{a_{w2}} \qquad R_{\max} = \frac{b_{w1}}{b_{w2}}$$

Then;

$$\frac{R - R_{\min}}{R_{\max} - R} \frac{a_{w2}}{b_{w2}} = K_s [M] \quad \Rightarrow \quad \log\left(\frac{R - R_{\min}}{R_{\max} - R}\right) = \log K_s \frac{b_{w2}}{a_{w2}} + \log [M]$$

By plotting the graphs, stability constants, K_s , and binding constants were easily calculated from the sigmodial curves and the slopes.

APPENDIX B

^1H NMR and ^{13}C NMR SPECTRUM

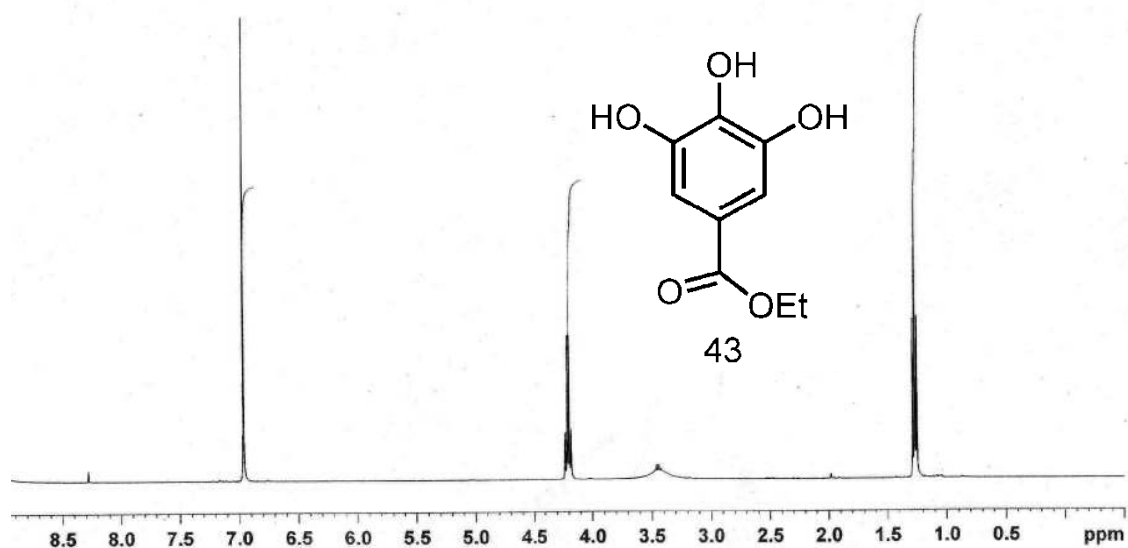


Figure 91 ^1H NMR spectra of the compound 43.

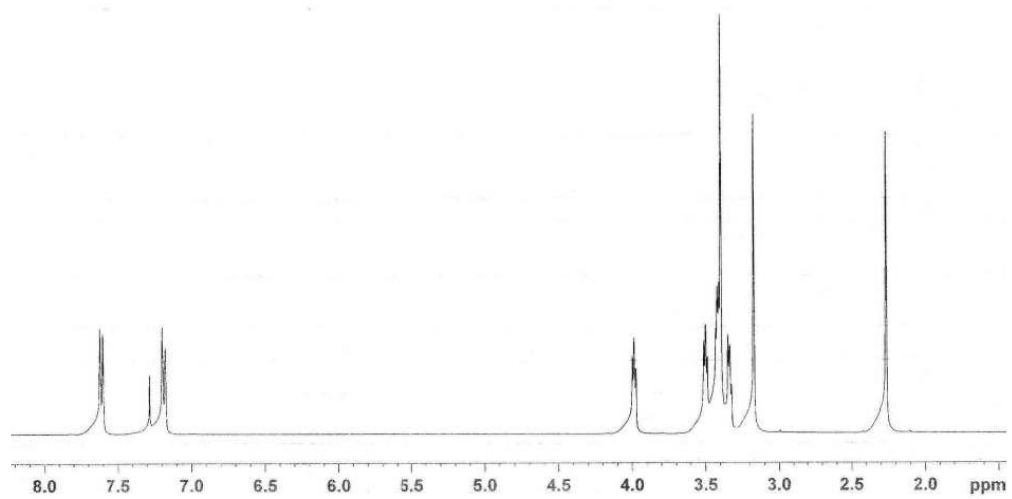


Figure 92 ^1H NMR spectra of the compound **45**

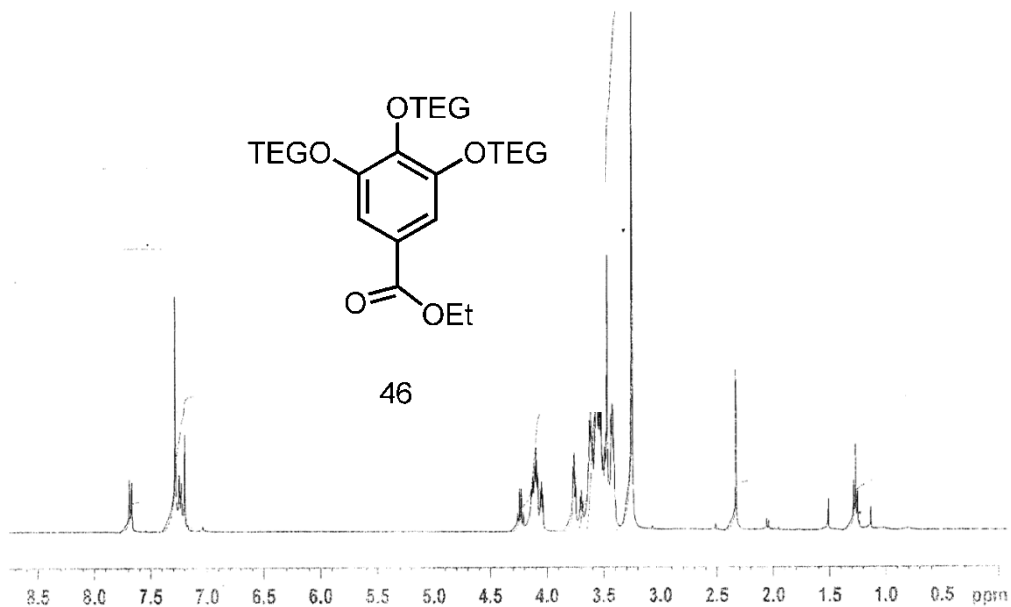


Figure 93 ¹H NMR spectra of the compound 46

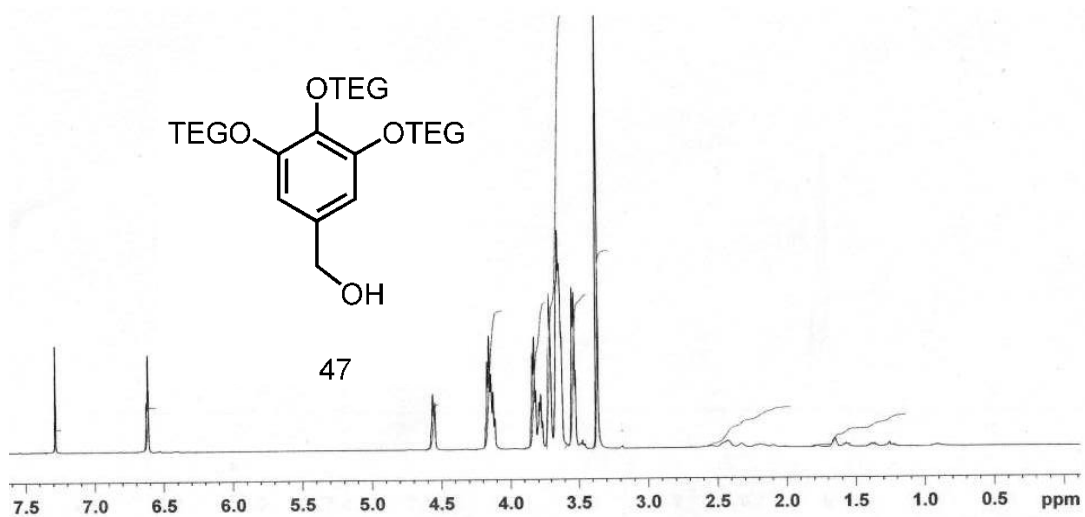


Figure 94 ¹H NMR spectra of the compound 47

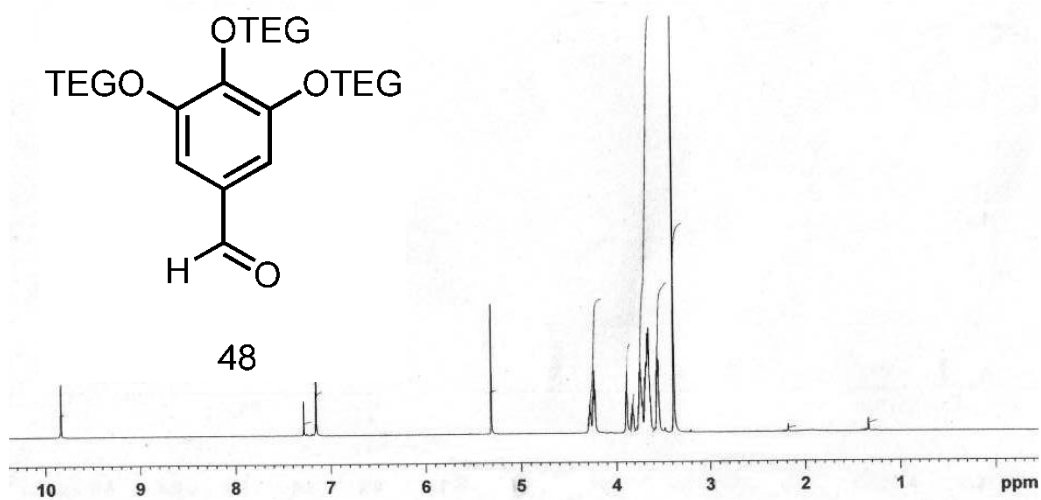


Figure 95 ¹H NMR spectra of the compound 48

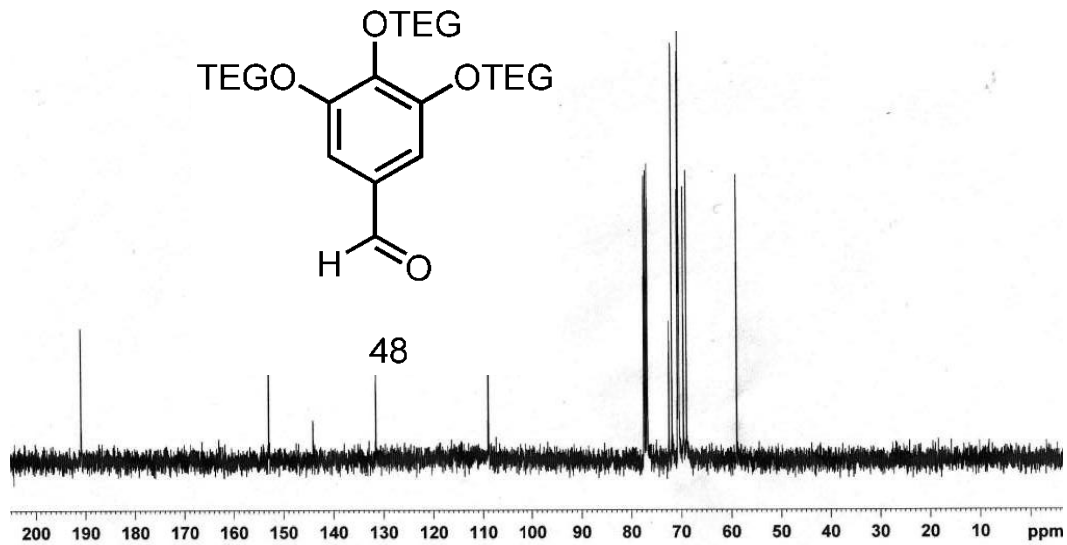


Figure 96 ¹³C NMR spectra of the compound 48

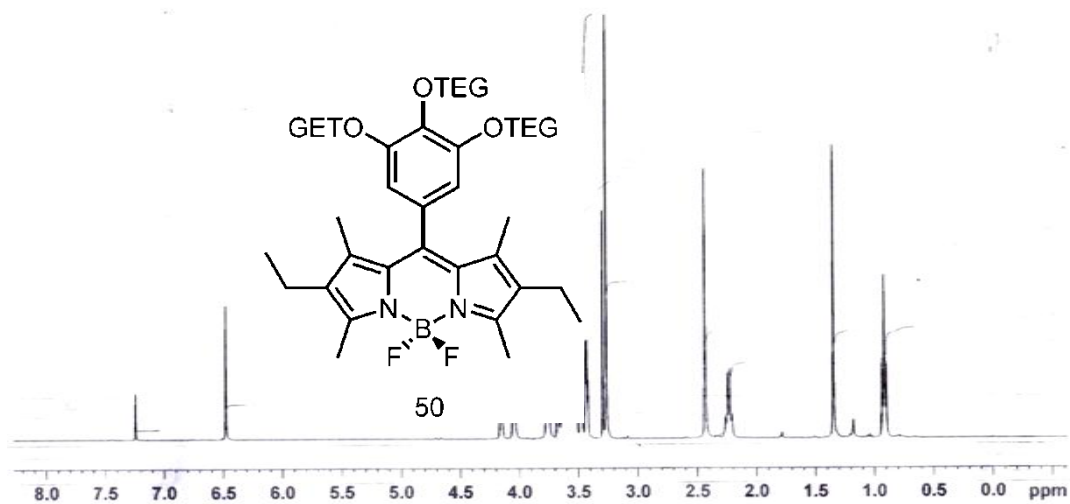


Figure 97 ^1H NMR spectra of the compound 50

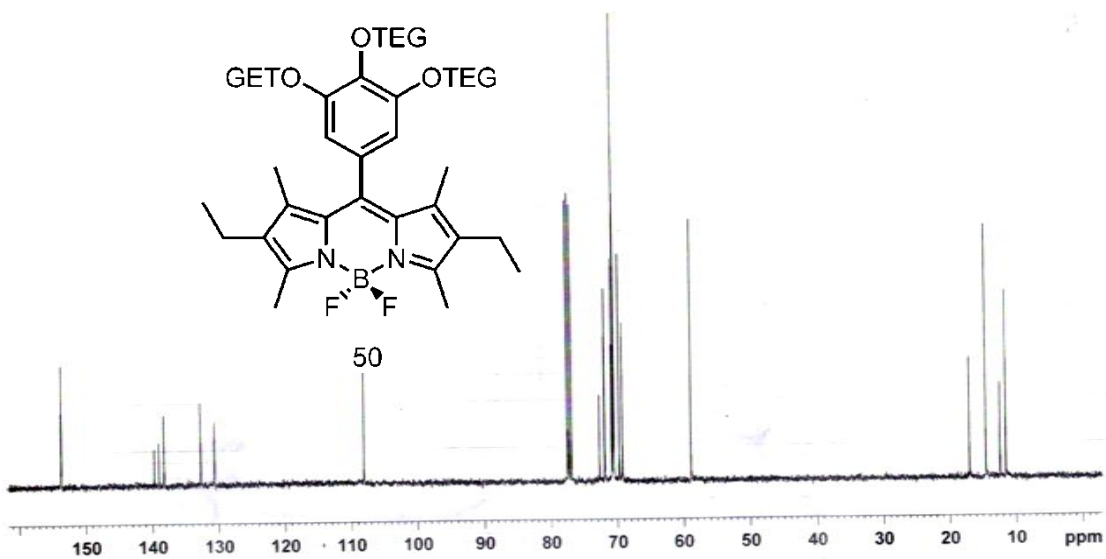


Figure 98 ^{13}C NMR spectra of the compound 50

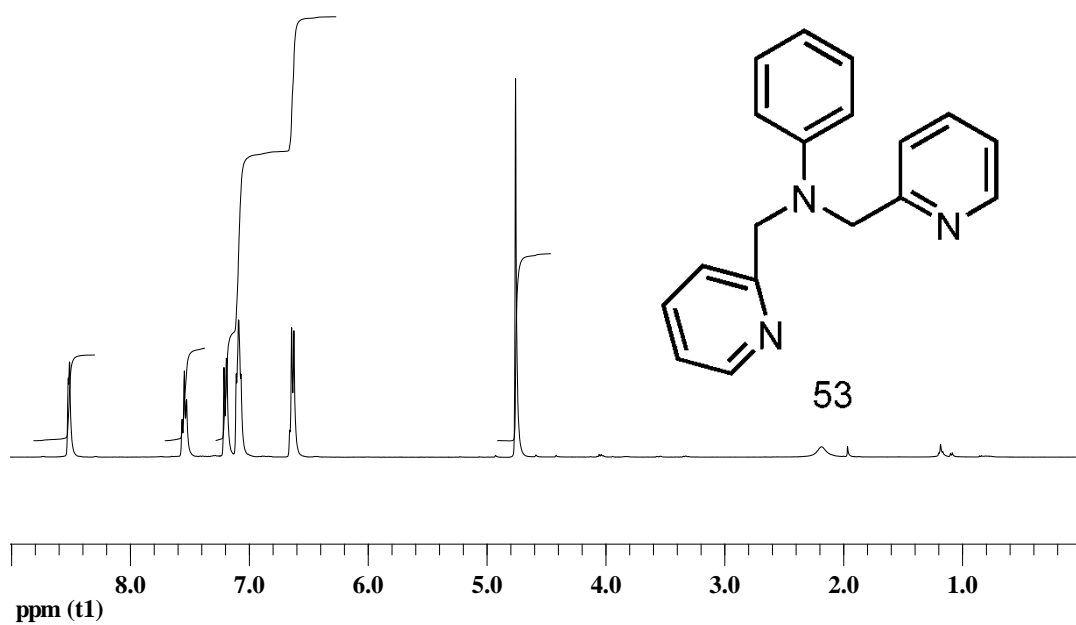


Figure 99 ¹H NMR spectra of the compound 53

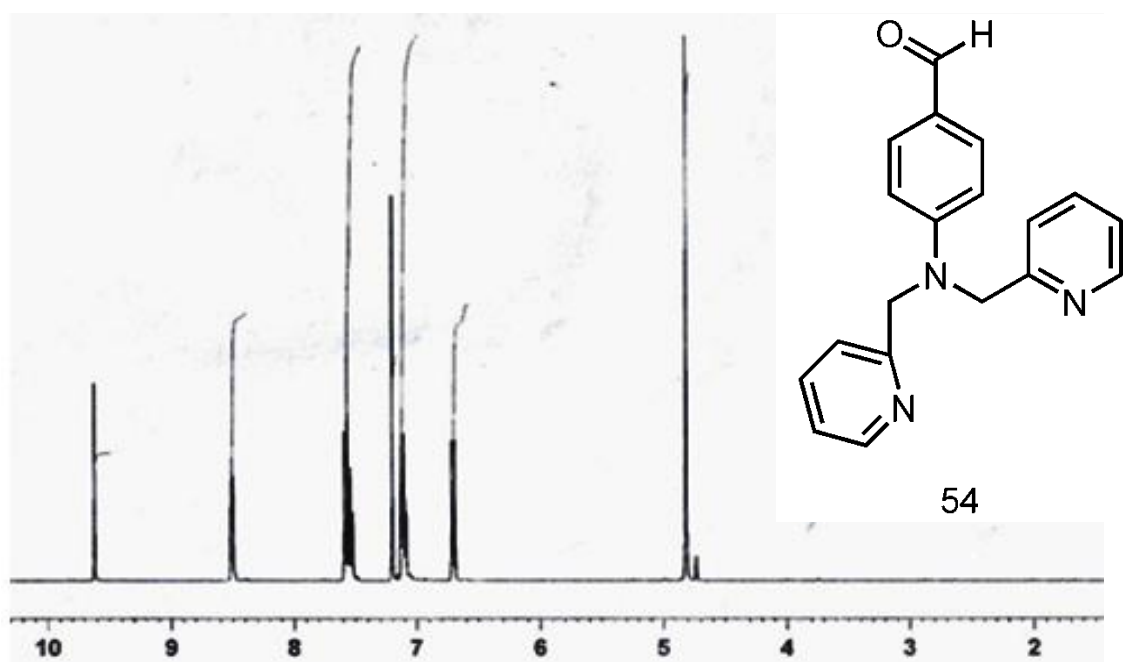


Figure 100 ¹H NMR spectra of the compound 54

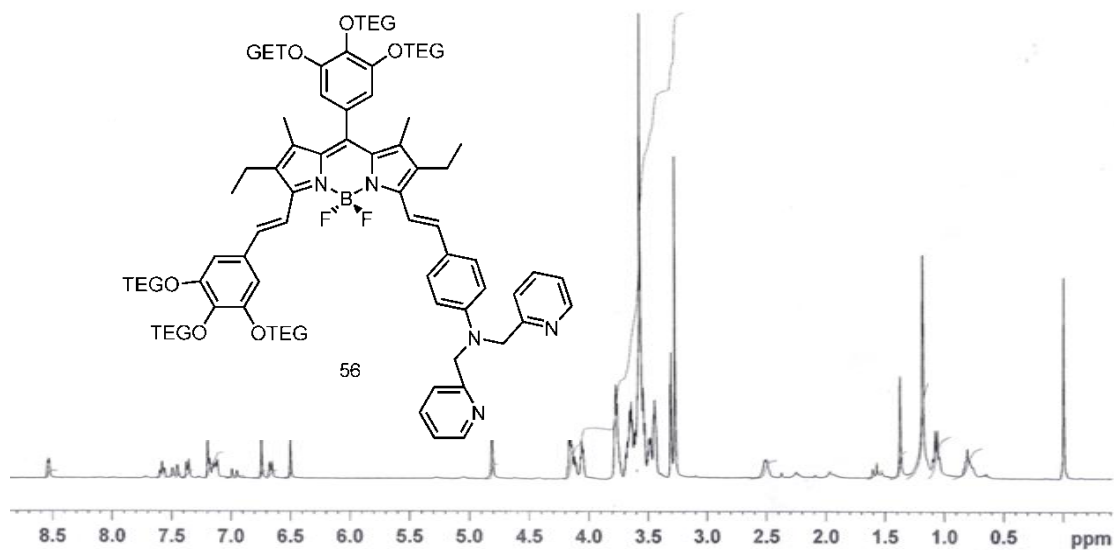


Figure 101 ^1H NMR spectra of the compound **56**

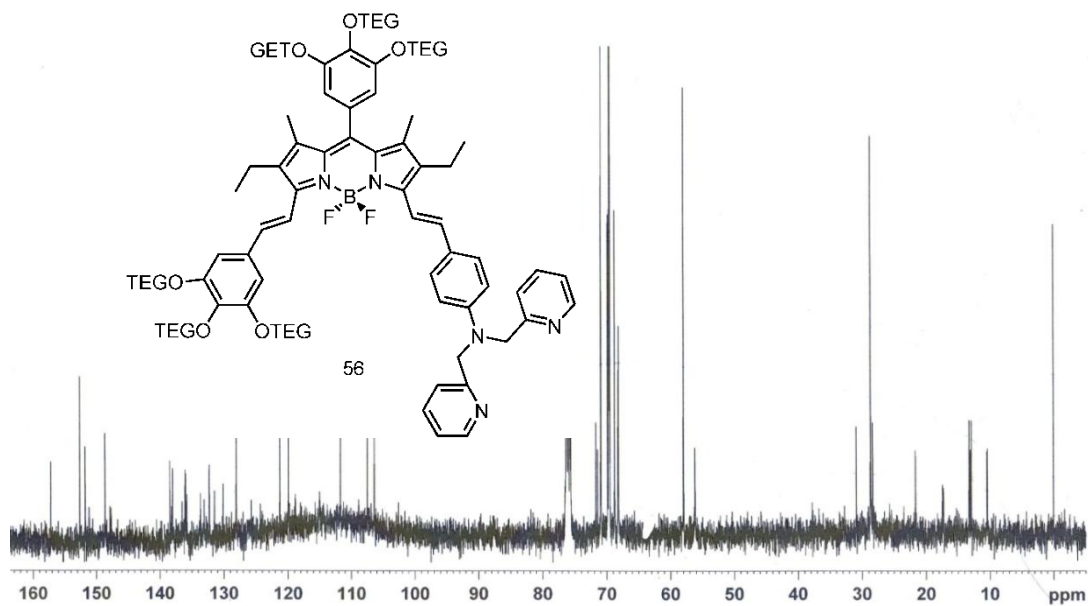


Figure 102 ^{13}C NMR spectra of the compound **56**

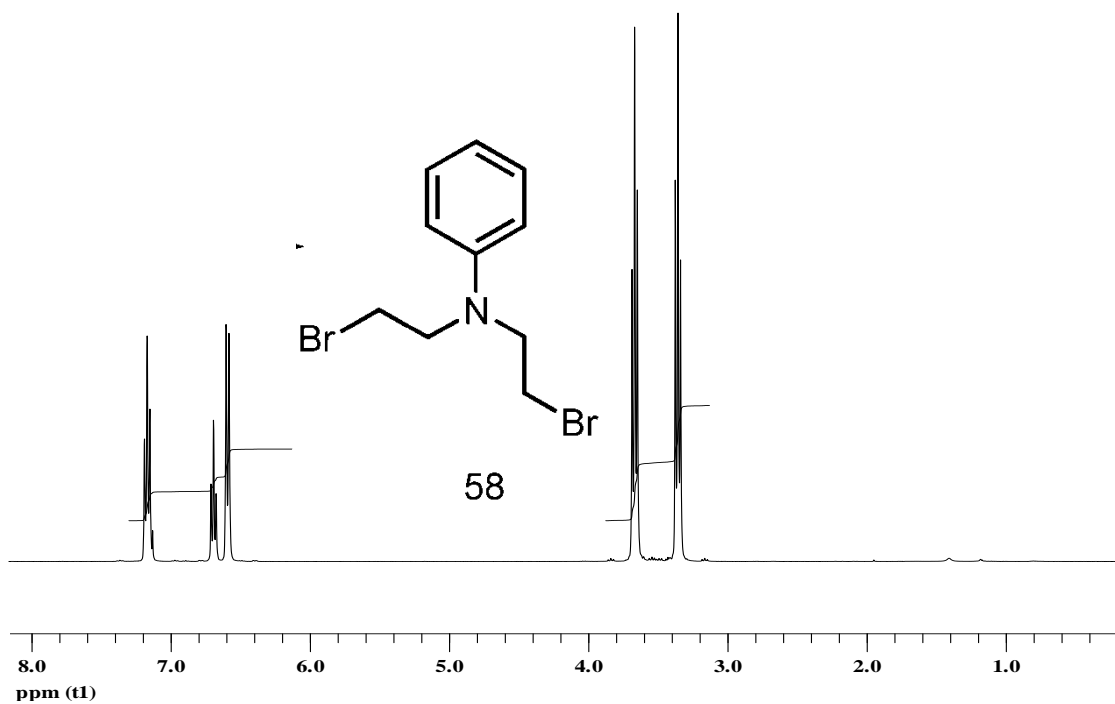


Figure 103 ^1H NMR spectra of the compound **58**

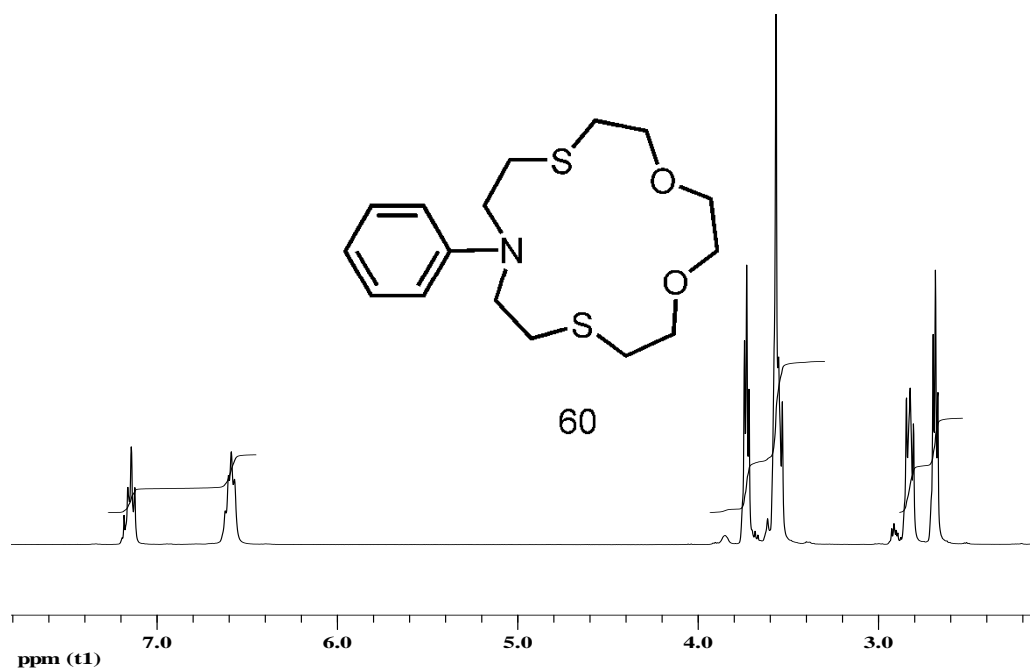


Figure 104 ^1H NMR spectra of the compound **60**

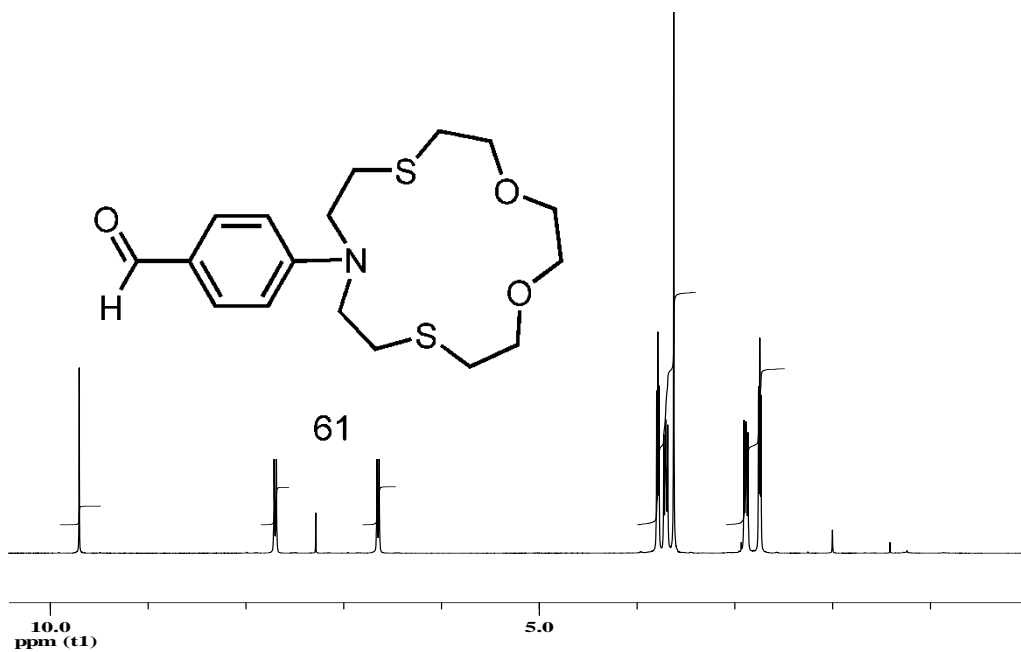


Figure 105 ^1H NMR spectra of the compound 61

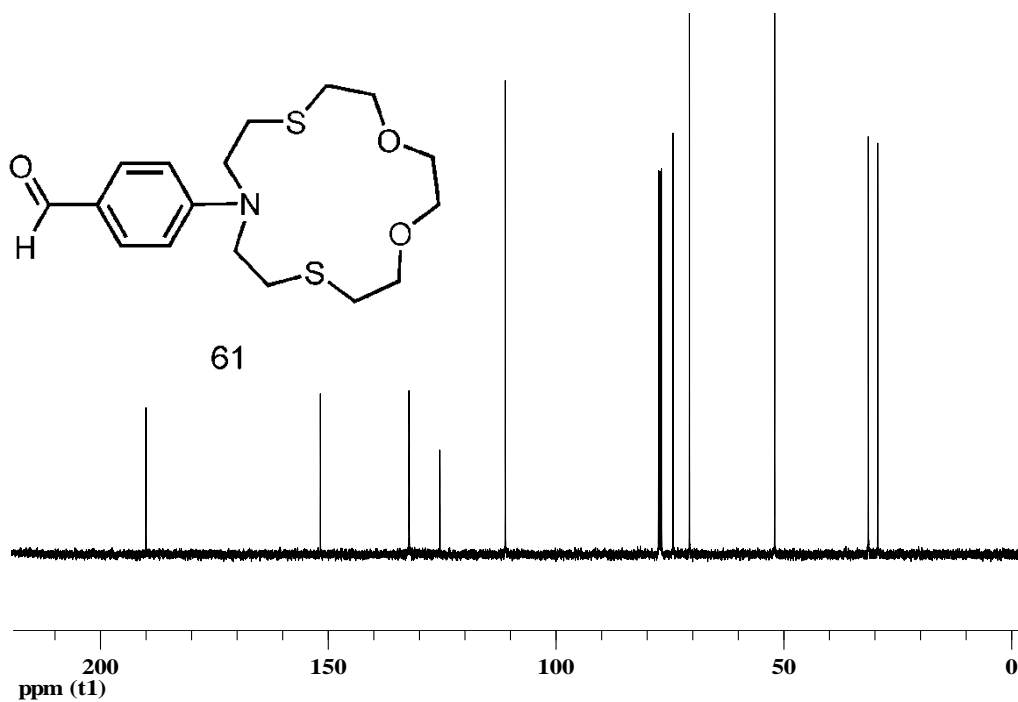


Figure 106 ^{13}C NMR spectra of the compound 61

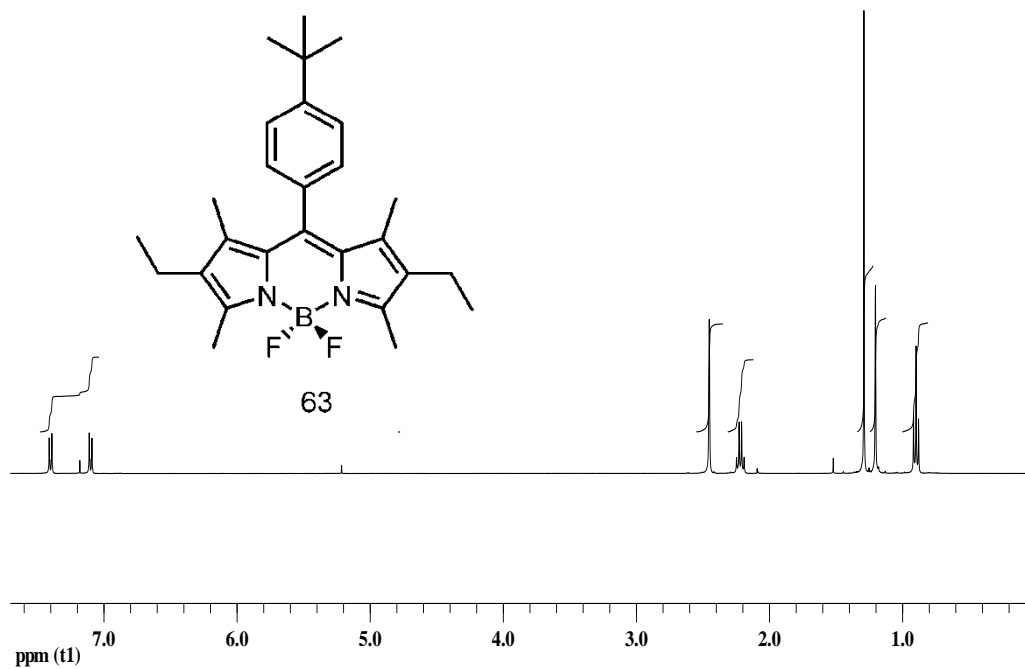


Figure 107 ¹H NMR spectra of the compound 63

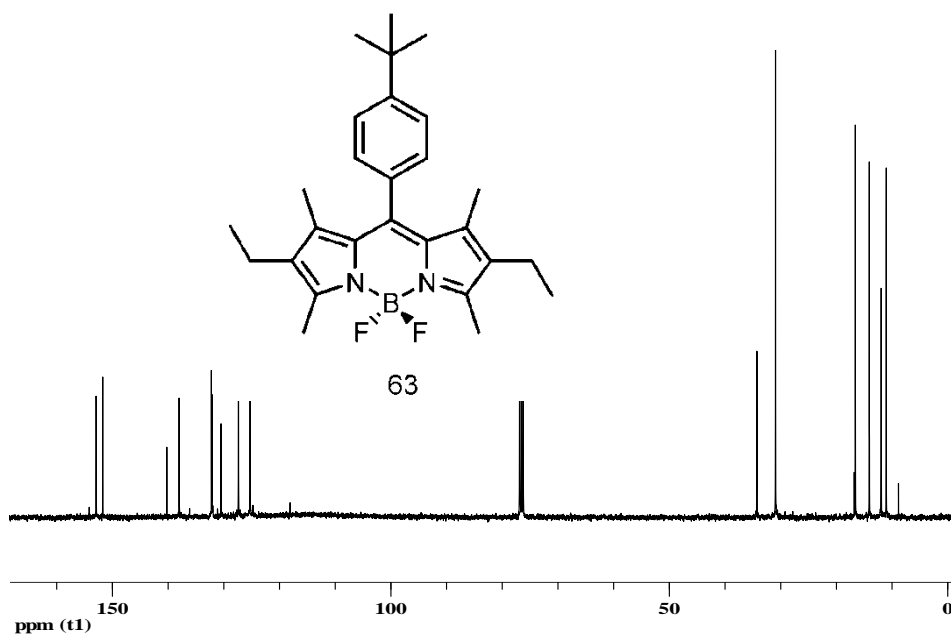


Figure 108 ¹³C NMR spectra of the compound 63

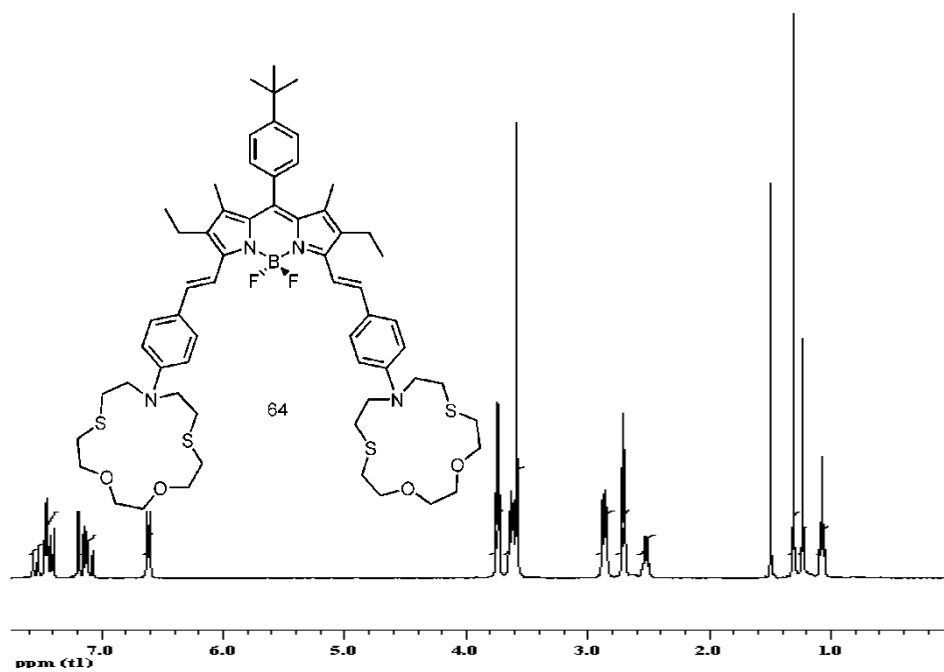


Figure 109 ^1H NMR spectra of the compound **64**

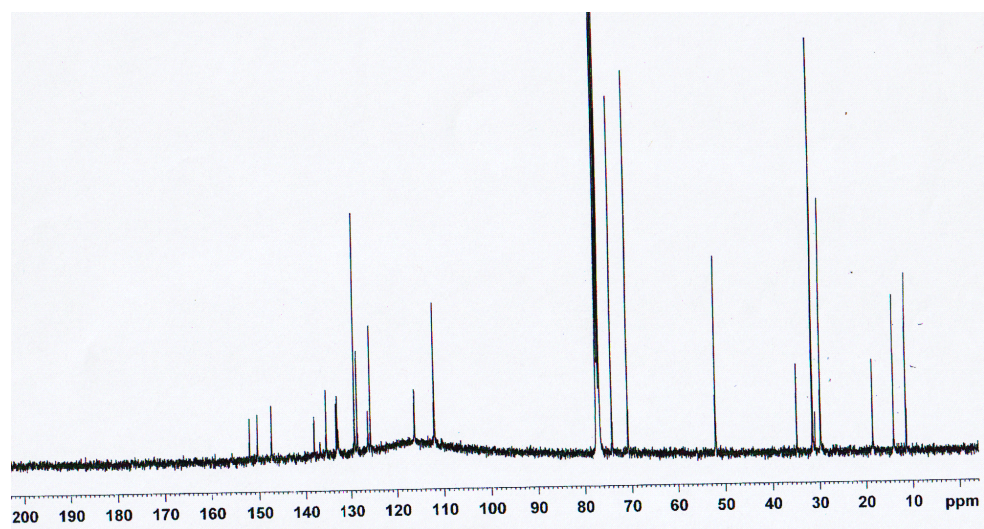


Figure 110 ^{13}C NMR spectra of the compound **64**

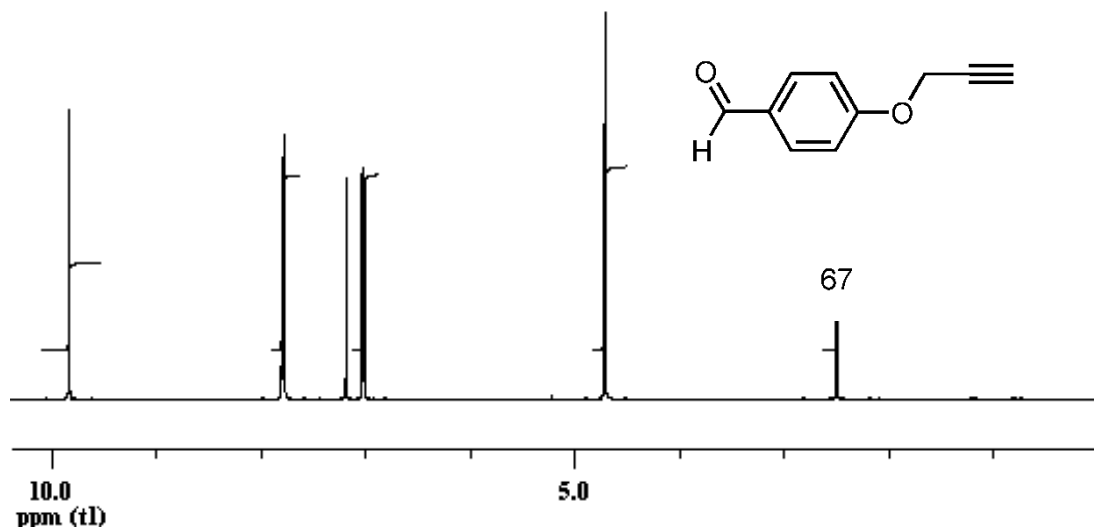


Figure 111 ^1H NMR spectra of the compound 67

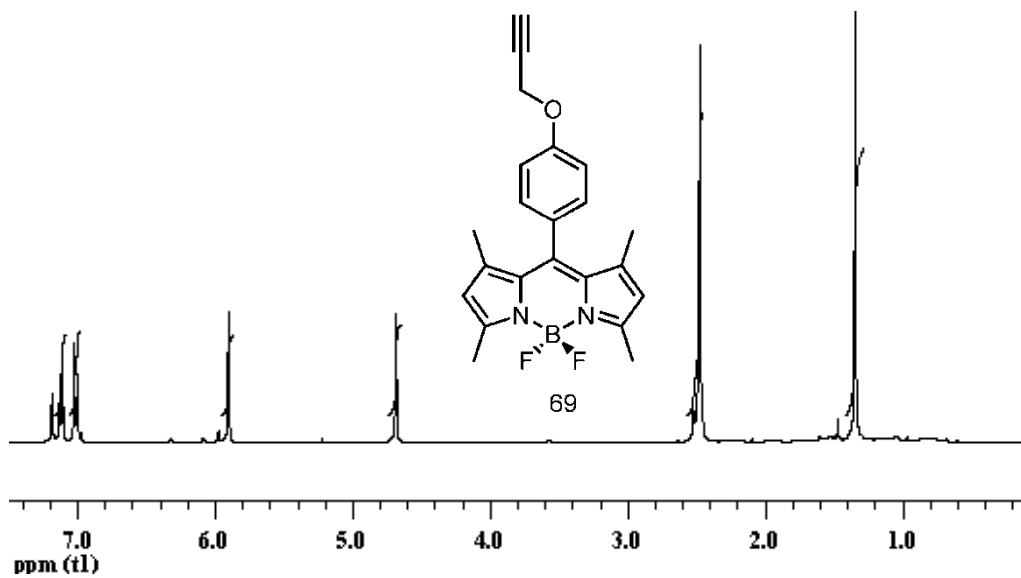


Figure 112 ^1H NMR spectra of the compound 69

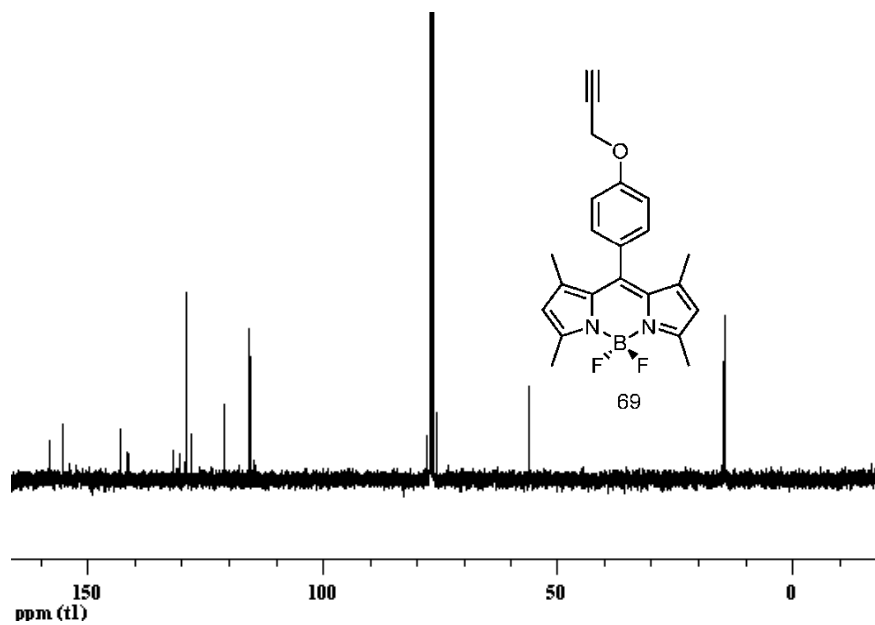


Figure 113 ^{13}C NMR spectra of the compound 69

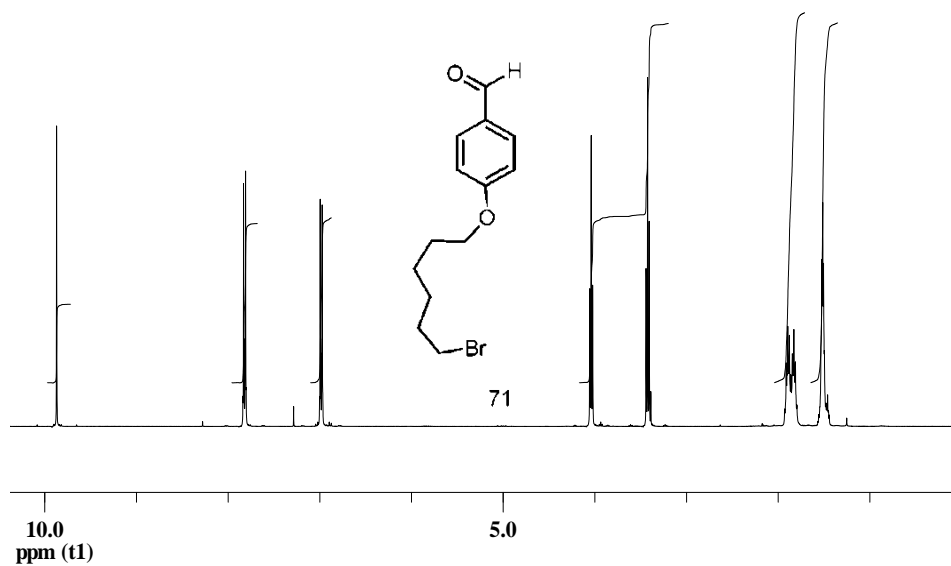


Figure 114 ^1H NMR spectra of the compound 71

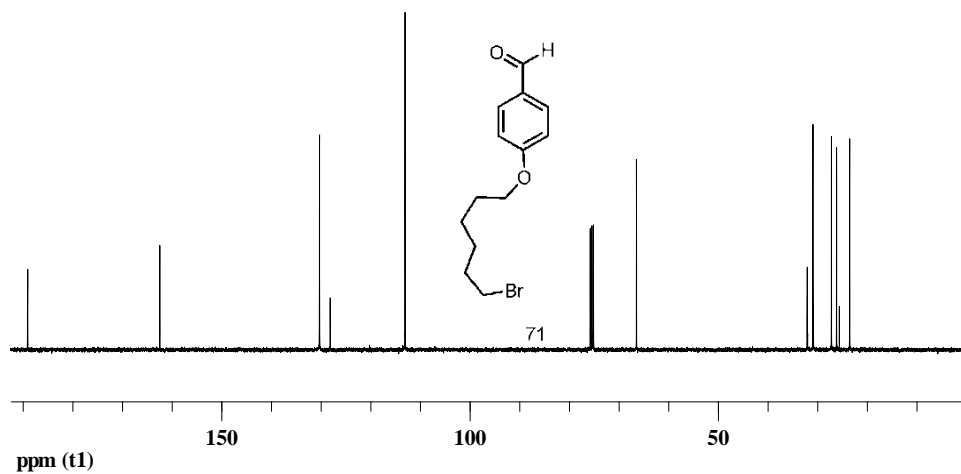


Figure 115 ^{13}C NMR spectra of the compound **71**

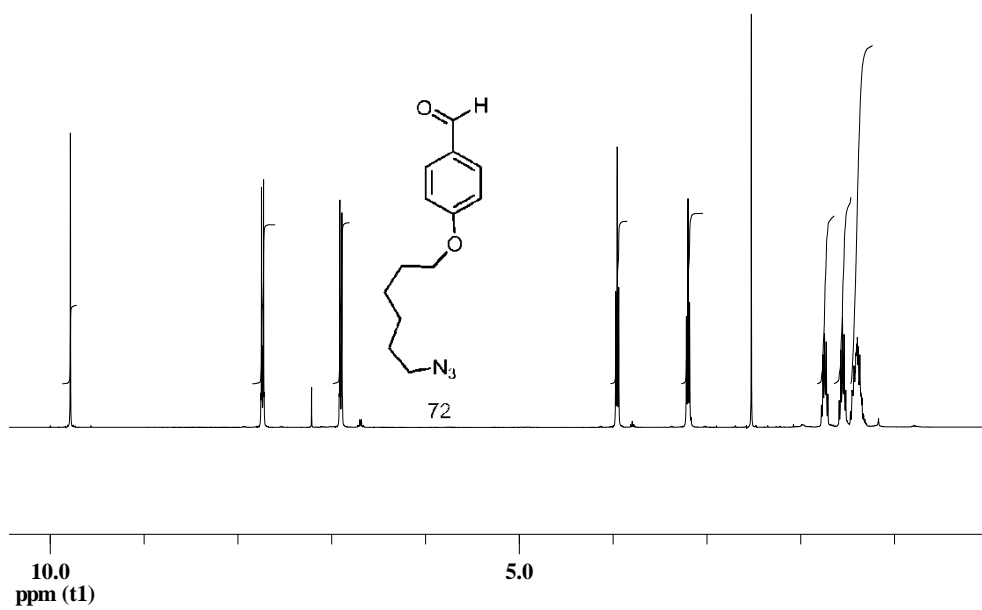


Figure 116 ^1H NMR spectra of the compound **72**

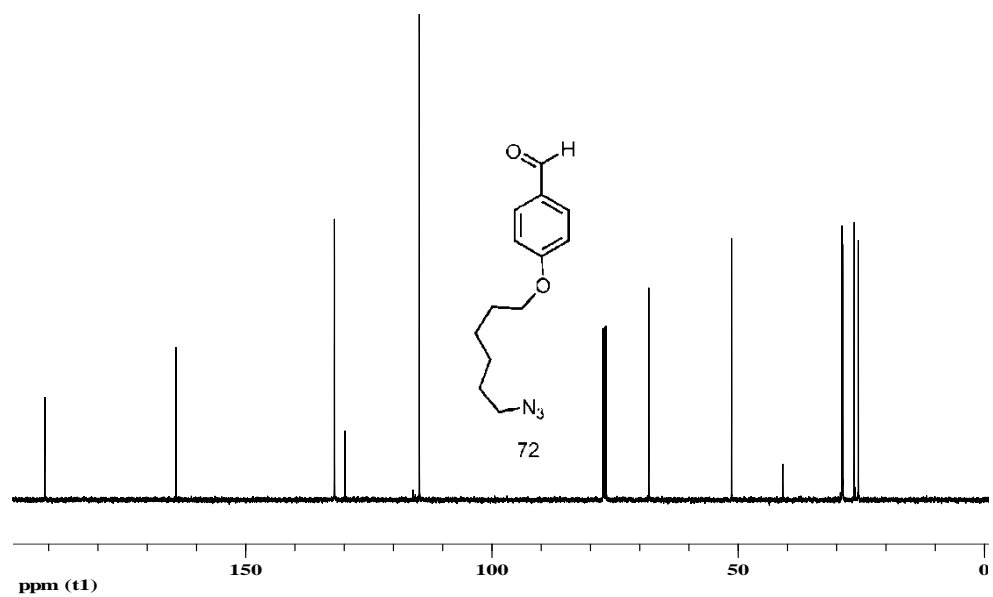


Figure 117 ^{13}C NMR spectra of the compound 72

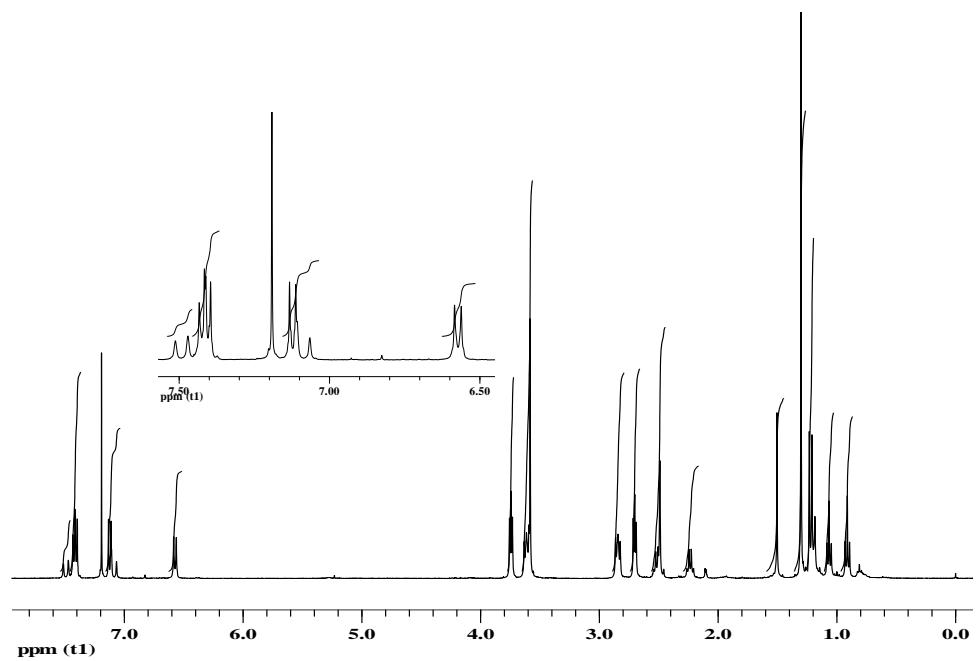


Figure 118 ^1H NMR spectra of the compound 73

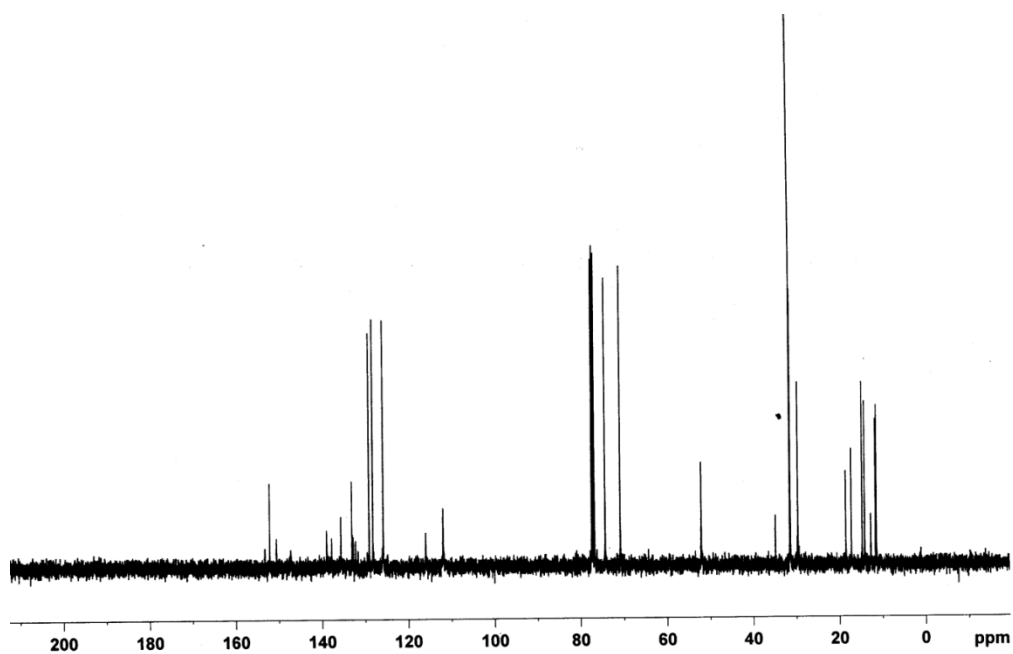


Figure 119 ^{13}C NMR spectra of the compound 73

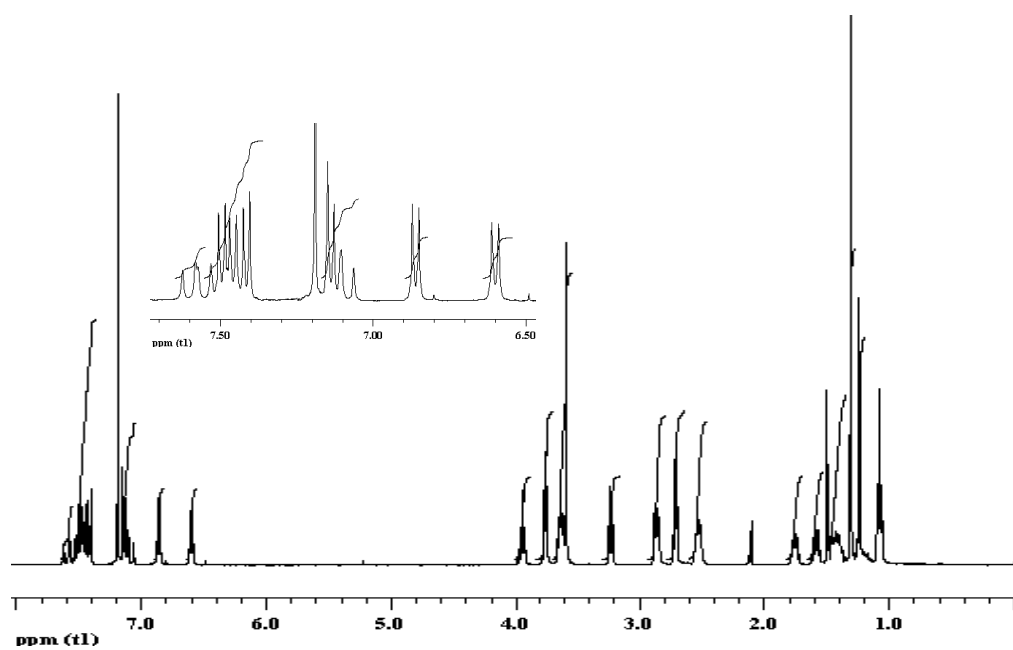


Figure 120 ^1H NMR spectra of the compound 74

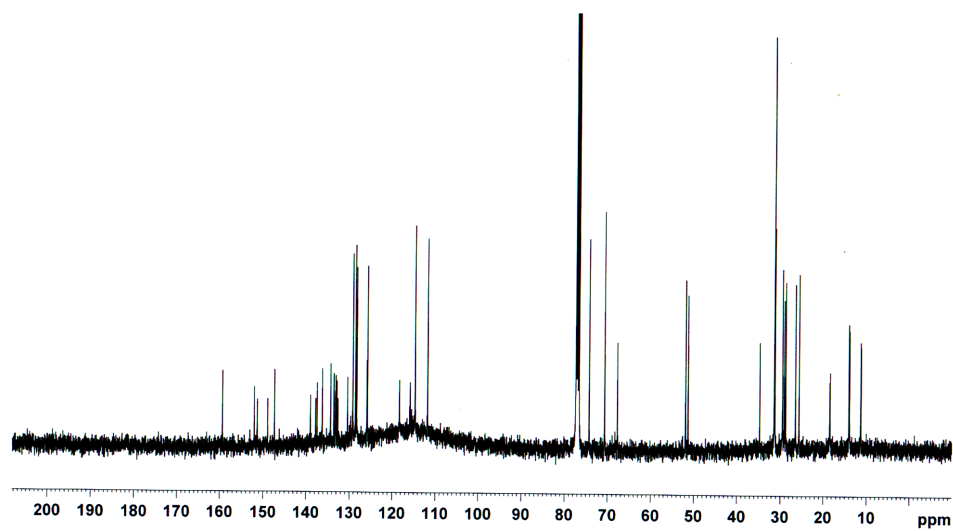


Figure 121 ^{13}C NMR spectra of the compound **74**

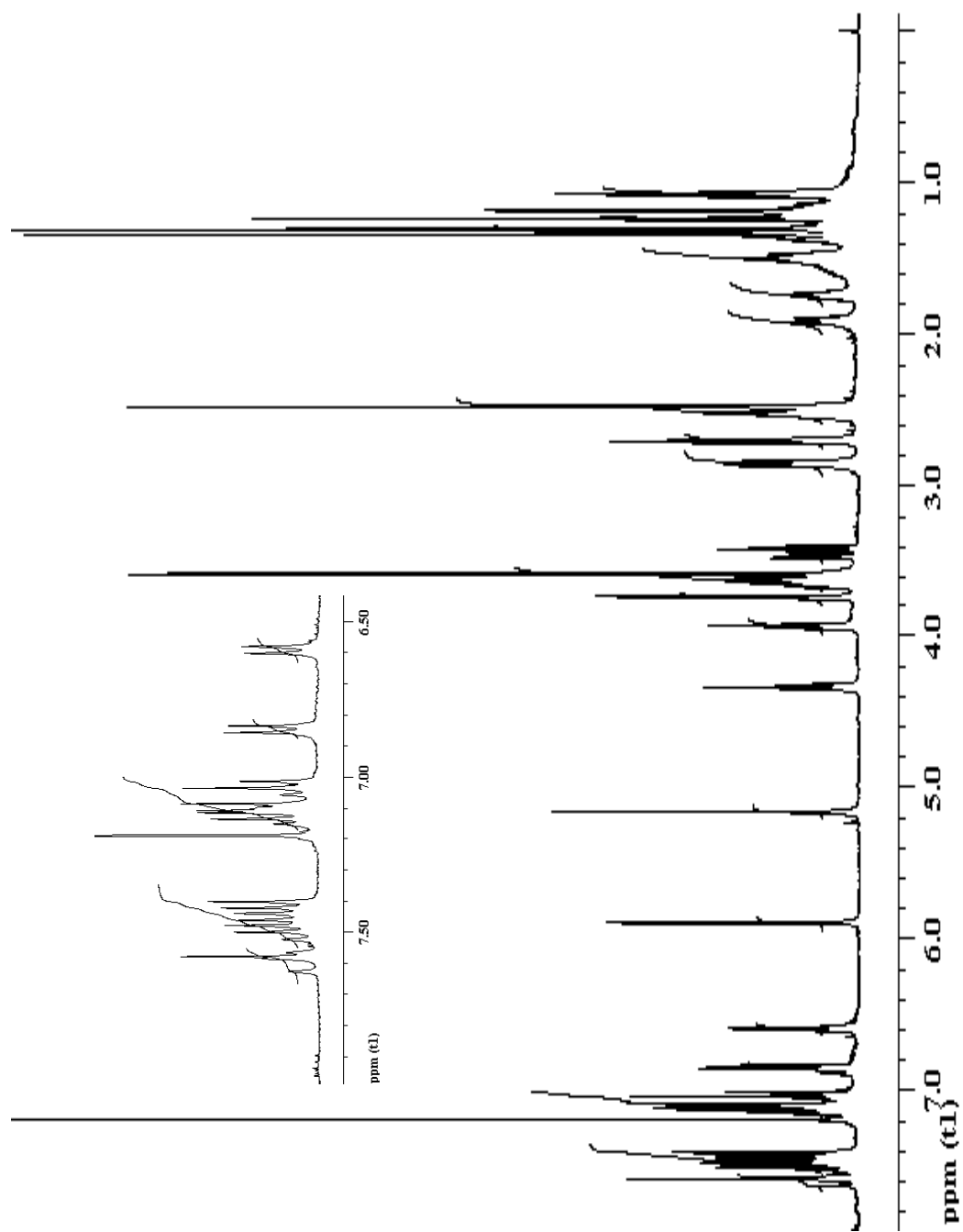


Figure 122 ^1H NMR spectra of the compound 75

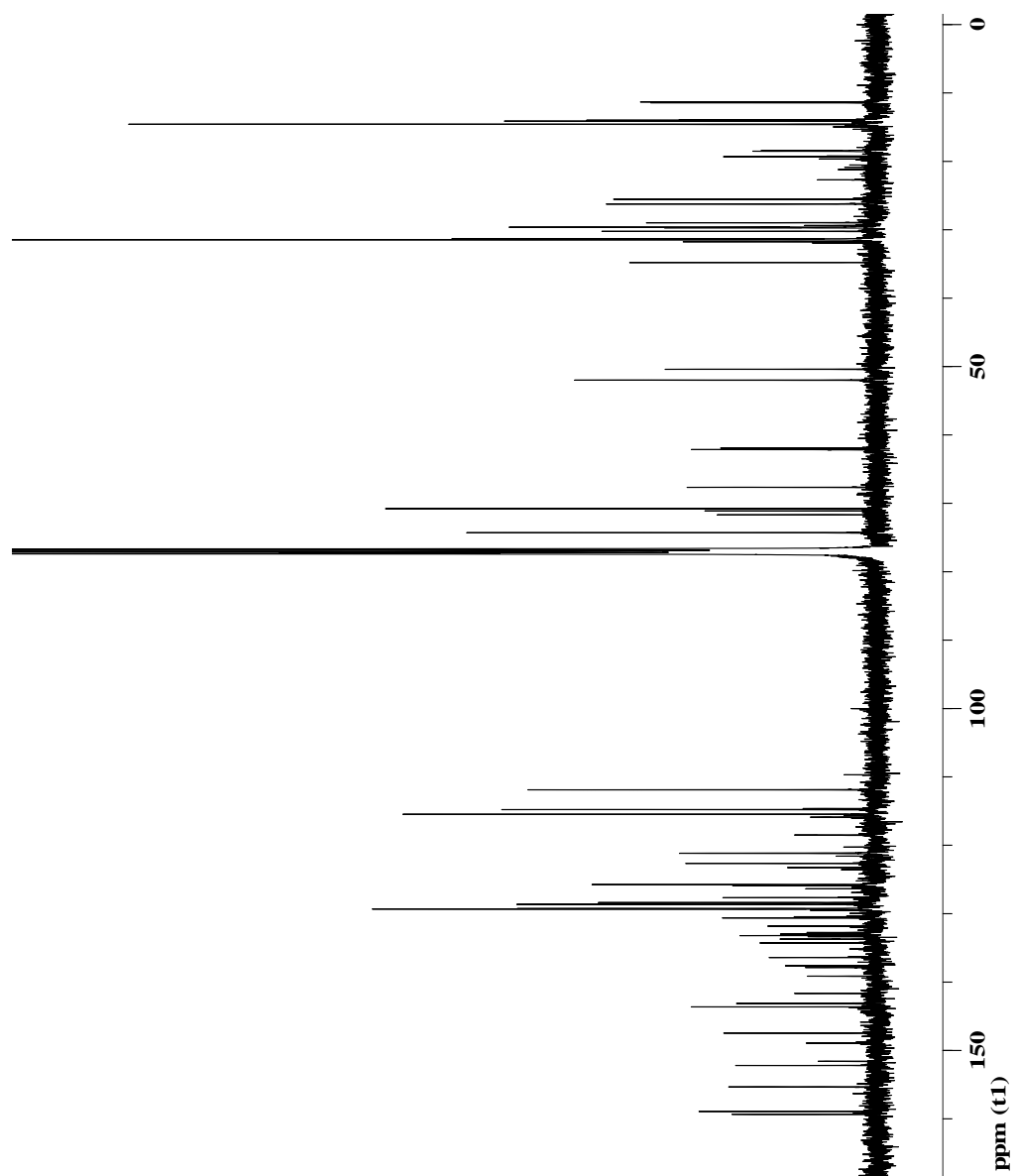


Figure 123 ^{13}C NMR spectra of the compound 75

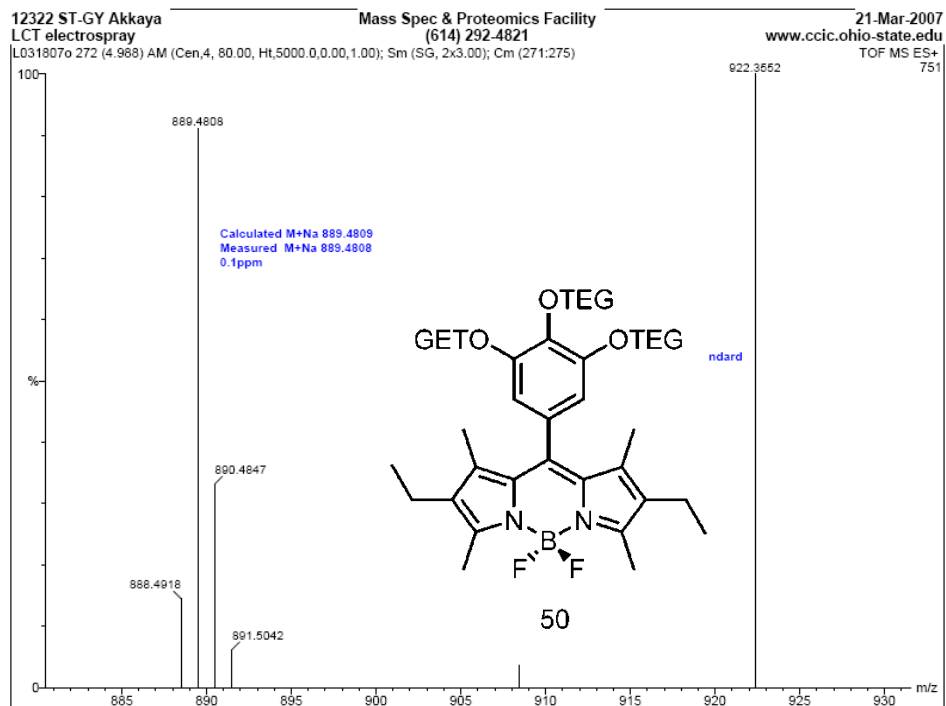


Figure 124 MALDI-TOF Mass spectra of the compound 50

12322 ST-GM Akkaya
Q-TOF2 Electrospray

Mass Spectrometry & Proteomics Facility
(614) 292-4821

22-Mar-2007
www.ccic.ohio-state.edu

Q032207G 358 (6.780) AM (Cen,4, 80.00, Ht,5000.0,0.00,1.00); Sm (SG, 2x3.00); Cm (352:358)

TOF MS ES+
1621.9321 305

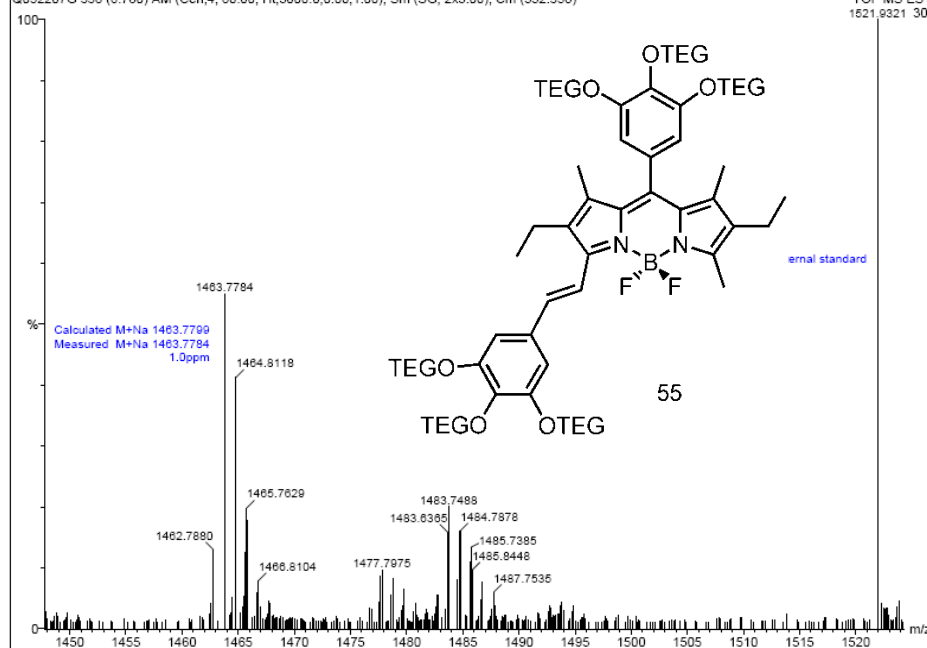


Figure 125 MALDI-TOF Mass spectra of the compound 55

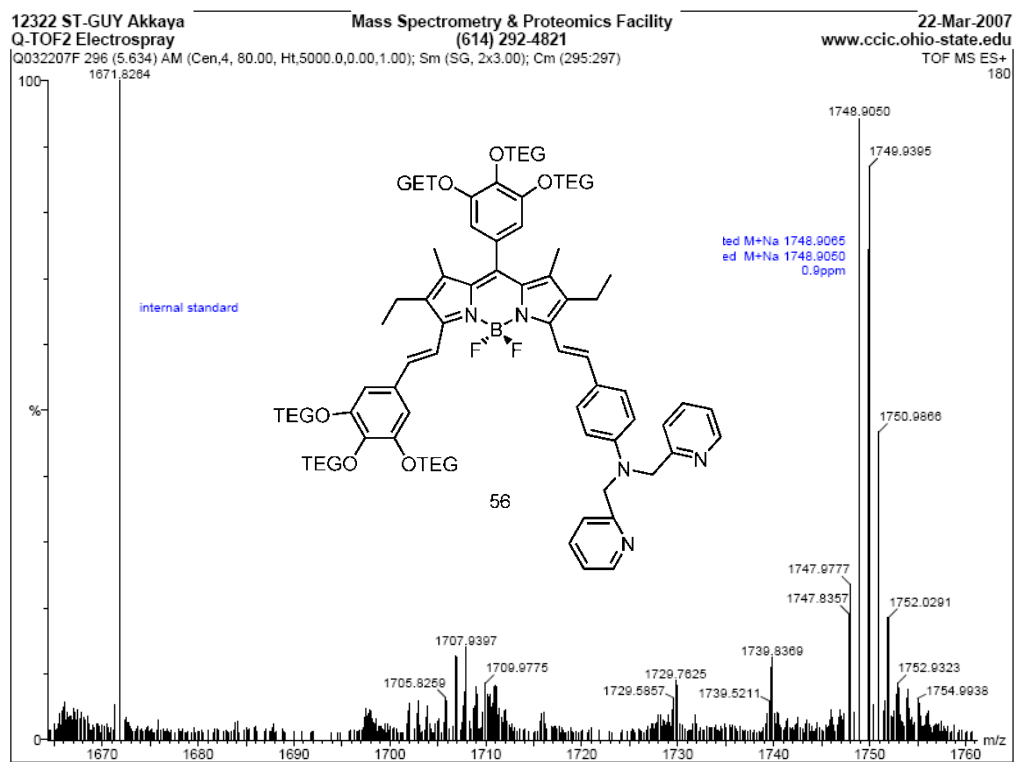


Figure 126 MALDI-TOF Mass spectra of the compound 56

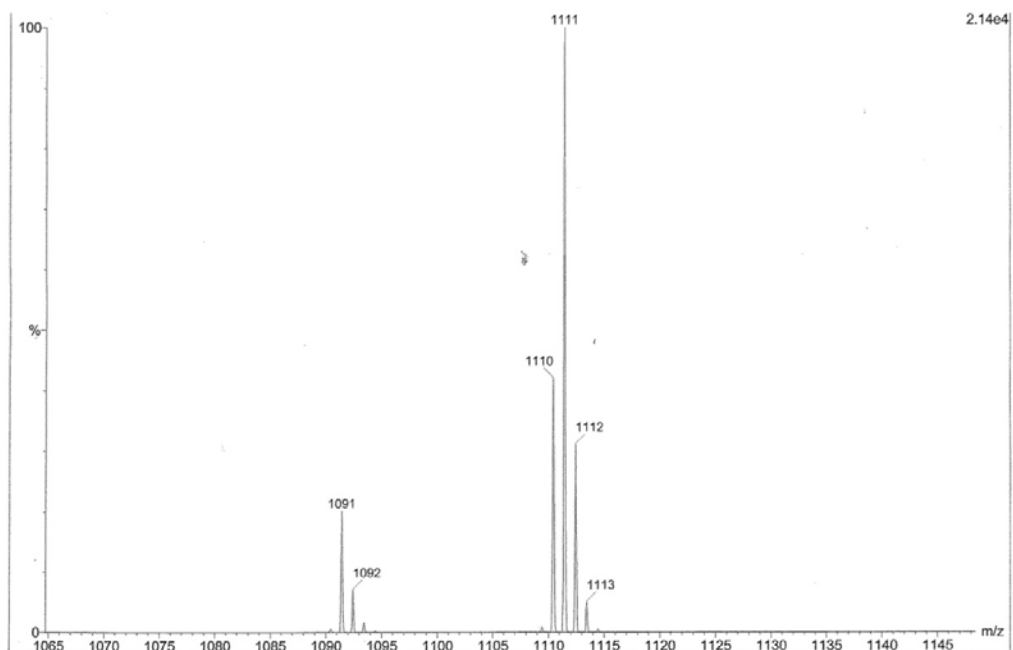


Figure 127 MALDI-TOF Mass spectra of the compound 64

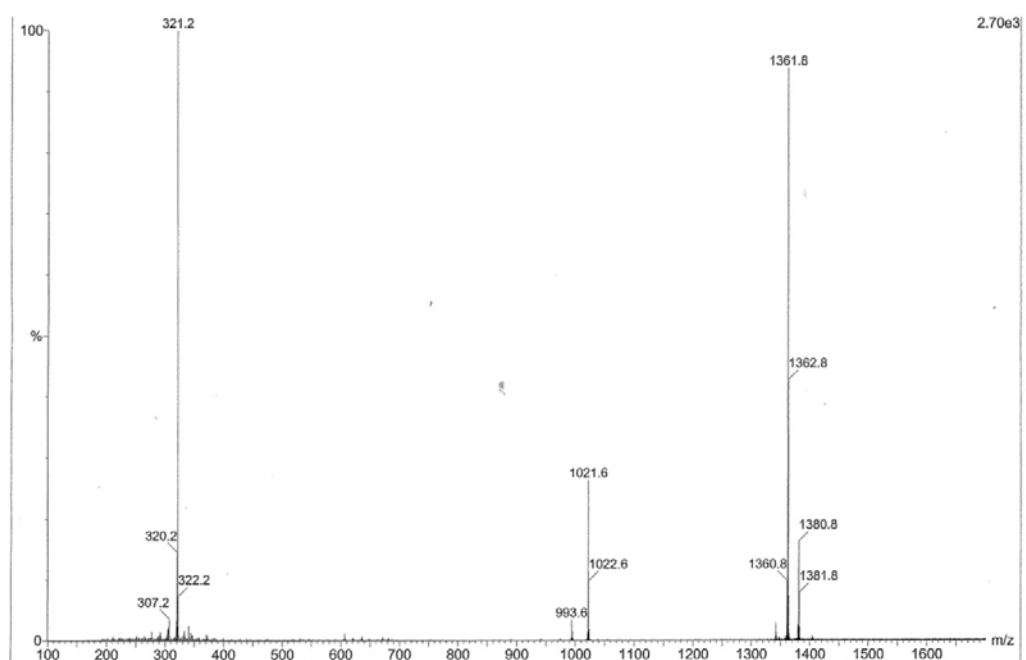


Figure 128 MALDI-TOF Mass spectra of the compound **75**

CURRICULUM VITAE

PERSONAL INFORMATION

Surname, Name: Atilgan, Serdar

Nationality: Turkish (TC)

Date and Place of Birth: 07/11/1980, Tokat

Marital Status: Married

Phone: +90 312 210 5153

Fax: +90 312 210 3200

email: atilganserdar@hotmail.com

EDUCATION

Degree Institution Year of Graduation

MS METU Chemistry Department 2006

BS AIBU Chemistry Department 2003

High School Gazi Osman Paşa High School, Tokat 1992

WORK EXPERIENCE

Year Place Enrollment

2004-2009 METU Department of Chemistry Department Research Assistant

FOREIGN LANGUAGES

Advanced English,

PUBLICATIONS

1. A calixpyridinium-pyranine complex as a selective anion sensing assembly via the indicator displacement strategy , Serdar Atılğan and Engin U. Akkaya. *Tetrahedron Lett.*, 2004, 45, 9269-9271, cited:9
2. Distyryl-Boradiazaindacenes: facile synthesis of novel near IR emitting fluorophores Zeynep Dost, Serdar Atılğan and Engin U. Akkaya; *Tetrahedron.*, 2006, 62, 8484-8488, cited:30
3. Water-Soluble distyryl-boradiazaindacenes as a efficient photosensitizers for photodynamic therapy; Serdar Atılğan, Zeynep Ekmekci, A.Lale Dogan, Dicle Guç and Engin U.Akkaya, *Chem. Comm*, 2006, 4349-4444. (Hot paper on this issue) and also published in *Chemical Science* with a title "Giving Red Light to cancer" cited;28
4. A sensitive and selective ratiometric near IR fluorescent probe for zinc ions based on the distyryl-bodipy fluorophore;Serdar Atılğan, Tugba Özdemir, Engin U. Akkaya, *Org. Let.* Volume: 10 Issue: 18 Pages: 4065-4067 Published: SEP 18 2008
5. Solid state emissive BODIPY dyes with bulky substituents as spacers, *Organic Letters*, Tugba Özdemir, Serdar Atılğan, İlker Kutuk, Mehmet Bayındır, Leyla Yıldırım Ahmet Tülek, Engin U.Akkaya, *Org Lett*, 2009, 11, 2105

ACHIVEMENTS

The best thesis of the year in Metu (M.Sc thesis) 2006.

-Scientific and Research Council of Turkey (TUBITAK), Ph.D scholarship, May 2006-2008(Project assistant scholarship)

-Scientific and Research Council of Turkey (TUBITAK),Undergraduate scholarship, January 2001-2003

-Graduation Degree, High Honour Student from İzzet Baysal foundation, July 2003

-Ranked first among all graduated student of the faculty of science and literature in 2003

-Ranked first among all graduated students of the bachelor's degree programs in Chemistry Department of Abant İzzet Baysal University 1998-2003 academic year.

-Ranked fourth among all graduated students of Abant İzzet Baysal University in 2003